การพัฒนาพอลิโพรพิลีนคอมพอสิตและพอลิแล็กทิกแอซิดคอมพอสิตที่ประกอบด้วยเซลลูโลสไฟบริล
ที่เตรียมโดยเทคนิคการละลาย/การตกตะกอน

นายสาริศ ถนอมชาติ

วิทยานิพนธ์นี้เป็นส่วนหนึ่งของการศึกษาตามหลักสูตรปริญญาวิทยาศาสตรดุษฎีบัณฑิต
สาขาวิชาวัสดุศาสตร์ ภาควิชาวัสดุศาสตร์
คณะวิทยาศาสตร์ จุฬาลงกรณ์มหาวิทยาลัย
ปีการศึกษา 2558

DEVELOPMENT OF POLYPROPYLENE COMPOSITES AND POLYLACTIC ACID COMPOSITES CONTAINING CELLULOSE FIBRIL PREPARED BY DISSOLUTION/PRECIPITATION TECHNIQUE

Mr. Sarit Thanomchat

A Dissertation Submitted in Partial Fulfillment of the Requirements
for the Degree of Doctor of Philosophy Program in Materials Science
Department of Materials Science
Faculty of Science
Chulalongkorn University
Academic Year 2015

Thesis Title	DEVELOPMENT OF POLYPROPYLENE COMPOSITES AND POLYLACTIC ACID COMPOSITES CONTAINING CELLULOSE FIBRIL PREPARED BY DISSOLUTION/PRECIPITATION TECHNIQUE
By	Mr. Sarit Thanomchat
Field of Study	Materials Science
Thesis Advisor	Associate Professor Kawee Srikulkit, Ph.D.

Accepted by the Faculty of Science, Chulalongkorn University in Partial Fulfillment of the Requirements for the Doctoral Degree

.....Dean of the Faculty of Science
(Associate Professor Polkit Sangvanich, Ph.D.)

THESIS COMMITTEE

.....Chairman
(Associate Professor Pranut Potiyaraj, Ph.D.)

.....Thesis Advisor
(Associate Professor Kawee Srikulkit, Ph.D.)

.....Examiner
(Assistant Professor Sireerat Charuchinda, Ph.D.)

.....Examiner
(Associate Professor Duangdao Aht-ong, Ph.D.)

.....External Examiner
(Assistant Professor Piyaporn Kampeerapappun, Ph.D.)

สาริศ ถนอมชาติ : การพัฒนาพอลิโพรพิลีนคอมพอสิตและพอลิแล็กทิกแอซิดคอมพอสิตที่ประกอบด้วยเซลลูโลสไฟบริลที่เตรียมโดยเทคนิคการละลาย/การตกตะกอน (DEVELOPMENT OF POLYPROPYLENE COMPOSITES AND POLYLACTIC ACID COMPOSITES CONTAINING CELLULOSE FIBRIL PREPARED BY DISSOLUTION/PRECIPITATION TECHNIQUE) อ.ที่ปรึกษาวิทยานิพนธ์หลัก: รศ. ดร. กาวี ศรีกูลกิจ, 155 หน้า.

งานวิจัยนี้มีจุดประสงค์เพื่อพัฒนาพอลิโพรพิลีนคอมพอสิตและพอลิแล็กทิกแอซิดคอมพอสิตที่เสริมแรงด้วยเซลลูโลสไฟบริลที่เตรียมได้จากเทคนิคการละลาย/การตกตะกอน โดยการละลายไมโครคริสตัลลีนเซลลูโลสในสารละลายโซเดียมไฮดรอกไซด์และยูเรียที่อุณหภูมิ -5 ℃ ซึ่งมีอัตราส่วนของโซเดียมไฮดรอกไซด์ ยูเรียและน้ำกลั่นเป็น 7:12:81 โดยน้ำหนัก แล้วจึงเติมสารละลายแป้งเพื่อทำหน้าที่เป็นสารกระจายตัวและป้องกันการรวมตัวกันของเซลลูโลสเนื่องจากแรงดึงดูดระหว่างพันธะไฮโดรเจน จากนั้นจึงนำมาตกตะกอนในสารละลายกรดไฮโดรคลอริก ได้เป็นเซลลูโลสไฟบริลที่มีโครงสร้างเป็นร่างแหและมีขนาดเส้นผ่านศูนย์กลางระหว่าง 10 ถึง 40 นาโนเมตรและมีค่าอมน้ำที่สูงเนื่องจากมีพื้นที่ผิวมาก ศึกษาการดัดแปรผิวของเซลลูโลสไฟบริลด้วยการใช้สารดัดแปรสองชนิดได้แก่ น้ำมันถั่วเหลืองมาลีเอตและเฮกซะเดซิลไตรเมทอกซีไซเลน โดยพบว่าเซลลูโลสไฟบริลที่ดัดแปรด้วยเฮกซะเดซิลไตรเมทอกซีไซเลน (Silane-g-CF) ทำหน้าที่เป็นสารเสริมแรงให้กับพอลิโพรพิลีนได้ดีกว่าเซลลูโลสไฟบริลที่ดัดแปรด้วยน้ำมันถั่วเหลืองมาลีเอต (Oil-g-CF) โดยเพิ่มอุณหภูมิเริ่มต้นการสลายตัวด้วยความร้อนของพอลิโพรพิลีนได้ถึง 20 ℃ และเพิ่มปริมาณผลึกได้ถึง 11 เปอร์เซ็นต์ นอกจากนี้ยังทำให้อุณหภูมิการเกิดผลึกของพอลิโพรพิลีนสูงขึ้น 4 ℃ จากนั้นจึงทำการเตรียมพอลิโพรพิลีนคอมพอสิตและพอลิแล็กทิกแอซิดคอมพอสิตที่มีปริมาณ Silane-g-CF เท่ากับ 0.5, 1.0, 3.0 และ 5.0 เปอร์เซ็นต์โดยน้ำหนัก ด้วยกระบวนการขึ้นรูปอัดรีดแบบเกลียวคู่และกระบวนการฉีดขึ้นรูป โดยพบว่าการใช้ Silane-g-CF เป็นสารเสริมแรงในพอลิโพรพิลีนสามารถช่วยเพิ่มเสถียรภาพทางความร้อน และทำหน้าที่เป็นสารก่อผลึกให้แก่พอลิโพรพิลีนโดยทำให้ปริมาณผลึกและอุณหภูมิการเกิดผลึกสูงขึ้น นอกจากนี้ยังสามารถปรับปรุงสมบัติเชิงกลโดยทำให้ความทนแรงกระแทกและมอดุลัสของยังมีค่าเพิ่มขึ้น 20 และ 10 เปอร์เซ็นต์ตามลำดับ เป็นผลมาจากความเข้ากันและแรงยึดเหนี่ยวระหว่างเฟสของสารเสริมแรงที่ดีขึ้นเนื่องจากการดัดแปรผิวของเซลลูโลสไฟบริล สังเกตได้จากผิวรอยแตกที่ขรุขระของพอลิโพรพิลีนคอมพอสิต ในกรณีของพอลิแล็กทิกแอซิดคอมพอสิตพบว่ามีเสถียรภาพทางความร้อนเพิ่มขึ้นเล็กน้อยและการทำหน้าที่เป็นสารก่อผลึกของ Silane-g-CF จะสังเกตได้อย่างชัดเจนเมื่อศึกษาสมบัติทางความร้อนด้วยการใช้อัตราการเย็นตัวของพอลิเมอร์หลอมเหลวที่ 1 ℃/นาที โดยพบการหายไปของอุณหภูมิเปลี่ยนสภาพแก้วและอุณหภูมิการเกิดผลึกระหว่างหลอมเหลว แต่ทำให้อุณหภูมิการเกิดผลึกเพิ่มขึ้น 5 ℃ และปริมาณผลึกเพิ่มขึ้น 30 เปอร์เซ็นต์ นอกจากนี้ Silane-g-CF ยังสามารถปรับปรุงสมบัติเชิงกลของพอลิแล็กทิกแอซิด โดยเพิ่มความทนแรงกระแทกได้ถึง 30 เปอร์เซ็นต์ และพอลิแล็กทิกแอซิดคอมพอสิตที่มีปริมาณ Silane-g-CF เท่ากับ 0.5 เปอร์เซ็นต์โดยน้ำหนักจะมีความยืดสูงสุด ณ จุดขาดเพิ่มขึ้น 50 เปอร์เซ็นต์ อย่างไรก็ตามเมื่อปริมาณสารเสริมแรงเพิ่มขึ้นจะทำให้ความยืดสูงสุด ณ จุดขาด ความทนต่อแรงดึงและมอดุลัสของยังมีค่าลดลง เป็นผลมาจากการทำหน้าที่เป็นสารเสริมสภาพพลาสติกของ Silane-g-CF เนื่องมาจากการดัดแปรด้วยออร์กาโนไซเลนที่ประกอบด้วยสายโซ่ยาวของหมู่แอลคิล

ภาควิชา วัสดุศาสตร์ ลายมือชื่อนิสิต .....

สาขาวิชา วัสดุศาสตร์ ลายมือชื่อ อ.ที่ปรึกษาหลัก .....

ปีการศึกษา 2558

5472860023 : MAJOR MATERIALS SCIENCE
KEYWORDS: CELLULOSE FIBRIL / SILANIZATION / SOYBEAN OIL / POLYPROPYLENE / POLYLACTIC ACID / COMPOSITES

SARIT THANOMCHAT: DEVELOPMENT OF POLYPROPYLENE COMPOSITES AND POLYLACTIC ACID COMPOSITES CONTAINING CELLULOSE FIBRIL PREPARED BY DISSOLUTION/PRECIPITATION TECHNIQUE. ADVISOR: ASSOC. PROF. KAWEE SRIKULKIT, Ph.D., 155 pp.

The aim of this research is to develop polypropylene (PP) and polylactic acid (PLA) composites reinforced with cellulose fibril which prepared from the novel technique via the dissolution and precipitation of cellulosic materials. Cellulose fibril was prepared from the dissolution of microcrystalline cellulose in NaOH/urea/distilled water (7:12:81 by weight) solution at -5 °C, followed by the addition of starch solution which plays a role as the dispersing agent and performs the anti-coagulation effect. The mixed solution was precipitated in HCl solution to obtain cellulose fibril (CF) which has a web-like morphology with the diameter ranging from 10-40 nm. The high surface area of CF results in the increasing of water retention value (WRV). The surface of CF was modified with two different modifying agents including malenized soybean oil and hexadecyltrimethoxysilane. The results indicate that hexadecyltrimethoxysilane modified cellulose fibril (Silane-g-CF) is the more efficient reinforcement for polypropylene than malenized soybean oil modified cellulose fibril (Oil-g-CF), judged by the rising of onset thermal degradation temperature by 20 °C, the increasing of degree of crystallinity up to 11% and the shift of crystallization peak to higher temperature by 4 °C. Subsequently, Silane-g-CF reinforced PP and PLA composites with the filler content of 0.5, 1.0, 3.0 and 5.0 wt% were prepared by the twin screw extrusion, followed by the injection molding. The results indicate that Silane-g-CF can improve the thermal stability of PP and plays a role as the nucleating agent by increasing the crystallization temperature up to 5 °C as well as the degree of crystallinity. Silane-g-CF/PP composites show the higher impact resistance and Young's modulus up to 20% and 10%, respectively when compared to neat PP. The enhancement of mechanical properties corresponds to the better compatibility and interfacial adhesion between CF and PP due to surface treatment, evidenced by the rough fracture surface of composites. In case of Silane-g-CF/PLA composites, the thermal stability is slightly increased. The nucleation effect of Silane-g-CF was observed clearly by DSC using the cooling rate of 1 °C/min. The glass transition temperature and the cold crystallization temperature are disappeared while the crystallization temperature is increased up to 5 °C as well as the increment of the degree of crystallinity by 30%. The addition of Silane-g-CF also improves the mechanical properties of PLA, resulting in the increasing of impact resistance up to 30%. At 0.5 wt% filler loading, the elongation at break of PLA is increased up to 50%. However, the decreasing of elongation at break, tensile strength, and Young's modulus is observed when filler loading is increased, attributing to the plasticization effect caused by the long alkyl chain of organosilane modifying agent.

Department: Materials Science Student's Signature .....
Field of Study: Materials Science Advisor's Signature .....
Academic Year: 2015

ACKNOWLEDGEMENTS

I would like to express my sincere gratitude to my thesis advisor, Associate Professor Dr. Kawee Srikulkit, who has always supported me throughout my research with his patience, motivation, encouragement, attention, advice and invaluable knowledge. His guidance helped me in all the time of my research and postgraduate education. I would not have achieved this far and this thesis would not have been completed without his supports. I really appreciate and respect him. Besides my advisor, I would like to thank my thesis committee sincerely, Associate Professor Dr. Pranut Potiyaraj, the chairman of thesis committee for his valuable advice, and also would like to express my appreciation to the thesis committee members, Assistant Professor Dr. Sireerat Charuchinda, Associate Professor Dr. Duangdao Aht-Ong and Assistant Professor Dr. Piyaporn Kampeerapappun, for the detailed review, invaluable suggestion, constructive criticism and excellence guidances.

I would like to thank and acknowledge The 90th Anniversary of Chulalongkorn University (Ratchadaphiseksomphot Endowment Fund GCUGR1125582011D), the Ratchadaphiseksomphot Endowment Fund of Chulalongkorn University (RES560530023-AM) and the Royal Golden Jubilee Ph.D. Program (PHD/0182/2553) for the financial support of this research and the DAAD-TRF Project based Personnel Exchange Program (PPP 2013) for the research collaboration.

I am really grateful the department of Materials Science, Faculty of Science, Chulalongkorn University for the necessary research instrument. Special thanks to my all teachers for giving me knowledge, the staff, the technicians, and my colleagues for the kind assistances and of course, my best friends for our good memories and friendship.

Last but not least, I would like to express a deep sense of gratitude to my parents who always stand by my side and believe in me. I owe my life for their constant love, encouragement, supports and blessing. Thanks to my brother for his understanding and care. Love them all.

CONTENTS

Page

Page

Page

Page

Page

Page

LIST OF TABLES

LIST OF FIGURES

CHAPTER I
INTRODUCTION

Over the past few decades, the awareness in the depletion of petroleum resources and the environmental pollution caused by the increasing of plastic wastes has led to the development of biodegradable plastics or sustainable materials to replace the consumption of petroleum-based polymers. Therefore, biopolymers or synthetic polymers reinforced with natural fibers, known as biocomposites, have attracted an attention from research and industrial fields due to their outstanding properties as well as environmental concern.

Cellulose is the most abundant natural polymer, good mechanical properties, light weight, biodegradability, renewability as well as low cost. Moreover, it can be used in several forms including film, fibers, microcrystalline cellulose, cellulose nanocrystal, cellulose nanowhisker or microfibrillated cellulose. Therefore, cellulose fibers have been considered as a reinforcement for polymers to obtain the biocomposites. Nowadays, the isolation, characterization, and searching for applications of cellulose novel forms have been increasing. There are several methods to isolate cellulose out of wood, forest/agricultural residues including chemical extraction (i.e. acid hydrolysis), enzymatic hydrolysis and mechanical process (ex. homogenizer, microfluidizer, grinding, etc.). However, the drawbacks of the conventional methods are the toxicity of chemical reagents, severe condition, high energy consumption as well as low yield. Therefore, the search for new novel methods of cellulose isolation becomes the challenge for the scientists. According to the hydrophilic nature of cellulose, the main problem for using cellulose fibers as the reinforcement of polymer composites is the incompatibility between cellulose and hydrophobic polymer matrices such as polyethylene, polypropylene, polylactic acid, etc., resulting in the non-uniform dispersion of filler, poor interfacial adhesion, and inferior properties. Therefore, the cellulose surface modification such as acetylation, silanization, application of coupling agents, grafting, corona/plasma discharges, and surface derivatization is carried out to enhance the hydrophobicity of cellulose.

Regarding the problems above, the aim of this research is to develop the cellulosic material reinforced polymer composites prepared by the novel technique. In this research, cellulose fibril (CF) was obtained from the dissolution of microcrystalline cellulose in NaOH/urea solution, followed by the precipitation in an acid solution. Normally, the dissolution of cellulose is carried out to destroy the strong hydrogen bonds between cellulose molecules and used for solution spinning process of rayon or Tencel fibers in the textile industry. There are several solvent systems for cellulose such as aqueous inorganic complexes (e.g. cuoxam, cuam, cuen), mineral acids, melts of inorganic salt hydrates, N,N-dimethyl-acetamide/LiCl, dimethylsulfoxide/triethylamine/SO_2, NH_3/NH_4SCN, CF_3COOH, HCOOH or N,N-dimethylformamide/N_2O_4 but NaOH systems, including NaOH/urea and NaOH/thiourea solution, are less toxicity, simple preparation and inexpensive.

To enhance the hydrophobicity of cellulose fibril, two different modifying agents were carried out. First, malenized soybean oil was synthesized and used as the modifying agent to obtain malenized soybean oil modified cellulose fibril (Oil-g-CF). Organosilane modified cellulose fibril (Silane-g-CF) was synthesized via silanization using hexadecyltrimethoxysilane as the modifying agent. The effects of modified cellulose fibril on the properties of thermoplastic including dispersibility, crystalline morphology, thermal degradation and thermal properties were investigated by using modified cellulose fibril as a reinforcing filler in polypropylene. The two composites of Oil-g-CF filled PP and Silane-g-CF filled PP were prepared through a simple melt mixing of modified CF and PP.

The composites of Silane-g-CF reinforced petroleum based polymer and bio-based polymer were prepared using polypropylene (PP) and polylactic acid (PLA) as a matrix. The biocomposites with various filler contents of 0.5, 1.0, 3.0 and 5.0 wt% were prepared using twin screw extrusion, followed by injection molding. Subsequently, the properties of modified cellulose fibril reinforced composites including thermal degradation, thermal properties, morphology, crystallinity, tensile properties and impact resistance were characterized and compared to the unmodified cellulose fibril reinforced composites.

CHAPTER II
THEORY AND LITERATURE REVIEWS

2.1 Cellulose

Cellulose is considered as the most abundant natural polymer on earth. Naturally, the major sources of cellulose are wood, plant fibers (cotton, flax, jute, sisal, etc.), sea animals (tunicate), algae, fungi, invertebrates, and bacteria. In case of plant source, cellulose occurs in leaf, fruit, seed, root, straw, stem, and wood. Cellulose is an odorless white-like fiber with an approximate density of 1.5 [1]. The estimated worldwide production of cellulose is 10^{10} to 10^{11} tons per year and about 6 x 10^{9} tons is processed by paper, textile, materials, and chemical industries [2, 3].

As shown in Figure 2.1, the chemical structure of cellulose is a linear homopolysaccharide of β-1, 4-linked anhydro-D-glucose units. The monomer unit is called anhydroglucose or AGU. Each repeating unit contains three hydroxyl groups of two secondary hydroxyl groups at C-2 and C-3 and one primary hydroxyl group at C-6. These three hydroxyl groups play an important role to cellulose properties due to their hydrophilic nature and the ability to form hydrogen bonds among cellulose molecules, resulting in strong crystalline regions [1]. Naturally, the degree of polymerization of cellulose chain is approximate to 10,000 [2].

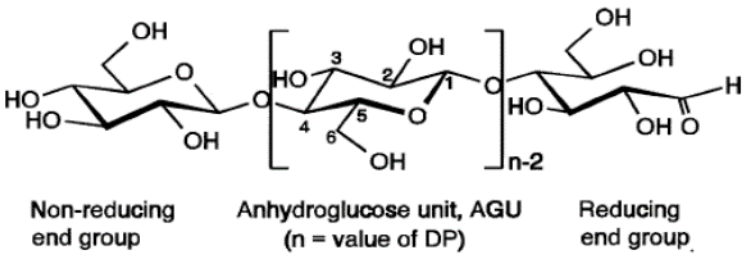

Figure 2.1 Chemical structure of cellulose [4]

Cellulose can be classified into four types by different polymorphs. Native cellulose named cellulose I is found in nature and presents in two allomorphs of Iα and Iβ. Cellulose II, also called regenerated cellulose, is obtained from precipitation,

recrystallization or mercerization in sodium hydroxide or alkali solution. Therefore, Cellulose I is unstable cellulose form but cellulose II is the stable form [5, 6]. The major different between two forms is presented in the layout of their atoms. Cellulose I is made up with the parallel chain whereas the chains of cellulose II run in the antiparallel direction [5] as shown in Figure 2.2.

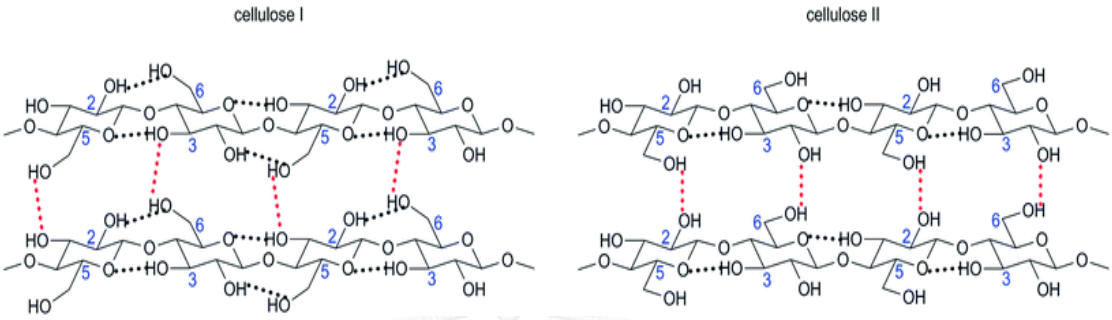

Figure 2.2 Supramolecular distinction between Cellulose I and Cellulose II [7]

Cellulose III_I and III_{II} result from the ammonia treatment of cellulose I and II, respectively while cellulose IV is obtained from the modification of cellulose III. The steps to obtain the various cellulose polymorphs and their models are displayed in Figure 2.3 and 2.4.

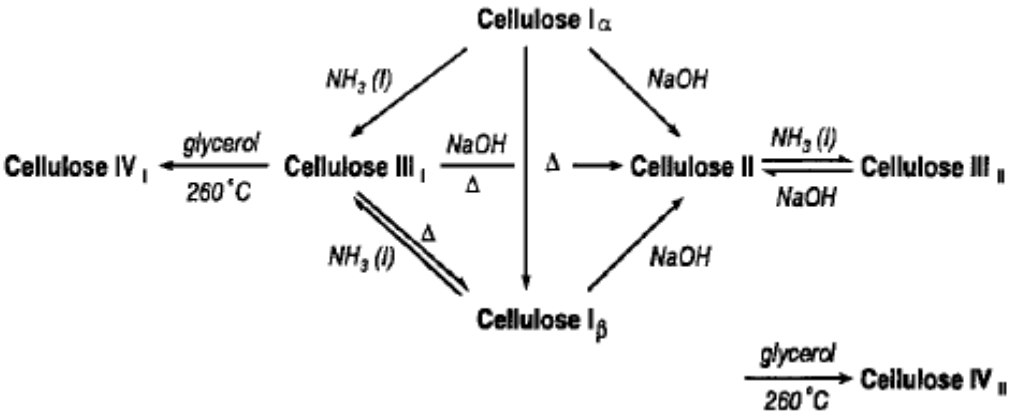

Figure 2.3 Transformation of cellulose into its various polymorphs [8]

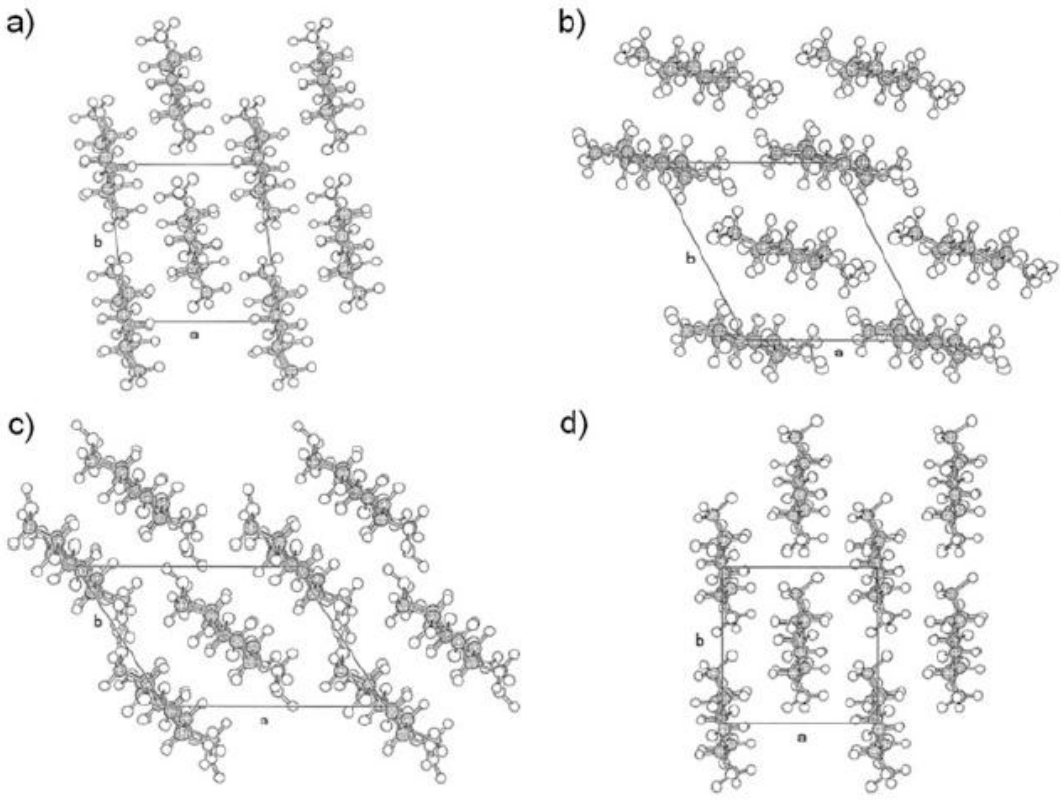

Figure 2.4 Model of a.) Cellulose Iβ, b.) Cellulose II, c.) Cellulose III_I and d.) Cellulose IV_I [9]

The details of cellulosic fibers are shown in Figure 2.5. About 36 individual cellulose molecules are brought together by biomass into the larger units called elementary fibrils or microfibrils. Each of microfibrils is packed into the larger units known as microfibrillated cellulose which assembles into the cellulosic fiber. The diameter of elementary fibrils is about 5 nm but microfibrillated cellulose has the diameter ranging from 20-50 nm and the length in several micrometers [10]. Microfibrillated cellulose consists of amorphous region and crystalline region of cellulose crystal which results from hydrogen bonding. Therefore, the two types of nanocellulose can be classified as i) cellulose nanocrystals and ii) cellulose microfibrils [1]. Nowadays, cellulosic materials have been received attentions in many fields due to its several advantages such as high strength and modulus, low density, biodegradability, renewability, abundant, and low cost [11].

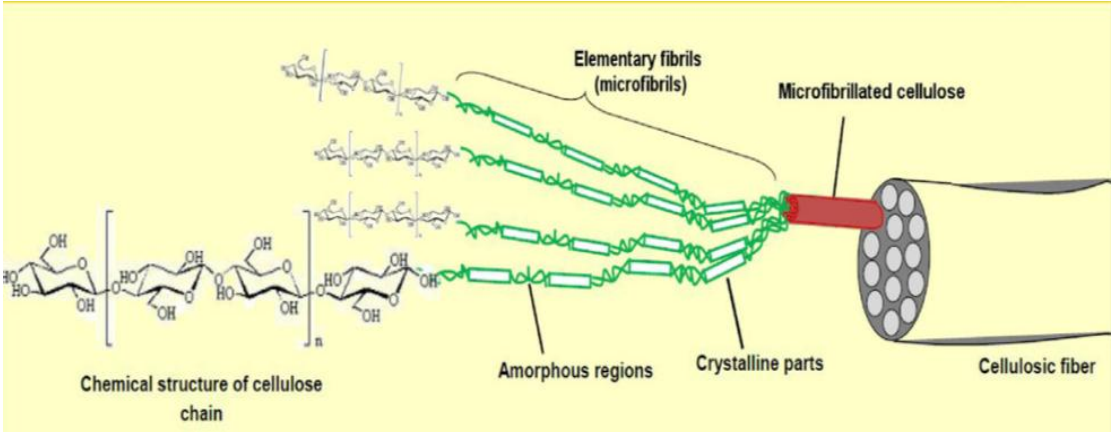

Figure 2.5 The details of cellulosic fiber [1]

2.2 Micro and Nanocellulose

As mentioned earlier, the crystalline structure, inter- and intra-molecular hydrogen bonds have an effect on the strength of cellulose microfibrils. Natural cellulosic fibers still have lower strength than the theoretical value due to the presence of amorphous region and other components such as hemicellulose. Therefore, the controlled disintegration of natural cellulose fibers or the growing of cellulose from bacterial sources are required to produce the unique properties of cellulose microfibrils, particularly high strength. Normally, the obtained cellulosic structure is found in micron or nanoscale which can exhibit the special properties when used as a reinforcement in polymer composites. In this section, the preparation methods and properties of microcrystalline cellulose, nanocrystalline cellulose, microfibrillated cellulose, and bacterial cellulose are discussed in detail [11].

2.2.1 Microcrystalline Cellulose

Microcrystalline cellulose (MCC) had been discovered since 1962 by Battista and Smith. They used a Waring Blender to disintegrate hydrolyzed cellulose suspension in water. The hydrolyzed cellulose was sliced by a sharp blade into small fragments of microcrystals in water. A stable colloidal suspension of microcrystalline is known in a commercial name as Avicel [11, 12].

Generally, MCC is obtained by the acid hydrolysis of cellulosic materials such as wood pulp. The amorphous regions of fibers are removed by acid, then cellulose microcrystals with an average diameter of 30 nm to 5 μm are obtained. Due to the

strong hydrogen bonding between the individual cellulose microcrystals, MCC is formed by the re-aggregation after drying process with a spongy, porous and random fine structure [11]. The SEM image of MCC in Figure 2.6 indicates the size of MCC which is in the wide range of several microns to several tens of microns. MCC can use as a rheology control agent or binder in a pharmaceutical industry.

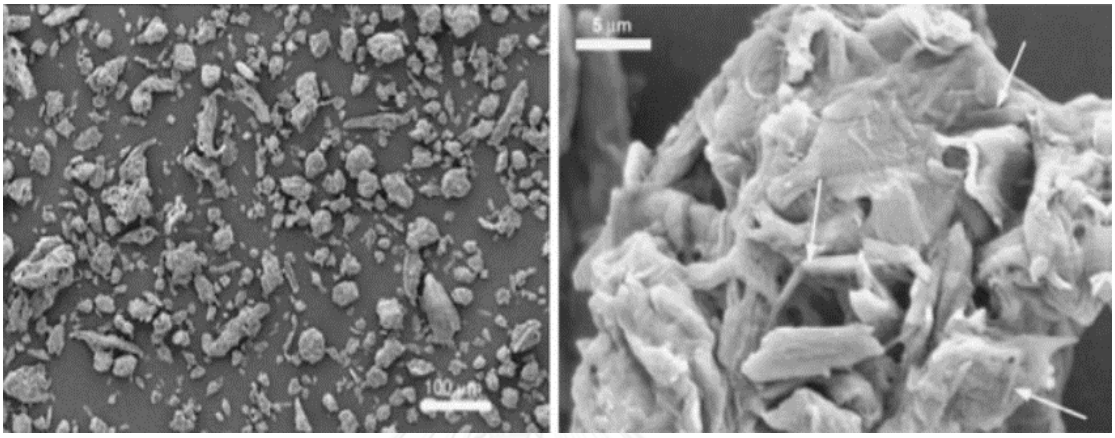

Figure 2.6 SEM micrograph of MCC at different magnification a.) Scale bar 100 µm and b.) Scale bar 5 µm (The arrows indicate the crystallites in MCC particle) [13]

2.2.2 Cellulose Nanocrystals

The discovery of cellulose nanocrystals began in 1870, Nageli and Schwendener found the presence of crystalline structures in amorphous regions of cellulosic materials. In 1950, Rånby and Ribi succeeded to produce the first cellulose nanocrystals using sulfuric hydrolysis of wood and cotton cellulose. They obtained a stable colloidal suspension of cellulose crystals with 50-60 nm in length and the diameter of 5-10 nm, approximately [1].

Cellulose nanocrystals, also called as nanocrystalline cellulose (NCC), cellulose nanowhiskers (CNW) or cellulose crystallites, is prepared from the strong acid hydrolysis combined with controlling of temperature, time and agitation. The amorphous regions are removed by acid, leaving the high crystalline regions as the intact domain [1]. Then, the CNC suspension is centrifuged or dialyzed using distilled water to remove the molecules of free acid. CNC can be extracted from a variety of sources such as cotton, wood pulp, tunicate, wheat straw, sugar beet, potato peel or MCC [14-19]. CNC has a rod-like shape with 5-70 nm width and a length varying from

100 nm to a few micrometers. The TEM images of CNC from different sources are shown in Figure 2.7. Regarding the mechanical properties, CNC has an approximate Young's modulus around 130 GPa to 250 GPa. Due to the high strength, CNC has a potential to use as a filler in composite materials [20-22].

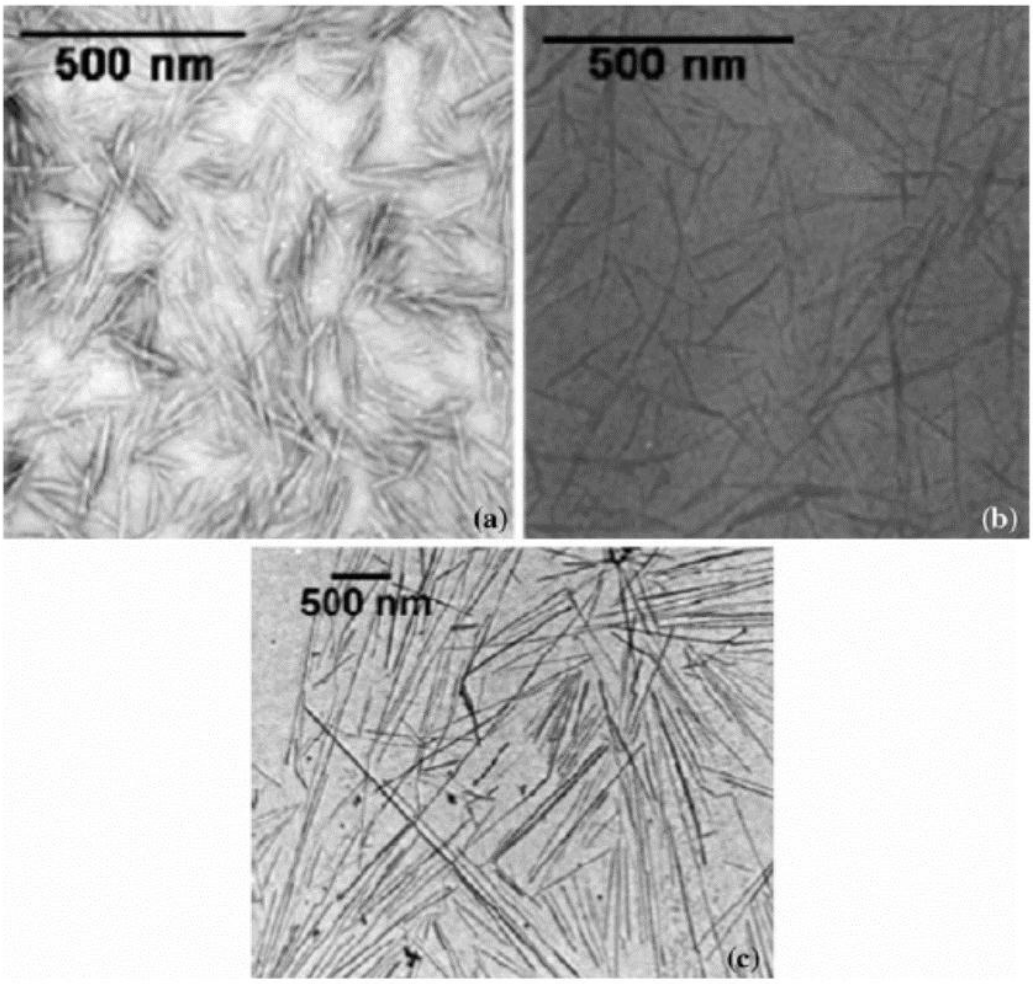

Figure 2.7 TEM images of CNC from a.) Cotton, b.) Sugar beet pulp and c.) Tunicate [11]

2.2.3 Microfibrillated Cellulose

Another type of nanocellulose is microfibrillated cellulose (MFC), also called cellulose microfibrils, microfibrillar cellulose or nanofibrillated cellulose (NFC). Unlike CNC, MFC has both amorphous and crystalline parts, web-like structure and prepared by mechanical extraction of cellulosic materials without the acid hydrolysis reaction. MFC consists of elementary fibrils aggregation, its diameter is in the range of 20-60 nm and the length is in several micrometers [1, 23].

The preparation of MFC by fibrillation of cellulose fibers into nano-scale requires intensive mechanical treatment. The first successful MFC production was reported in 1983 by Herrick et al. and Turbak et al by using a Gaulin laboratory homogenizer. In this method, the dilute slurries of cut cellulose fibers from softwood pulp were passed through a mechanical homogenizer with a large pressure drop under high shear forces to facilitate microfibrillation [1, 23, 24]. Microfluidizer is a recent alternative equipment for MFC preparation by passing the wood pulp through the thin z-shaped chamber under high pressure and shear rate for the formation of very thin cellulose nanofibers [4]. The other methods of MFC preparation by mechanical treatment are grinding and cryo-crushing. The principle of grinding process is the breakdown of cell wall structure by the shear force generated from grinding stones. The pulp is passed between a static grindstone and a rotating grindstone at about 1500 rpm. Then, the nano-sized fibers in a multilayer structure are individualized from the pulp. Cryo-crushing is the rarely used technique. This technique consists of the crushing of pulp which was frozen in liquid nitrogen and applying the high impact forces to the frozen fibers. Then, the ice crystals of the cell wall are ruptured to liberate nanofibers [1, 24]. Figure 2.8 presents the TEM images of MFC from rutabaga produced by the cryo-crushing process.

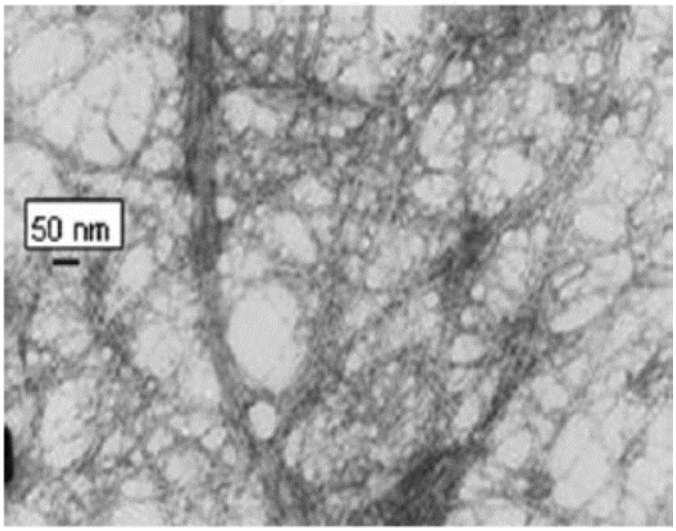

Figure 2.8 TEM images of MFC from rutabaga produced by cryo-crushing process [25]

The sources of MFC consist of wood (ex. bleached kraft pulp, bleached sulfite pulp, etc.) and non-wood source (ex. cotton, flax, hemp, jute, sisal, ramie, sugar beet pulp, wheat straw and soy hull, palm trees, etc.) [26]. MFC can be used as thickeners, emulsifiers or additives in food, paints, cosmetic, packaging with high barrier properties and pharmaceutical products. As a result of many advantages of MFC such as high strength and stiffness, high surface area, good barrier properties, light weight, renewability, biodegradability, abundance and low cost, MFC is being extensively used as the reinforcement of composite materials in several applications such as automotive components, shipping crates/pallets, storage bins, toys, outdoor furniture as well as biomedical applications [27]. The preparation of CNC and MFC is shown in Figure 2.9

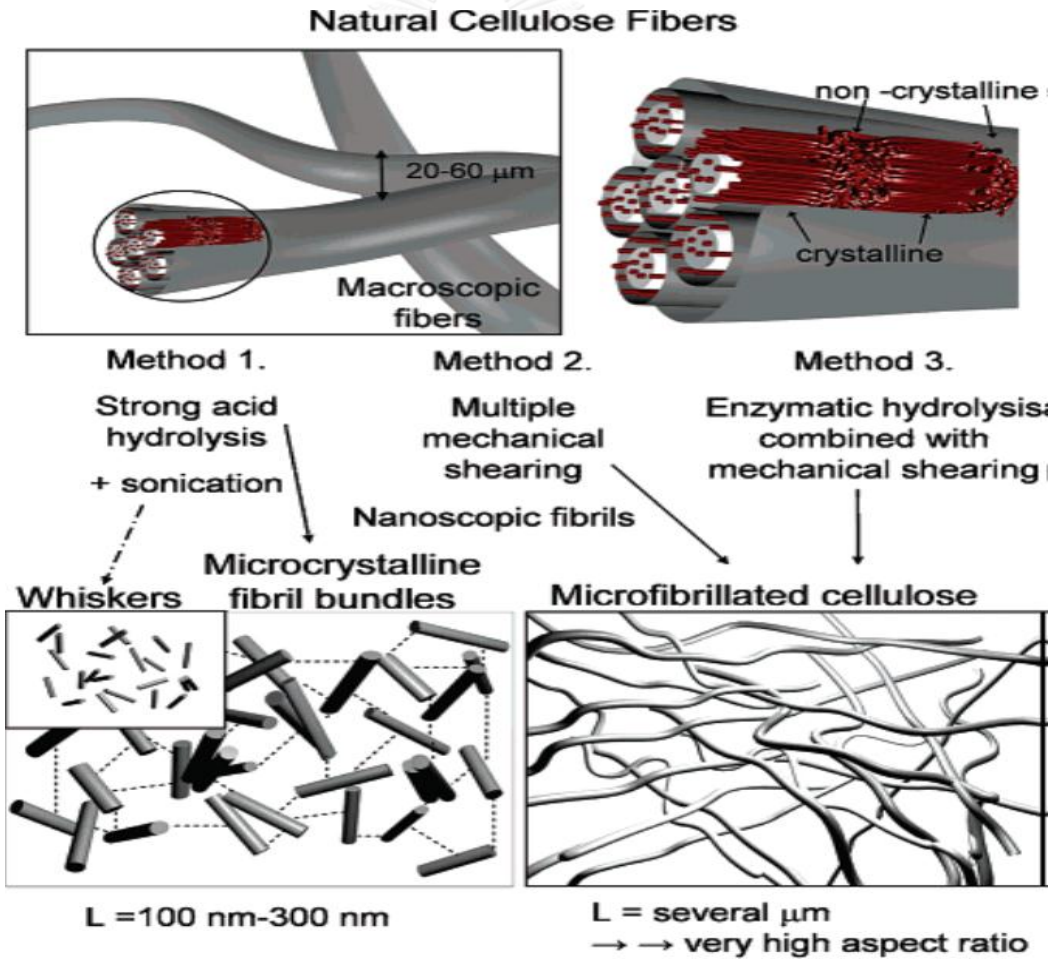

Figure 2.9 Preparation of cellulose nanocrystals and microfibrillated cellulose from the fiber suspension [28]

2.2.4 Bacterial Cellulose

Besides plant source, nanocellulose can be synthesized from some kind of bacteria species such as *Gluconacetobacter* [1] or *Acetobacter xylinium* [11]. This kind of cellulose nanofibers is called bacterial cellulose or BC. Seidel et al. [29] synthesized BC from *A. xylinium* using Hestrin-Schrammn as a medium at 30 °C for several days. They extruded glucan chains, which can aggregate into microfibrils when the bacteria grew in the medium. Then, the microfibrils packed together and formed microbial cellulose ribbons. BC was harvested from the culture medium, followed by washing with alkaline solution and water extensively. BC exhibits a network structure made by an assembly of ribbon-shaped fibrils randomly. The diameter of fibrils which contain the bundle of many fine microfibrils is less than 100 nm. The SEM image of BC is shown in Figure 2.10.

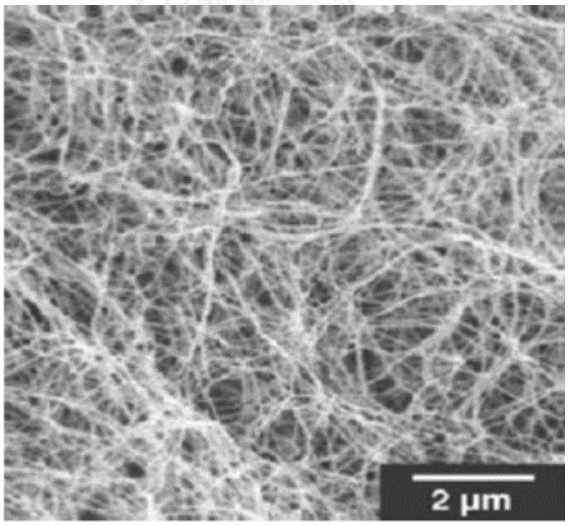

Figure 2.10 SEM image of bacterial cellulose [30]

Due to the high purity and high strength of bacterial cellulose [11], it has been studied for several applications including biomedical materials, reinforcement of nanocomposites, electronic paper, and fuel cell membranes [31-34].

2.3 Cellulose Reinforced Polymer Composites

2.3.1 Composite

Composite is a material that composes of two or more components with significantly different physical, mechanical or chemical properties to enhance or improve mechanical properties and superior functionalities. A strong and stiff component of composite, which called a reinforcement, will be embedded in a softer component called a matrix. Therefore, the properties of composite are lying between the properties of matrix and reinforcement. Figure 2.11 illustrates the mechanical properties of reinforcements, matrices, and composites.

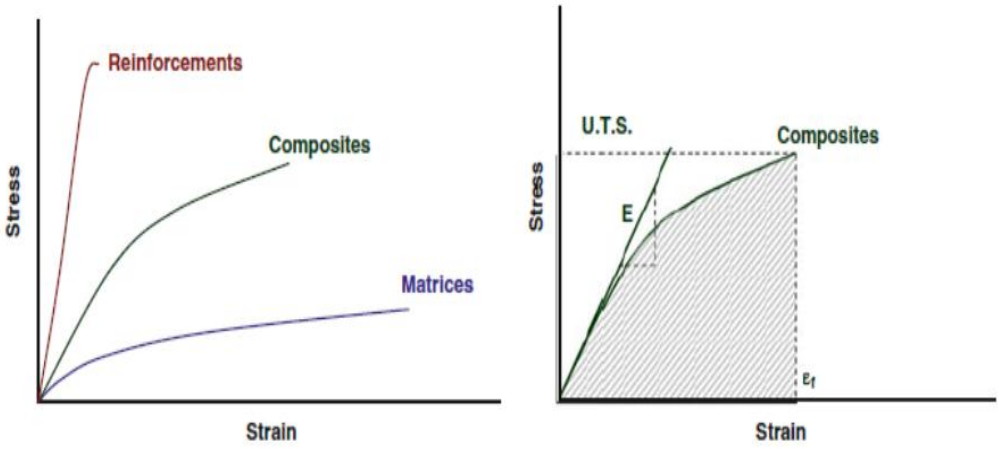

Figure 2.11 The illustration of mechanical properties of reinforcements, matrices, and composites [11]

Some types of natural materials are composite such as wood fibers (cellulose microfibrils in an amorphous matrix of lignin and hemicellulose), bone or teeth (inorganic crystals in a matrix of collagen). Composite can be classified into three types by the types of matrix: 1) Metal matrix composites (MMCs), 2) Ceramic matrix composites (CMCs) and 3) Polymer matrix composites (PMCs). In case of PMCs, thermoset resin and thermoplastic such as unsaturated polyester, phenolic resin, epoxy resin, rubber, PP, PE, PVC, PEO [35-42], etc., are conventionally used as the matrix. Recently, biodegradable polymers or polymers obtained from natural resources e.g. polylactic acid, poly(hydroxybutyrate), poly(hydroxyoctanoate), starch or cellulose

[43-47] have been used as the matrix to achieve the sustainable materials and overcome the environmental problems.

The reinforcements of composites can be classified by their structure as woven, continuous fibers, short fibers, and particles, or judged by the physical size as macroscopic, microscopic and nanoscopic. Conventionally, a macroscopic cloth or microscopic short fibers are used as the reinforcement for composites but the using of nanoscale reinforcement which has at least one dimension in the nanometer range (less than 100 nm), can improve the properties of conventional composites due to its high specific area. Generally, the factors that affect the properties of polymer composites are [11]

- The properties of reinforcement including intrinsic properties, shape and size
- The properties of matrix
- The interfacial interactions at the phase boundaries and the compatibility of matrix and reinforcement
- The dispersion of reinforcements in matrix
- The processing condition

The examples of conventional reinforcements for polymer composites are listed in Table 2.1.

Table 2.1 The examples of conventional reinforcements [11]

Types	d (μm)	L (μm)	Examples
Monofilament (large-diameter single fibers)	100-150	∞	SiC, Boron
Multifilaments (tow or woven rovings with up to 14,000 fibers/strand)	7-30	∞	Carbon, Glass, Aramid fibers
Short fibers (staple fibers aggregated into blankets, tapes, wool, etc.)	1-10	50-5000	Saffil™, Kaowool™, Fiberfax™
Micro-whiskers (fine single crystals in loose aggregates)	0.1-1	5-100	SiC, Al_2O_3
Micro-particulate (powders)	5-20	5-20	SiC, Al_2O_3, B_4C, Microcrystalline Cellulose
Nano-reinforcements (fibers, whiskers, platelets, particles)	0.002-0.1	0.1-2 (fibers and whiskers) <0.1 (particles)	Silicate clays, carbon nanotubes, cellulose nanocrystals

2.3.2 Biocomposite

Over the past few decades, the awakening in the depletion of petroleum resources and the environmental pollution caused by the increasing of plastic wastes has led to the development of biodegradable plastics or sustainable materials to replace the consumption of petroleum-based polymers. Biopolymers or synthetic polymers reinforced with natural fibers, known as biocomposites, have attracted an attention of scientists because of their several advantages compared to the conventional composites [48].

The broad definition of biocomposite is a composite material made from natural/bio fibers and petroleum-based polymer (PE, PP) or biodegradable polymer (PLA, PHA) [49]. Mohanty et al. [50] define biocomposite as a composite material which at least one component is derived from natural resources. The history of natural fibers reinforced plastics started in 1908 with cellulosic fibers reinforced phenolic resin, followed by urea and melamine [49]. Currently, the market of natural fiber reinforced composites is growing. The report of Lucintel, (Global market research firm), on the topic of "Natural Fibre Composites Market Trend and Forecast 2011–2016: Trend, Forecast and Opportunity Analysis" reveals the global natural fiber composites market that reached US $289.3 million in 2015, with compound annual growth rate (CAGR) of 15% higher than 2010 and will reach US $531.3 million in 2016 with the increasing of CAGR up to 11% over the next five years. The trend report is shown in Figure 2.12.

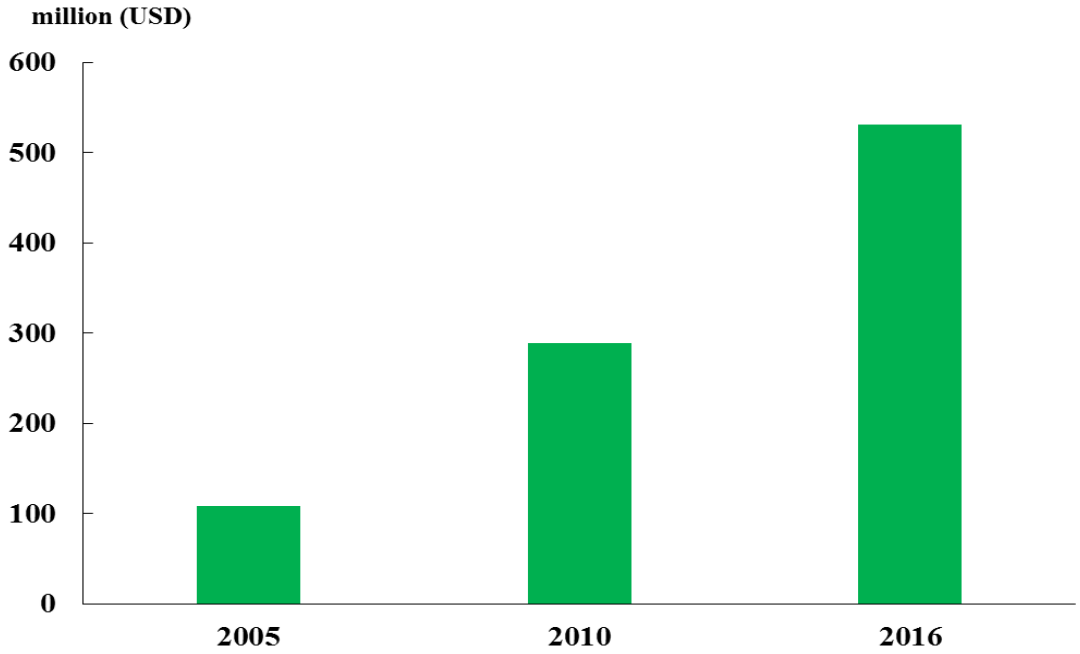

Figure 2.12 Global natural fiber composites market trend and forecast [51]

2.3.3 Cellulose Fiber Reinforcements

As shown in Table 2.2, wood is the major source of cellulosic fibers production especially found in pulp and paper industry, followed by the other plant sources such as bamboo, cotton, jute, kenaf, etc. Biofibers can be considered as the composite of cellulose fibrils which embed in the matrix of lignin and hemicellulose [52]. Figure 2.13 reveals the structure of biofiber. Each fibril has a complex layered structure of one primary wall and three secondary walls. The thick middle layer of the secondary wall, which consists of the helically wound of cellular microfibrils, affects the mechanical properties of the fiber. The microfibrils are made of 30-100 cellulose molecules in extended chain conformation and the diameter of microfibrils is around 10-30 nm [49] The fiber structure, microfibrillar angle, cell dimension, defects and chemical composition are the main factors of fiber properties [53] for example tensile strength and Young's modulus increase with an increasing of cellulose content while the microfibrillar angle affects the stiffness of fibers [49].

Table 2.2 The world production and sources of commercially important fibers [54]

Fiber	Species	World Production (10^3 tons)	Origin
Wood	>10,000 species	1,750,000	Stem
Bamboo	>1,250 species	10,000	Stem
Cotton lint	Gossypium sp	18.450	Fruit
Jute	Corchorus sp	2,300	Stem
Kenaf	Hibiscus cannadbinus	970	Stem
Flax	Linum usitatissimum	830	Stem
Sisal	Agave sisilana	378	Leaf
Hemp	Cannabis sativa	214	Stem
Coir	Cocos nucifera	100	Fruit

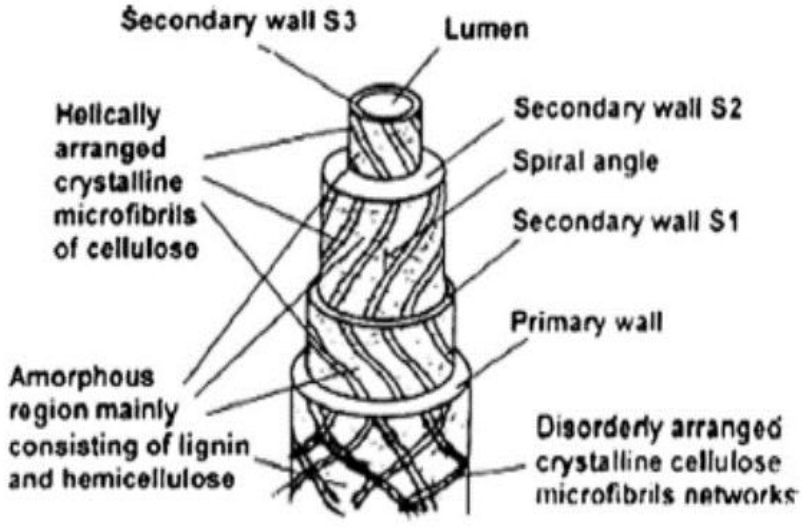

Figure 2.13 The detailed structure of biofiber [49]

The advantages of using cellulosic fiber as the reinforcement are [49]

- Economical production due to the few requirements of equipment
- Low specific weight
- High strength and stiffness
- Safer handling and working conditions compared to synthetic fibers
- Non-abrasion to mixing and molding equipment
- Environmental friendly material
- Renewability
- Consuming less energy for production
- Releasing low CO_2 into atmosphere when they are composted or combusted
- High electrical resistance
- Thermal recycling
- Good insulating properties

However, the major drawback of cellulosic fibers is the hydrophilic nature of cellulose that leads to non-uniform dispersion of fibers in hydrophobic or non-polar polymer matrices. The other drawbacks are the limited processing temperature ($\sim$ 200 $^{\circ}$C), high moisture absorption, resulting in the swelling, occurring of voids at the interface as well as low microbial resistance [11, 49]

2.4 Surface Modification of Cellulose

As mentioned earlier, the drawback of cellulose is the hydrophilic nature resulting in the non-uniform dispersion in non-polar polymer matrices such as PE, PP, PLA, etc. Therefore, several surface modification methods such as acetylation, silanization, application of coupling agents, grafting, corona/plasma discharges and surface derivatization are carried out in order to enhance the hydrophobicity and compatibility with polymer matrix [23, 24].

2.4.1 Acetylation

Acetylation is a type of chemical modification which acetyl groups react with the hydroxyl groups of cellulose, resulting in the more hydrophobic cellulose. Tingaut et al. [55] studied the surface modification of nanofibrillated cellulose (NFC) by adding the acetyl moieties on NFC surface using a large excess of acetic anhydride. The mechanism is presented in Figure 2.14.

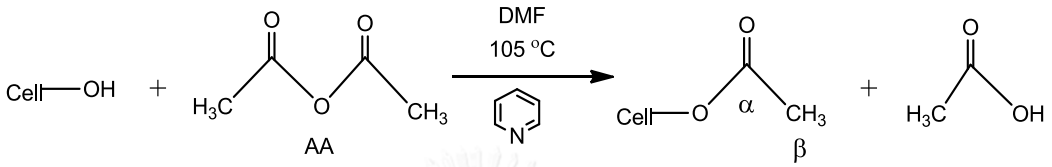

Figure 2.14 Acetylation reaction of nanofibrillated cellulose with acetic anhydride [55]

Bulota et al. [56] synthesized acetylated MFC to use as a toughening agent in polylactic acid. The MFC surface was modified via acetylation reaction with acetic anhydride at 105 °C in toluene for 15 and 30 min. The DS values of 15 and 30 min reaction time were 0.24 and 0.43, respectively. The FT-IR spectra of carbonyl stretching of the acetyl group at the wave number 1740 cm^{-1} was observed. The agglomerations of modified MFC were disappeared in PLA matrix when DS value was 0.43. The DS of MFC played an important role in altering mechanical properties because the dispersion was improved and the aggregation of MFC was impeded with higher DS. At 20 wt% MFC loading, the tensile strength increased up to 60 and 35% for DS of 0.43 and 0.24, respectively.

2.4.2 Silylation

Goussé et al. [57] modified cellulose microfibrils obtained from the homogenization of parenchymal by using isopropyl dimethylchlorosilane. They found that cellulose microfibrils could retain their morphology under mild silylation condition and disperse in an organic solvent without flocculating manner. Anderson et al. [58] also used the same silylation agent to modified MFC. The results indicated that NFC was partially solubilized and lost its nanostructure when silylation conditions were too harsh. The reaction of isopropyl dimethylchlorosilane and cellulose fibers is shown in Figure 2.15.

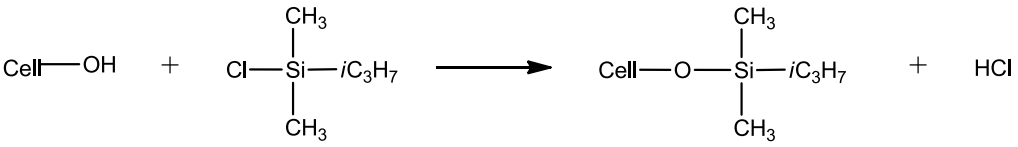

Figure 2.15 Silylation reaction between isopropyldimethylchlorosilane and cellulose fibers [57]

2.4.3 Silanization

Functional trialkoxysilanes, $R'Si(OR)_3$, are widely used as coupling agents to enhance the adhesion between polymer matrix and filler [58-62]. The alkoxy groups (-OR) enable the silane to be anchored to surfaces bearing hydroxyl groups while the organic functionality (R′; amine, methacrylic, vinylic, etc.) helps improve the compatibility, or even copolymerization with the matrix to enhance the interfacial adhesion between two phases [63, 64]. The organosilane surface treatment is carried out with silane water-alcohol solution with a concentration range of 0.5-2% by weight [65]. The water induces the hydrolysis of silane leading to silanol derivative (R'-$Si(OH)_3$) which promotes the silane adsorption onto the surface of cellulose by hydrogen bonding. Consequently, after heat treatment or solvent evaporation, the residual silanol groups may undergo a further condensation with the hydroxyl groups of cellulose substrate or form a polysiloxane network on the surface by self-condensation [66-71]. The reaction mechanism between silanol derivative and the OH-rich substrate is shown in Figure 2.16.

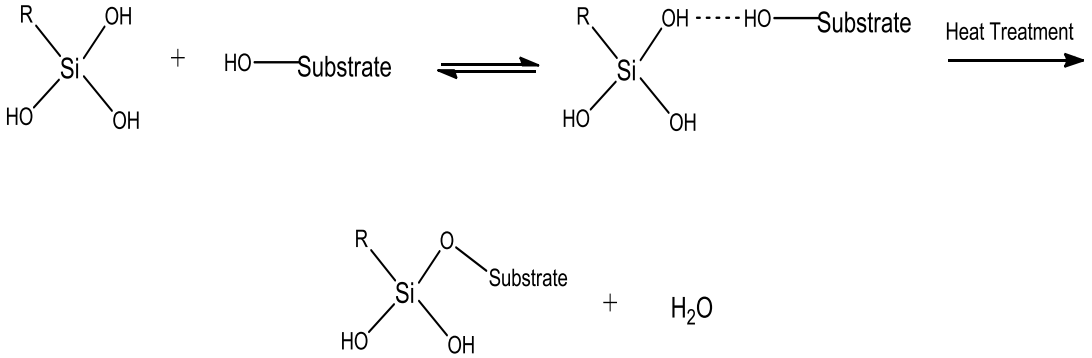

Figure 2.16 Chemical reaction of silanol and hydroxyl substrate [65]

However, in aqueous solution, the condensation of silanol groups can occur with each other or alkoxy groups to form a dimeric and an oligomeric structure as presented in Figure 2.17, leading to gel-like networks which precipitate in the form of colloidal particles.

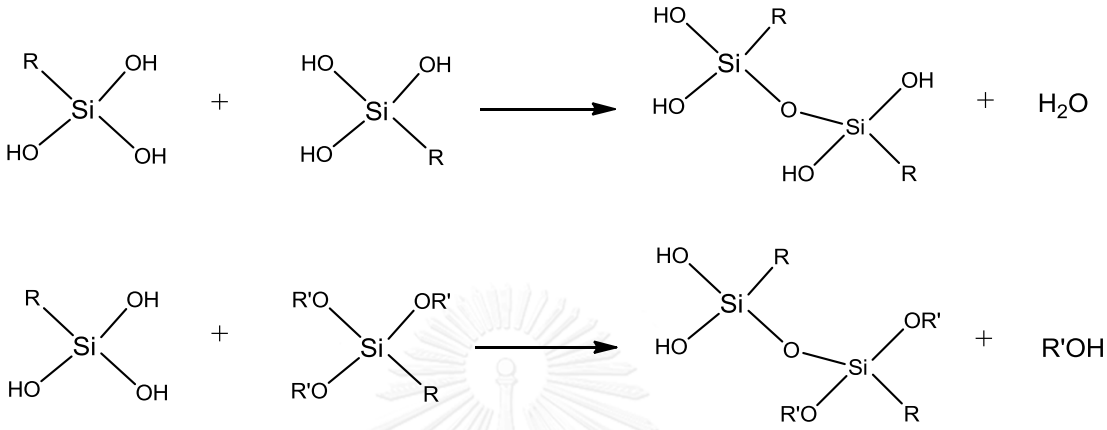

Figure 2.17 The dimeric and the oligomeric structure obtained by the condensation reaction of silanol-silanol groups or silanol-alkoxy groups [65]

Both hydrolysis and condensation reaction of organosilane are affected by the structure of organic parts of silane and the medium composition including temperature, pH, concentration, amount of water and catalyst [68, 69]. An insufficient water leads to an incomplete monolayer on the cellulose surface whereas an excess of water may induce silane polymerization rather than the reaction with cellulose [72]. Valadez-Gonzalez et al. [73] studied the effect of silane concentration. They found that silane binding to henequen fibers was decreased when the silane concentration was higher than 0.01, attributing to the perfect formation of polysiloxanes. Salon et al. [74] found that the acidic media favored hydrolysis reaction and can limit the self-condensation of silanol groups.

Abdelmouleh et al. [75] modified cellulosic fibers surface by using organofunctional silane coupling agents (γ-methacryloxypropyltrimethoxyslane (MPS), γ-aminopropyltriethoxysilane (APS), and γ-mercaptopropyltrimethoxysilane (MRPS)), followed by grafting with the monomer including styrene, methylmethacrylate and epoxy. The amount of silane was added to a 5 wt% of cellulose suspension in an 80/20 v/v ethanol/water mixture by stirring for 2 h. The cellulose fibers were

centrifuged and dried at room temperature for 2 days. Modified fibers were cured at 120 °C under a nitrogen atmosphere for 2 h and then extracted by soxhlet with THF for 24 h and dried. The MPS modified fibers were copolymerized with styrene monomer and methylmethacrylate monomer whereas epoxy was used to graft APS and MRPS modified fibers. The grafting of polymer chains on the silane modified fibers enhanced their hydrophobicity, judged by increasing of contact angle value.

2.4.4 Application of Coupling Agents

Another important technique of cellulose surface functionalization is the using of coupling agents. Lu et al. [76] studied the surface modification of MFC with three different coupling agents: 3-aminopropyltriethoxysilane (APS), 3-glycidoxypropyltrimethoxysilane (GPS) and titanate coupling agent (Lica 38). The modification of cellulose with silane coupling agent involves hydrolysis and condensation reaction of triethoxysilane to form Si-O-C bonds with hydroxyl groups of cellulose at room temperature. Silane was added to MFC acetone suspension and stirred for 24 h. The silane treated MFC was filtered and dried at room temperature for 24 h, followed by heat treatment at 120 °C for 2 h in the air. The mechanism of titanate coupling agent is quite different from silanes. It is proposed to occur via alcoholysis, surface chelation or coordination exchange [77]. The monoalkoxy- and neoalkoxy-type titanium-derived coupling agents react with the hydroxyl groups of cellulose to form a monomolecular layer. Titanate coupling agent or Lica 38 was dissolved in a small amount of acetone and added to MFC acetone suspension. The suspension was stirred for 3 h, filtered and washed several times with acetone and then dried at room temperature for 24 h. The reaction mechanism of titanate coupling agent on the cellulose surface is shown in Figure 2.18. The water contact angle of all samples was measured and the contact angle of untreated, APS treated, GPS treated and titanate treated MFC was 15, 90, 64 and 110°, respectively. The titanate treated

MFC showed the highest contact angle due to the effect of the long alkyl chain of titanate coupling agent.

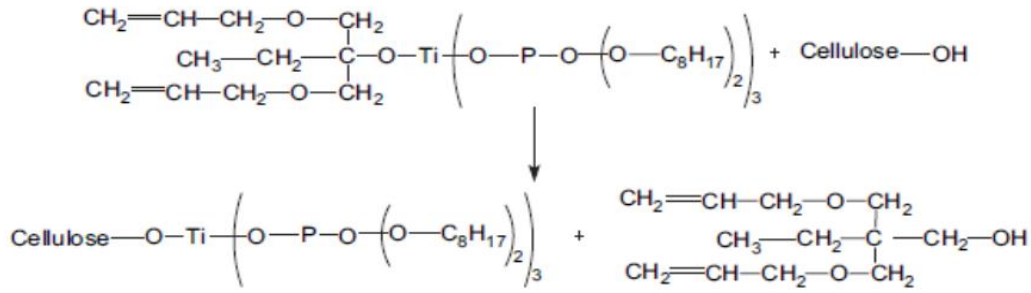

Figure 2.18 The reaction mechanism of titanate coupling agent on cellulose surface [76]

2.4.5 Grafting

Lönnberg et al. [78] grafted microfibrillated cellulose with poly(ε-caprolactone) via ring opening polymerization as illustrated in Figure 2.19. The success of MFC grafted with PCL was confirmed via FTIR analysis. The adsorption peak of carbonyl group of PCL was observed at 1729 cm^{-1}. The change of MFC surface was observed by the dispersion of modified and unmodified MFC in a non-polar solvent (THF) by adding the same amount of modified and unmodified MFC in THF, followed by the sonication for 5 min 3 times in a bath. The result showed the dispersibility of MFC was improved after grafting with PCL.

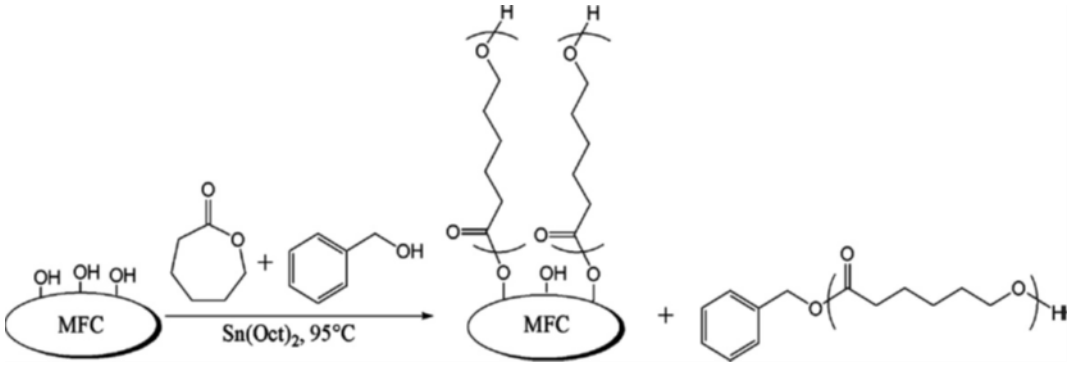

Figure 2.19 Ring-opening polymerization of ε-CL from MFC, using benzyl alcohol as co-initiator [78]

2.4.6 Other Chemical Methods

There are other chemical methods developed by the researchers to enhance the surface hydrophobicity of cellulose such as cationic modification, alkali treatment or synthesis of amino functionalized cellulose [79]. Syverud et al. [80] modified the surface of cellulose nanofibrils by cationic modification using n-hexadecyl trimethyl ammonium bromide (cetyltrimethylammonium bromide, CTAB) as a cationic surfactant. Nakagaito et al. [81] treated the surface of NFC with an alkali solution. The dry sheet of NFC was immersed in NaOH aqueous solution of 5 and 20 wt% concentration and kept at a reduced pressure of 0.01 MPa for 2 h, followed by keeping at ambient pressure for 10 h. They found that the 5 wt% alkali solution treated sheet showed no variations in dimension and remained cellulose I crystalline structure. The synthesis of amino functionalized NFC by click chemistry was studied by Pahimanolis et al. [82] and the reaction is illustrated in Figure 2.20. Firstly, the surface of NFC was reacted with 1-azido-2,3-epoxypropane by etherification under alkaline condition using copper catalyzed azide-alkyne cyclo-addition (CuAAC) as a catalyst.

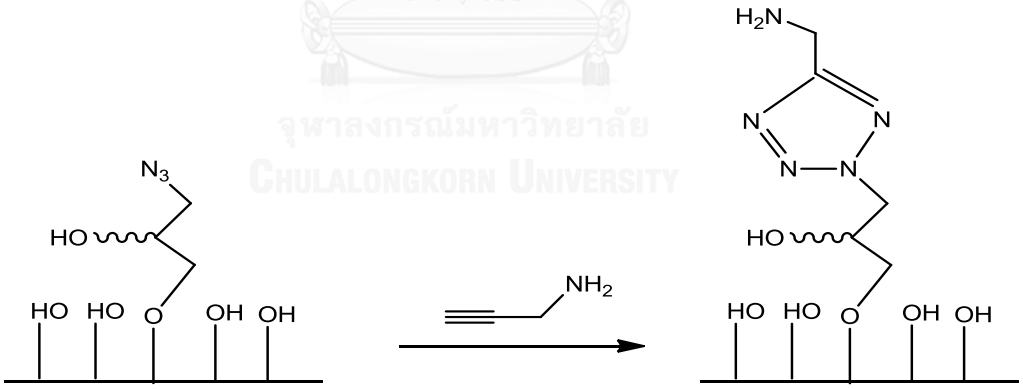

Figure 2.20 Synthesis of Azide functionalized NFC [82]

Figure 2.21 shows the synthesis of amine grafting on oxidized cellulose microfibrils. Lasseuguette [83] prepared oxidized native cellulose with catalytic amounts of radical TEMPO, sodium hypochlorite and sodium bromide in water. Then coupling of amines derivatives was grafted on oxidized cellulose using carbodiimide as catalyst and hydroxysuccinimide as an amidation agent.

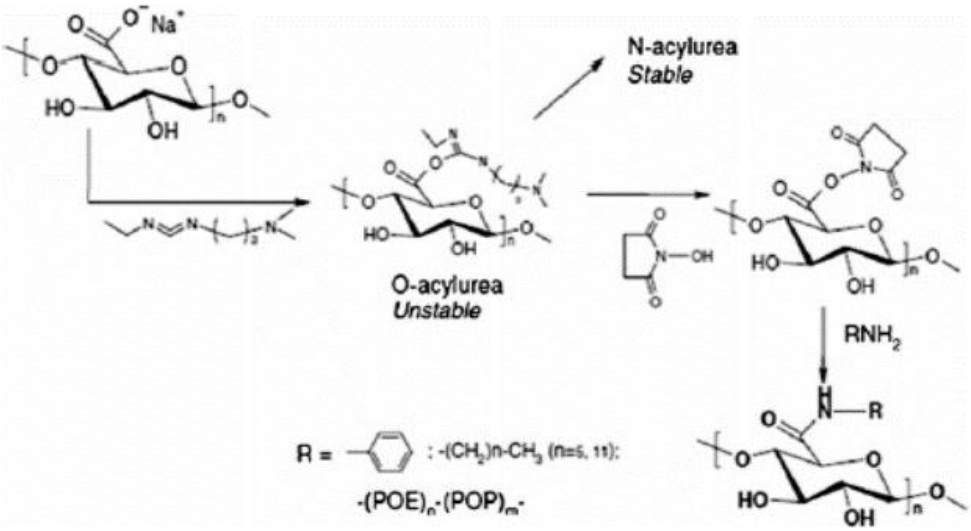

Figure 2.21 Chemical reaction of amine grafting onto oxidized cellulose [83]

2.5 Cellulose/Polymer Composites

2.5.1 Cellulose/Polypropylene Composites

2.5.1.1 Polypropylene

Polypropylene or PP had been discovered since 1954 by Giulio Natta. PP is a petrochemical product from an addition polymerization process using a monomer called propylene. The two-third of propylene monomer is produced to PP as seen in Figure 2.22. Propylene monomer is from three major sources. The largest propylene production comes from the steam cracking process of naphtha. The second source is the refining process of gasoline, followed by the hydrogenation of propane [84]. The polymerization process of PP requires heat, high-energy radiation, and an initiator or a catalyst to combine propylene monomers together. Then, propylene molecules are polymerized into long polymer chains. PP is a vinyl polymer which every carbon atom is attached to a methyl group. The chemical structure of propylene monomer and polypropylene are exhibited in Figure 2.23.

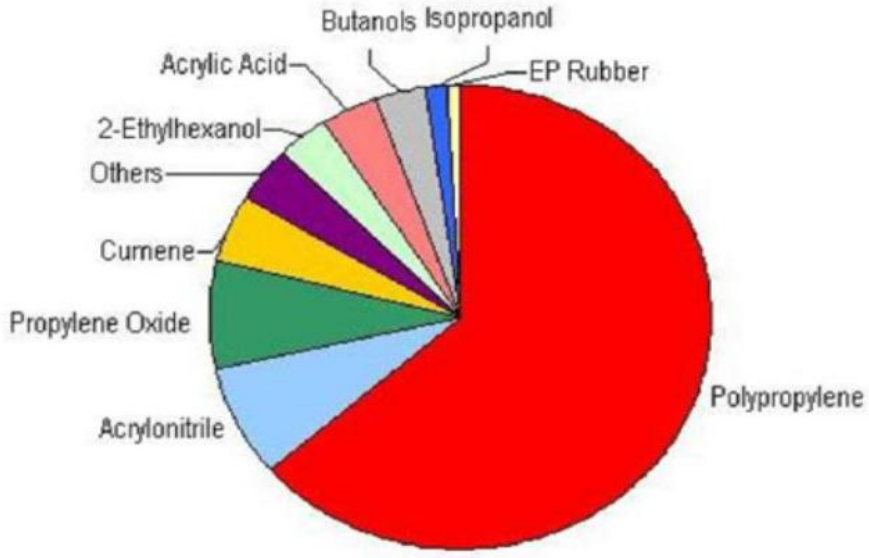

Figure 2.22 The global consumption of propylene monomer [84]

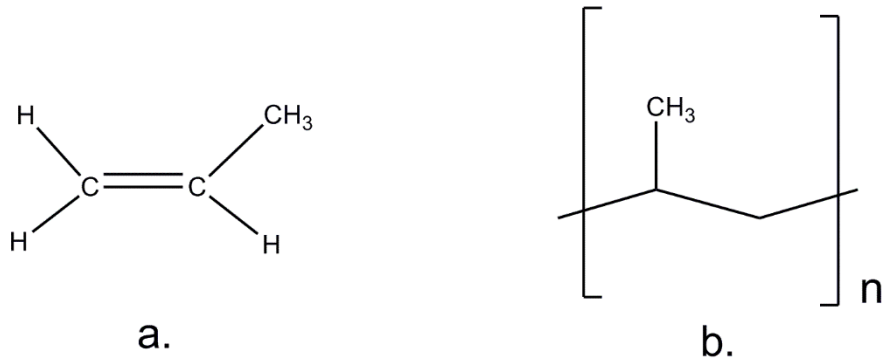

Figure 2.23 Chemical structures of a.) Propylene monomer and b.) Polypropylene

The stereo configuration of PP is classified into three types depending on an arrangement of methyl groups [84]:

1. Isotactic; the methyl groups are on the one side of polymer backbone
2. Syndiotactic; the methyl groups alternate on both side
3. Atactic; the arrangement of methyl groups are random or irregular

The three stereo configurations of PP are presented in Figure 2.24.

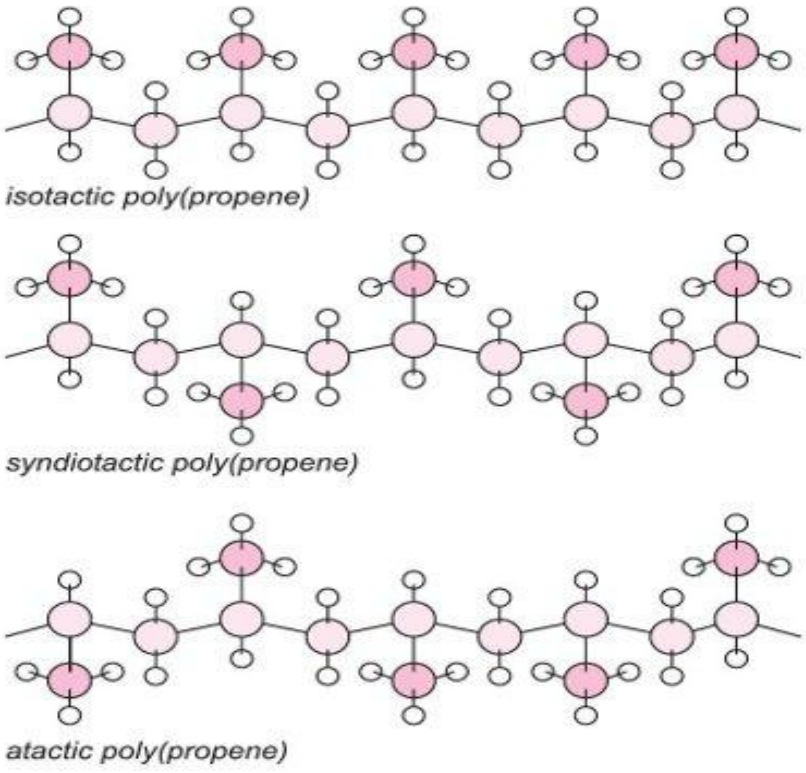

Figure 2.24 The stereo configurations of polypropylene [85]

PP is one of the widely used polymers due to its dominant properties including low density, high melting temperature, good mechanical properties, chemical resistance, good duration, dimension stability, flame resistance, low water absorption and good electrical resistance [84]. Some thermal and mechanical properties of commercial PP are shown in Table 2.3. Moreover, the other advantages of PP are reasonable production cost, easy to mold by conventional methods, and suitable for blending, reinforcing or filling to enhance the properties. Therefore, the cooperation between PP and natural fibers is one of the most promising ways to fabricate natural fibers/synthetic polymer composites [86].

Table 2.3 Thermal and mechanical properties of commercial PP [86]

Properties	**Test Method**	**Homopolymer**		
MFI	a	3.0	0.7	0.2
Tensile stength (MN/m^2)	b	34	30	29
Elongation at break (%)	b	350	115	175
Flexural modulus (MN/m^2)	-	1310	1170	1100
Brittleness temperature (^oC)	I.CI./ASTM D746	+15	0	0
Vicat softening point (^oC)	BS 2782	145-150	148	148
Rockwell hardness	-	95	90	90
Impact strength (Ft.lb)	-	10	25	34

[a]Standard polyethylene grader: load 2.16 kg at 230 ^oC

[b]Straining rate of 18 in/min

2.5.1.2 Literature Reviews of Cellulose/Polypropylene Composites

Panaitescu et al. [87] prepared two types of cellulose/polypropylene composites using microcrystalline cellulose (MCC) and cellulose microfibrils (MF) as a reinforcement. To enhance the compatibility between fillers and matrix, two compatibilizing methods were applied using maleic anhydride modified PP (MA-PP) and a silane-coupling agent. Neat PP showed the two steps of melting behavior as a shoulder at a lower temperature between 159 and 162 °C and a distinct peak at 165.6 °C due to the recrystallization melting mechanism. The addition of MCC without and with MA-PP increased crystallization temperature as well as the degree of crystallinity of PP, indicating that MCC could act as a nucleating agent for PP. The addition of 20 wt% of MF with MA-PP in PP decreased the melting temperature around 5 °C and the shoulder peak was absence that could be explained by the compatibilizing effect of MA-PP. The increasing of crystallization temperature around 10 °C of the composite filled with MF and MA-PP indicating the nucleating effect caused by both MF and MA-PP. The addition of MCC in PP decreased tensile strength due to a weak composite structure induced by the filler and a discontinuous stress transfer whereas the presence of MA-PP could raise the tensile strength of PP indicating the improved interfacial bonding between filler and matrix. The modulus of elasticity of PP was enhanced by MCC and the value was higher when the compatibilizer was added. The similar trends of mechanical properties were observed in case of MF filled PP confirming that the compatibilizer improved the interaction between MF and PP as well as stress transfer. PP composite with 10 wt% silanized MF showed the higher tensile strength and elongation at break when compared to PP composite with untreated MF. However, there was no significant change in mechanical properties of silane treated MCC, corresponding to the poorer interaction between silane coupling agent and MCC.

Ljungberg et al. [88] investigated the properties of isotactic polypropylene nanocomposites reinforced with cellulose whisker extracted from tunicates. Three types of whisker were prepared for using as a reinforcement: AGWH (no surface modification), GRWH (cellulose whisker grafted with maleated polypropylene) and

SUWH (surface coated whisker with phosphoric ester). Nanocomposites films were prepared by solvent casting. The XRD patterns of neat PP and all nanocomposites with three difference fillers showed the characteristic peaks of α-phase. The peaks which corresponded to the β-phase were observed only in SUWH and AGWH/PP nanocomposites. However, the dominant β-peaks were found in AGWH/PP nanocomposites, indicating that the β-phase preferred more hydrophilic of whiskers. The XRD results revealed the ability of cellulose whisker and a presence of surfactant could induce the nucleating effect. The addition of 6 wt% AGHW decreased tensile strength and elongation at break of PP corresponding to the fillers aggregation whereas GRWH/PP nanocomposites showed the higher tensile strength and elongation at break than PP due to the better compatibility and stress-transfer properties. The most improved mechanical properties were observed in SUWH/PP nanocomposites as a result of the surface modification.

Iwamoto et al. [89] studied the mechanical properties of PP composites filled with uncoated-surface microfibrillated cellulose (MFC) and polyoxyethylene nonylphenyl ether (PNE) coated-surface microfibrillated cellulose. The composites were prepared by melt compounding using a twin screw extruder, followed by compression and injection molding. In case of compression molded specimens, the uncoated MFC/PP composites showed the higher Young's modulus than neat PP and other composites as a result of the rigidity of MFC and hydrogen bonding interaction between MFC. When maleic anhydride grafted PP was added, the Young's modulus was slightly decreased but yield strength and strain at break were higher due to the improved interfacial adhesion between PP-MFC and the better MFC dispersion. The addition of PNE-coated MFC enhanced strain at break indicating the good dispersion of filler in matrix while Young's modulus and yield strength were similar with neat PP. Therefore, MAPP was added to improve the adhesive interaction between MFC and matrix, resulting in the increasing of Young's modulus and yield strength. The preparation of composites by injection molding showed the higher Young's modulus and yield strength than neat PP around 45 and 52%, respectively. These values were also higher than compression molding method due to the good alignment of MFC

along the injection direction. However, the strain at break was found lower than neat PP but the composites showed a large plastic deformation as seen in case of compression molded specimens.

Nakatani et al. [90] investigated the effects of maleated polypropylene (MAPP) as a compatibilizer and silanized (3-aminopropyltriethoxysilane, APTES) fibrous cellulose (FC) on the morphology and tensile properties of syndiotactic polypropylene (SPP) composites. An SEM micrograph of fracture surface of SPP filled with 30% of FC exhibited many aggregations of FC. When compared to neat SPP, the Young's modulus of FC/SPP composites was higher while tensile strength and elongation at break were lower due to the poor interfacial adhesion between SPP and FC. The addition of MAPP could improve the interface between filler and matrix resulting in the higher Young's modulus and tensile strength than FC/SPP composites up to 20 and 70%, respectively. The better interfacial adhesion was evidenced by many rodlike FCs which were attached to SPP matrix. The SEM micrograph and EDS analysis of silanized FC/SPP composites showed the detecting of Si atoms and partial adhesion between FC and SPP confirming that FC was extensively covered by APTES. The Young's modulus of silanized FC/SPP composites was higher than FC/PP and FC/SPP/MAPP composites whereas tensile strength was lower than FC/SPP/MAPP composites and similar to FC/SPP composites, corresponding to the good dispersion of filler but poor interfacial adhesion.

Cheng et al. [91] worked on the study of morphology and tensile properties of polypropylene composites reinforced with cellulose fibril aggregates which were isolated from Lyocell fiber. The composites of PP fibers and cellulose fibril aggregates was obtained from the compression molding. The tensile test results revealed the higher tensile strength and modulus than neat PP. The tensile modulus was increased up to 93% and 130% by adding 10% and 20% cellulose fibril, respectively. The SEM micrograph of fracture surface of composites showed the good dispersion of fibril aggregates in PP. However, some holes in PP and some gaps between fibers and PP matrix were observed indicating the non-perfect adhesion between filler and matrix.

2.5.2 Cellulose/Polylactic acid Composites

2.5.2.1 Polylactic acid

Polylactic acid or PLA is a biodegradable and compostable thermoplastic derived from natural renewable resources such as starch and sugarcane [92]. It belongs to the family of aliphatic polyesters, which are made from α-hydroxy acids [93]. According to the biodegradability, PLA is considered as a solution of plastic wastes disposal problem [93, 94]. The degradation time of PLA is approximate to six months to two years compared to 50 to 1000 years of conventional polymers such as polyethylene (PE) or polystyrene (PS) [95]. Due to the low toxicity and being eco-friendly, PLA is an ideal material for food packaging products and other consumer products [96].

The basic building block of PLA is a lactic acid which made by the fermentation of sugar from natural resources e.g. sugarcane [92, 93]. Lactic acid (2-hydroxypropiniic acid), CH_3-CHOHCOOH, is a simple chiral molecule which can exist in two enantiomers of L- or D-lactic acid as seen in Figure 2.25 [92, 93]. These enantiomers are different in their optical activity to polarized light. The optically inactive D, L or meso form is an equimolar or racemic mixture of D(-) and L(+) isomers [97]. Due to the two isomers of lactic acid, polylactic acid refers to the family of polymers including pure poly-L-lactic acid (PLLA), pure poly-D-lactic acid (PDLA) and poly-D,L-lactic acid (PDLLA) [98] when the L-isomer is the main fraction of PLA produced from renewable resources. PLA can crystallize into three forms of α, β and γ, depending on the composition of L and D,L-enantiomers [92].

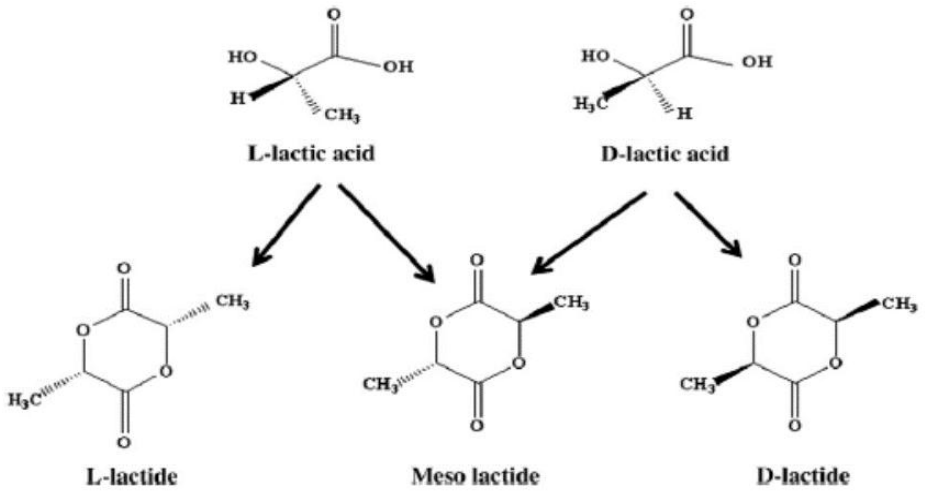

Figure 2.25 The steroforms of lactides [99]

PLA was first discovered in 1932 by Carothers. He heated lactic acid under vacuum and obtained a low molecular weight PLA. Later on, Du Pont succeeded in synthesis and patent of a high molecular weight polymer in 1954. PLA can be produced by several polymerization processes from lactic acid including azeotropic dehydrative condensation, direct condensation polymerization, and polymerization through lactide formation as shown in Figure 2.26. Currently, the high molecular weight PLA is most synthesized by ring opening polymerization [92, 93].

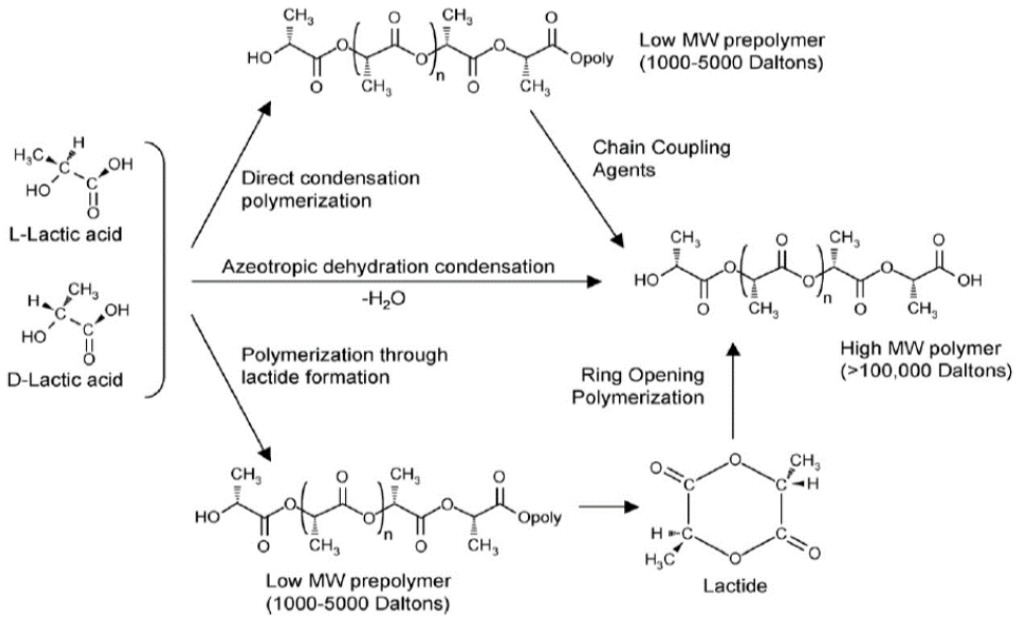

Figure 2.26 Synthesis methods of PLA from L- and D-lactic acids [92]

Commercially, PLA is a copolymer of poly(L-lactic acid) and poly(D, L-lactic acid), which are made of L-lactide and D, L-lactide monomers [94]. PLA with the L-content higher than 90% tends to be crystalline whereas the lower optical purity is amorphous. The decreasing of L-isomer content leads to the decreasing of glass transition temperature (T_g) and melting temperature (T_m) [94]. Therefore, the properties of PLA depend on the component isomers, processing temperature, annealing time and molecular weight [99]. The physical properties of PLA such as density, heat capacity, and mechanical properties depend on the transitions temperatures [100]. The crystallinity of PLLA is around 73% with the glass transition temperature and melting temperature ranging from 50-80 °C and 173-178 °C, respectively [99]. Due to the stereoregular chain structure, the optically pure polylactide, then PLLA and PDLA are semicrystalline. The density of amorphous and crystalline PLLA is 1.248 g/cm^3 and 1.290 g/cm^3, respectively [94]. Generally, PLA products can be dissolved in dioxane, acetonitrile, chloroform, methylene chloride, 1, 1, 2-trichloroethane and dichloroacetic acid but partially dissolved in cold ethyl benzene, toluene, acetone, and tetrahydrofuran when it is heated to boiling temperature [101]. Glass transition temperature, melting temperature, density, and solubility of lactic acid polymers are presented in Table 2.4.

Table 2.4 Some properties of polylactic acid [101]

Lactic acid polymer	T_g (°C)	T_m (°C)	Density (g/cm^3)	Good solubility in solvents
PLLA	55-80	173-178	1.29	Chloroform, furan, dioxane and dioxolane
PDLLA	43-53	120-170	1.25	PLLA solvents and acetone
PDLA	40-50	120-150	1.248	Ethyl lactate, tetrahydrofuran, ethyl acetate, dimethylsulfoxide, N, N xylene and dimethylformamide

Compared to the petroleum-based polymers, PLA has reasonably good optical, physical, barrier and mechanical properties [102]. The permeability coefficient of CO_2, O_2, and H_2O of PLA is higher than poly(ethylene terephthalate) (PET) but lower than polystyrene (PS) [103-105]. However, the barrier properties of PLA on organic permeants such as ethyl acetate or D-limonene are similar to PET [106]. An unoriented PLA has good strength and stiffness but brittle while an oriented PLA has better performances than oriented PS but approximate to PET [104]. Young's modulus and the flexural modulus of PLA are higher than HDPE, PP, and PS but the Izod impact strength and elongation at break are lower [107]. PLA can be degraded by hydrolysis reaction after several months under the moisture environment. The degradation consists of two stages including the random non-enzymatic chain scission of the ester groups which leads to the reducing of molecular weight, then the molecular weight is reduced until the lactic acid and the low molecular weight oligomers are metabolized by microorganisms to obtain carbon dioxide and water [101]. PLA is easily processed by melt processing using injection molding, thermoforming or melt extrusion [93]. The examples of PLA applications are disposable cutleries, bottles, containers, cups, extruded cast, oriented films, melt spun fibers, textiles and carpets [96, 108, 109]. Moreover, it can be used as a housing of laptop computer [109-112]. Nowadays, to obtain the superior performances, PLA is fabricated to composite materials using nanoclays, biofibers, glassfibers or cellulose as the reinforcement [92].

2.5.2.2 Literature Reviews of Cellulose/Polylactic acid Composites

Polylactic acid or PLA is a biopolymer which derived from 100% renewable resources (e.g. corn, wood residues, agricultural crops or other biomass) and has approximate properties to petroleum-based polymers. However, some drawbacks of PLA such as brittleness, low thermal stability, insufficient gas and vapor barrier and relatively high price limit the field of its applications [24]. Therefore, several approaches have been studied to improve PLA properties for example polymer blend, copolymerization, and composite or nanocomposite preparation.

Cellulose fibers reinforced PLA composites or nanocomposites have attracted the attentions of both research and industries to replace the using of man-made fibers or inorganic fillers such as glass fibers, aramid fibers, talcum powder or clay [113-115] due to the several advantages of cellulose such as renewability, high strength and modulus, low density, high specific area, biodegradability, non-abrasion as well as low cost [91]. Moreover, the fully bio-based composites are obtained. Therefore, much research of cellulose reinforced PLA has been increased and reported during the past few decades.

Suryanegara et al. [116] studied the thermo-mechanical properties of MFC reinforced PLA. A compound of MFC/PLA with a fiber content of 10 wt% was prepared by solvent casting, followed by crushing into small pieces and then pressed into sheets at 180 °C in three steps: preheating for 5 min, pressed at 0.5 MPa for 5 min and pressed at 1 MPa for 5 min. The molten samples were quenched in liquid N_2 to obtain the fully amorphous sheets. Then, the samples were annealed at 80 °C with varied time to study the effect on the degree of crystallinity. The DSC and DMA results indicated that the partially crystallized composites (X_c ~ 17%) was obtained by using the annealing time around one-seventh of that required for fully crystallized PLA (X_c ~ 41%) but the storage modulus of the composite was higher than the fully crystallized PLA. Therefore, it could be concluded that MFC could enhance the mechanical properties and induce the faster crystallization time of PLA. This effect was important to reduce the fabrication time of PLA parts.

Lu et al. [117] investigated the effect of different scales cellulose fibers on the mechanical properties and crystallization of PLA by using bamboo cellulosic fiber (BCF), microcrystalline cellulose (MCC) and bacterial cellulose (BC) as the reinforcement. It was found that all types of cellulosic fibers could increase the stiffness of PLA but MCC reinforced PLA exhibited the greatest stiffness due to the rough surface and large surface area. The Young's modulus and impact strength of MFC/PLA composites were increased by 44% and 59%, respectively whereas the decrease in tensile strength was found in BCF and BC composites due to the poor adhesion and poor dispersion in PLA. The DSC results indicated that the crystallization of PLA could be improved by the three types of cellulosic fibers. However, the smallest grain size and the highest crystallinity could be found in case of BC due to its smallest size.

Petersson et al. [118] studied the thermal stability and the dynamic mechanical properties of cellulose nanowhisker (CNW) reinforced PLA. A *tert*-butanol treated CNW and a surfactant treated CNW were synthesized. Then 5 wt% of treated CNW was incorporated into PLA by solution casting technique. The TGA analysis indicated that the thermal stability of PLA and both PLA composites were stable in the same region of 25-220 $^{\circ}$C. The DMA results showed that both treated CNW could improve the storage modulus of PLA in the plastic zone and the shift of tan δ peak by 20 $^{\circ}$C was found in case of *tert*-butanol treated CNW/PLA nanocomposite. The TEM micrograph confirmed the better dispersion of both treated fillers in PLA matrix.

Jonoobi et al. [119] investigated the tensile properties and the dynamic mechanical properties of cellulose nanofiber (CNF) reinforced PLA. The nanocomposites with the filler content of 1, 3 and 5 wt% were prepared by the dilution of a masterbatch using a twin screw extruder. The tensile properties showed an increase in strength and modulus when filler content was higher, corresponding to the good interaction between PLA and CNF. Contradictory, the decreasing of maximum strain was found due to the increasing of filler content. However, the large standard deviation indicated the non-homogeneous distribution of fillers. The results from dynamic mechanical analysis revealed the enhancement of storage modulus and tan δ peak of PLA when filler content was increased indicating the entanglement of

CNF as well as the physical interaction between filler and matrix. In addition, the study of CNF/PLA nanocomposites transparency exhibited white spots of CNF aggregations at 5 wt% filler loading.

In 2012, Jonoobi et al. [120] studied the effect of unmodified and acetylated modified cellulose nanofibers on the thermal stability, tensile properties and dynamic mechanical properties of PLA. The TG thermograms showed the starting degradation of modified and unmodified nanofibers at 240 and 266 $^{\circ}$C, respectively while the main degradation step of modified and unmodified nanofibers was found at 330 and 350 $^{\circ}$C. The decrease in thermal stability of acetylated nanofiber could be explained by the decreasing of the crystallinity when the hydroxyl groups were substituted by the acetyl groups, resulting in the partially crystalline structures of nanofibers. Both nanocomposites exhibited the improved tensile strength and modulus when compared to neat PLA while the maximum strain was found lower than neat PLA. However, the acetylated cellulose nanofibers had no significant effects on tensile properties compared to non-acetylated cellulose nanofibers. This results might be attributed to the poorer interaction between particle-particle due to the increasing of surface hydrophobicity. In case of dynamic mechanical properties, the addition of acetylated and non-acetylated cellulose nanofibers at 5 wt% showed the improved storage modulus of neat PLA at 70 $^{\circ}$C around 2800 and 2400%, respectively. Both acetylated and non-acetylated CNF increased the tan δ peak of PLA to the higher temperature up to 7 $^{\circ}$C, approximately. Obviously, the modification of CNF did not show the significant improvement in the dynamic mechanical properties as well as the tensile properties

Pei et al. [121] modified cellulose nanocrystals through partial silylation reaction using n-dodecyldimethylchlorosilane as a modifying agent to obtain silylated cellulose nanocrystals (SCNC). SCNC was used as a nucleating agent and reinforcement for poly(L-lactide) (PLLA). Nanocomposites films of PLLA filled with CNC and SCNC were prepared via solution casting. The DSC results revealed the similar melting temperature of neat PLLA and nanocomposites. The increase in the degree of crystallinity of PLLA from 14.3% to 30.4% was found in 1 wt% SCNC/PLLA

nanocomposite while CNC/PLLA nanocomposites showed the similar degree of crystallinity as PLLA, indicating the capability of SCNC as the nucleating agent. The crystallization peak of SCNC/PLLA nanocomposites was found at a higher temperature with high intensity when compared to neat PLLA confirming the nucleation effect of SCNC which related to the better dispersion of modified cellulose nanocrystals in PLLA. The addition of 1 wt% SCNC in PLLA increased tensile modulus and tensile strength up to 27% and 21%, respectively whereas the addition of CNC did not improve tensile modulus and tensile strength. However, the elongation at break was decreased in both nanocomposites due to the substantial local stress concentration and failure strain caused by the stiff reinforcement of CNC.

Raquez et al. [122] studied the effect of the difference functional trialkoxysilanes modified cellulose nanowhiskers (CNWs) on the thermal properties and the thermomechanical properties of PLA. The DSC thermogram of neat PLA showed the glass transition at 60 °C but the melting temperature was not clear indicating the high amorphous of PLA. In case of organosilane modified CNWs/PLA nanocomposites, the two melting peaks were observed around 150 and 157 °C together with a cold crystallization temperature which was lower than 130 °C, corresponding to the increasing of nucleus density originated by the nucleation effect of modified CNWs as well as the good dispersion in PLA matrix. The dynamic mechanical thermal analysis (DMTA) measurement exhibited the increasing of the storage modulus of PLA at 25 °C from 1300 MPa to 4200 MPa when 3 wt% of modified CNW was added. However, the type of silanization agents did not affect the storage modulus except amino-based CNWs due to an aminolysis reaction during the preparation of nanocomposites via the extrusion process.

Frone et al. [123] investigated the properties of difference cellulose fiber reinforced PLA composites using acid hydrolyzed microcrystalline crystalline cellulose (HMCC) and cellulose microfibrils (MF) obtained from the mechanical disintegration of regenerated wood fibers as a reinforcing filler. The surface of both cellulose fibers was treated by 3-aminopropyltriethoxysilane (APS) via silanization reaction. PLA composites with 2.5% of treated and untreated HMCC and MF were prepared via a two-roll mill,

followed by the compression molding to obtain composite sheets. The fracture surface morphology of silane treated cellulose/PLA composites showed the better fibers distribution when compared to untreated cellulose/PLA composites. Both treated and untreated cellulose fibers could enhance the storage modulus of PLA in the glassy state due to the decreasing of polymer chains mobility. HMCC composites showed the higher storage modulus than MF composites, corresponding to its high aspect ratio which led to the better stress transfer between filler and matrix. The silanization of cellulose fibers enhanced the storage modulus of PLA, attributing to the stronger fiber-matrix interfacial adhesion.

2.6 Dissolution of Cellulose

To destroy the strong hydrogen bonds between cellulose molecules, the dissolution of cellulose has been investigated and normally found in the fiber spinning and related processes [4]. Many solvent systems have been created to dissolve cellulose such as aqueous inorganic complexes (e.g. cuoxam, cuam, cuen), aqueous bases (e.g. 10% NaOH), mineral acids, melts of inorganic salt hydrates, N, N-dimethyl-acetamide/LiCl, dimethylsulfoxide/triethylamine/SO_2, NH_3/NH_4SCN, CF_3COOH, HCOOH and N,N-dimethylformamide/N_2O_4 [4, 124]. However, these solvent systems are restricted only in the laboratory use due to volatility, toxicity, and high cost [125]. Consequently, the aqueous NaOH systems including NaOH/urea and NaOH/thiourea solution has been recently developed for cotton linter and other natural cellulose materials. The advantages of the aqueous NaOH systems are simple, less toxicity and inexpensive [126-128]. Cellulose could be dissolved completely in the pre-cooled solvent of 7 wt% NaOH/12 wt% urea system on a typical laboratory scale and a large scale. The regenerated cellulose materials and functional materials with excellent properties have been prepared from this solvent system. Furthermore, NaOH/urea system is a suitable medium for the homogeneous reaction of cellulose etherification that cellulose ethers such as methylcellulose and hydroxyethyl cellulose have been successfully synthesized under mild conditions [128].

Qi et al. [129] studied the influence of temperature on the dissolution of cellulose in NaOH/urea solution. Cellulose from cotton linter pulp was dissolved in 7

wt% NaOH/12 wt% urea aqueous solution at different temperature (60, 25, 0, -6, -10 and -12.6 °C) for 2 minutes and the dissolution state of each cellulose solution was captured by an optical microscope. The results indicated that cellulose was dissolved completely at -12.6°C and became a transparent solution.

In 2009, Qi et al. [128] succeeded in dissolving two kinds of cellulose samples (Avicel and cotton linter) in the solution of NaOH, urea and distilled water (7:12:81 by weight) for the completely homogeneous carboxymethylation reaction of cellulose. The cellulose solution was stirred to obtain a slurry mixture and then kept in a refrigerator to pre-cool at -12.5°C. The mixture was brought to stir at ambient temperature until the solution became transparent. Therefore, the aqueous solution of 7 wt% NaOH/12 wt% urea has been proved as the powerful solvent for cellulose.

Cai et al. [130] studied the rapid dissolution of cellulose in NaOH/urea solution at different times. Cellulose from cotton pulps was dissolved in a pre-cooled solution of 7 wt% NaOH/12 wt% urea at -10°C for 5, 10, 30 and 60 s. The optical microscope images showed the dissolution of cellulose that occurred rapidly and the solubility was increased depending on the increasing of the dissolution time from 5 to 60 s.

CHAPTER III
METHODOLOGY

3.1 Materials

All materials and chemicals used in this research are shown Table 3.1

Table 3.1 Materials and sources

Material	Grade	Source
Cotton fabric waste	-	Local textile producer
Sodium Hydroxide Pellet (NaOH)	Analytical Grade	Ajax Finechem, Pty., Ltd
Urea	Analytical Grade	Ajax Finechem, Pty., Ltd
Hydrochloric acid (HCl), 37%	Analytical Grade	QRëc
Hexadecyltrimethoxysilane (HDTMS/Dynasylan 9116)	Analytical Grade	Evonik
Glacial acetic acid (CH_3COOH)	Analytical Grade	VWR
Nonylphenolethoxylate EO15 (EO15/TERGINOLTM)	Analytical Grade	Dow Chemical Co., Ltd
Disperse BYK 2008	Analytical Grade	BYK Asia Pacific Pte. Ltd.
Soybean oil	Analytical Grade	Siam Chemical Industry, Co., Ltd.
Maleic anhydride	Analytical Grade	Fluka
Dicumyl peroxide, 98%	Analytical Grade	Sigma Aldrich
Aryphosphite (Alkanox 246)	Analytical Grade	Songnok Company
Acetone	Commercial Grade	Local supplier

Material	Grade	Source
Methanol	Commercial Grade	Local supplier
Potassium permanganate	Commercial Grade	Local supplier
Sulfuric acid, 98%	Analytical Grade	QRëc
Orthophosphoric acid, 85%	Analytical Grade	Sigma Aldrich
Tapioca starch	Food Grade	Local supplier
Polypropylene (PP) flakes	HP561R	HMC Polymers
Polylactic acid (PLA) pellets	2003D	Naturework®

3.2 Equipment and Instruments

All instruments in this research are shown in the list

1. Centrifuge machine, TD5M-WS, Senova, China
2. Scanning electron microscope, JSM 6460 LV, Joel, Japan
3. Transmission electron microscope, TECNAI T20 G2, FEI, Netherlands
4. Fourier transform spectrometer, Nicolet 6700, Thermo Electron Corporation
5. Particle size analyzer, Brookhaven Instruments Corp., USA
6. Polarized optical microscope (CX31), Olympus, Japan
7. Polarized optical microscope (DMR), Leica, Germany equipped with a hotstage of Mettler Toledo, USA
8. Thermogravimetric analyzer (TGA/STDA851), Mettler Toledo, USA
9. Differential scanning calorimeter (DSC1), Mettler Toledo, USA
10. X-ray diffractometer (D8 Advance), Bruker, Germany
11. Universal testing machine (LR100K), LLOYD, Germany)
12. Impact testing machine (GT-7045-MD, GOTECH, Taiwan)

13. Twin screw extruder (LTE-26-44), Labtech Scientific, Labtech Engineering, Thailand
14. Cutting machine, Labtech Scientific, Labtech Engineering, Thailand
15. Hopper dryer, SHINI Plastic Technologies
16. Injection molding machine, NEX80, Nissei, USA
17. Hotplate
18. Overhead stirrer
19. Hot air oven
20. Homogenizer
21. 100 mesh sieve

3.3 Microcrystalline Cellulose Preparation

Microcrystalline cellulose (MCC) was obtained by the acid hydrolysis of cotton fabric, following the method of Usarat et al. [131]. The cotton fabric was cut into small sizes of 2 cm x 2 cm, approximately. Then, the fabrics were heated in 2.5 N HCl solution at 60 °C for 2 h with continuous stirring using an overhead stirrer. The amorphous regions of cellulose were removed by hydrolysis reaction leaving highly crystalline cellulose. At the end of the reaction, MCC dispersion was filtered and washed with distilled water until the pH became neutral to obtain MCC powder. The powder was dried in an oven at 60 °C.

3.4 Cellulose Fibril Preparation

A 5 %w/v of MCC solution was prepared by adding the MCC powder from section 3.3 into a cooled NaOH/urea/distilled water solution (7:12:81 by weight) at -5 °C with continuous stirring until MCC particles were completely dissolved and the solution became transparent. A 5 %w/v of starch solution was prepared in parallel, tapioca starch was dissolved in water, then a 5 %w/v NaOH solution was dropped to gelatinize starch until a transparent gel-like solution was obtained. The obtained starch solution was mixed with MCC solution, the mixed solution was stirred until

homogeneous. The MCC/starch solution was precipitated in a 1.0 M HCl and left for 6 h to hydrolyze starch. In acidic media, cellulose fibrils (CF) colloid was formed and stabilized by the starch gel which acts the anti-coagulating agent. The leaving cellulose fibrils dispersion was filtered and washed with distilled water to remove HCl until the pH was approximately 5. Then, the solvent exchange of CF was carried out using methanol.

3.5 Surface Modification of Cellulose Fibril

3.5.1 Synthesis of Soybean Oil Modified Cellulose Fibril (Oil-g-CF)

Malenized soybean oil was synthesized via the reaction between soybean oil and maleic anhydride using dicumyl peroxide as an initiator, following the method of Kiangkitiwan and Srikulkit [132]. Firstly, 20 g of maleic anhydride (20 wt% of soybean oil) was added into a 500 ml Erlenmeyer flask containing 100 g of soybean oil, followed by 1 g of dicumyl peroxide (5 wt% of maleic anhydride). The mixture was stirred and heated to 170 $^{\circ}$C and retained at this temperature for 3 h. Finally, the viscous yellowish liquid of malenized soybean oil was obtained and then left at ambient temperature overnight to precipitate unreacted maleic anhydride. Afterward, the malenized soybean oil modified cellulose fibril was synthesized, following the method of Thanomchat and Srikulkit [133]. The 40 g of malenized soybean oil was decanted to another container of 200 g (10 g on dry weight) of acetone-extracted cellulose fibrils gel. A 200 ml of dry acetone was added to reduce the viscosity of modified oil. The mixture of cellulose fibrils and modified oil was stirred for 2 h and then cured at 120 $^{\circ}$C in the oven. The excessive malenized soybean oil was washed with acetone, resulting in soybean oil modified cellulose fibrils (Oil-g-CF). Oil-g-CF was ground and screened by a 100 mesh sieve. The tentative structure of Oil-g-CF is shown in Figure 3.1.

3.5.2 Synthesis of Organosilane Modified Cellulose Fibril (Silane-g-CF)

According to the method of Thanomchat and Srikulkit [133], a 200 g of wet CF (equivalent to 10 g of dry CF) was dispersed into 200 ml of water and stirred by an overhead stirrer. In parallel, a mix solution between 20 ml of 10 %w/v EO15 solution

and 5 ml of 2.5 %w/v DISPERBYK2008 was prepared using a homogenizer to obtain a milky solution. The solution was poured slowly into CF dispersion. A homogeneous CF mixture was carried out by the homogenizer. Then, 25 g of hexadecyltrimethoxysilane (HDTMS, $C_{19}H_{42}O_3Si$) was added into CF mixture with the weight ratio of CF: HDTMS as 1:2.5 and stirred for 30 min. A 60 ml of methanol was added to the mixture and continuously stirred for 30 min, followed by an addition of HCl drop by drop until pH was approximately 2 and the mixture became more viscous. The viscous mixture was poured into a tray and left at the ambient temperature until dry, then Silane-g-CF was obtained. Silane-g-CF was frozen in a refrigerator overnight to extract the excess of water. Then, it was washed with distilled water until pH reached to 5, followed by freezing overnight once again. Later on, the frozen Silane-g-CF was defrosted at ambient temperature and dried in an oven at 60 °C. Finally, Silane-g-CF was ground and screened through the 100 mesh sieve. The tentative structure of Silane-g-CF is shown in figure 3.1 also.

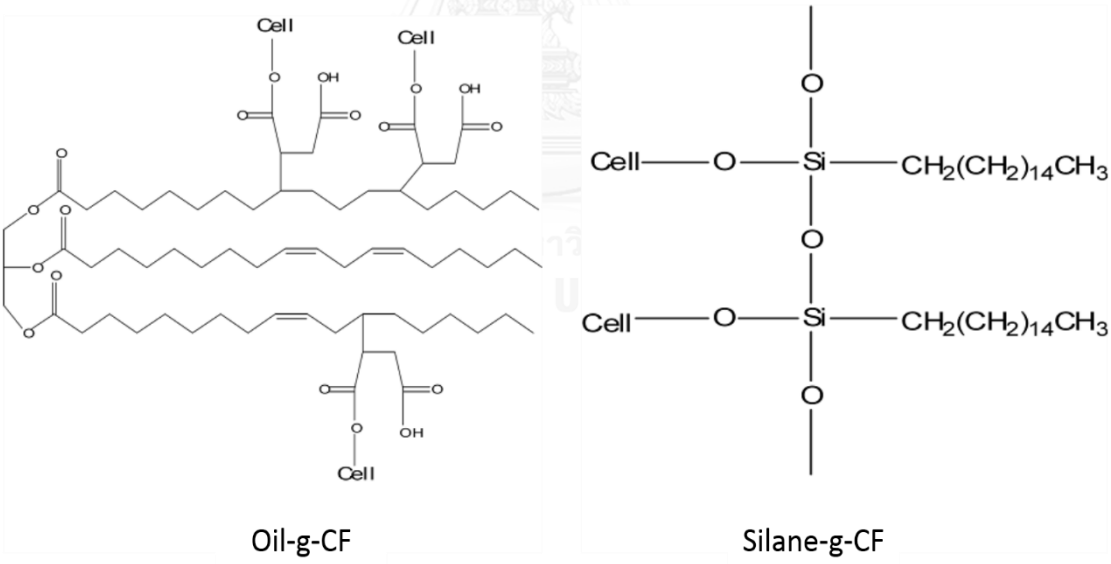

Figure 3.1 Chemical structure of Oil-g-CF and Silane-g-CF [133]

3.6 Preparation of Oil-g-CF/PP Composite and Silane-g-CF/PP Composite by Simple Melt Mixing

To study the properties of the different reinforcing fillers, both Oil-g-CF filled PP composite and Silane-g-CF filled PP composite were prepared by a simple melt mixing on a hotplate. Modified CF powder to PP weight ratio of 1:24 (4 wt% modified CF/PP composite) was chosen. Firstly, the PP flakes were physically mixed with modified CF and then placed between polyimide films. The compound was heated to 210 °C for 2 min and flatted to obtain a thin film. The thin film was removed from the hotplate to cool down, then folded and molten again for 4 times, resulting in the modified CF/PP composite film with an approximate thickness of 25 μm.

3.7 Preparation of Silane-g-CF/Polymer Composites via Melt Extrusion Process

3.7.1 Silane-g-CF/Polypropylene Composites

A 1 kg of 20 wt% Silane-g-CF/PP masterbatch was prepared by melt extrusion. The sample preparation steps were carried out as follows: 10 g of arylphosphite (heat stabilizer) was dissolved in 100 ml of toluene, followed by an addition of Silane-g-CF (200 g). Then, 800 g of PP flakes were added into Silane-g-CF dispersion. The mixture was mechanically mixed and then left standing to allow Silane-g-CF precipitate onto PP surface during toluene evaporation in a fume hood. When toluene was completely evaporated, modified CF coated PP flakes were obtained. The sample was put in an oven at 60 °C for 24 h prior to melt extrusion. The masterbatch was prepared using a twin-screw extruder (LTE-26-44, Labtech Scientific, Labtech Engineering, Thailand) with a screw diameter of 26 mm and L/D (length/diameter) of 44. The temperature profile from feed zone to die zone was set as 170/180/180/190/190/200/200/200/205/205/205 °C, respectively using the screw speed of 30 rpm. The extruded Silane-g-CF/PP masterbatch was cooled in a water bath and then cut into pellets by a cutting machine (Labtech Scientific, Labtech Engineering, Thailand). The masterbatch was dried in a hopper dryer (SHINI Plastic Technologies) at 80 °C.

The PP composites with the Silane-g-CF content of 0.5, 1.0, 3.0 and 5.0 wt% were prepared by mixing the calculated amount of masterbatch with virgin PP flakes. 1.0 wt% of heat stabilizer was added and physically mixed. The compound was fed into the same twin-screw extruder. The extrusion was conducted using the same condition as the masterbatch preparation.

The test specimens of PP composites for tensile test and impact resistance test were prepared via an injection molding machine (NEX80, Nissei, USA). The temperature profile from feed zone to nozzle was set as 30/190/190/195/195/210 °C, respectively. The tensile specimen is type I model, according to ASTM D638. The specimens for the impact test were molded into the required dimension, following ASTM D256.

3.7.2 Silane-g-CF/Polylactic acid Composites

A 1 kg of 20 wt% Silane-g-CF/PLA masterbatch was prepared by the melt extrusion process, following the steps of Silane-g-CF/PP composites in the section 3.7.1. The masterbatch was prepared using the same twin-screw extruder with the screw diameter of 26 mm and L/D of 44. The temperature profile from feed zone to die zone was set as 140/150/160/170/170/175/175/175/180/180/180 °C, respectively and the screw speed was set at 30 rpm. The extruded masterbatch was cooled in a water bath and then cut into pellets by the cutting machine. The masterbatch was dried in the hopper dryer at 60 °C.

The PLA composites with the Silane-g-CF content of 0.5, 1.0, 3.0 and 5.0 wt% were prepared by mixing the calculated amount of masterbatch with virgin PLA pellets. 1.0 wt% of heat stabilizer was added and physically mixed. The compound was fed to the same twin-screw extruder. The extrusion was carried out using the same condition as the masterbatch preparation.

The test specimens of PLA composites for tensile test and impact test were also prepared via the same injection molding machine as Silane-g-CF/PP composites. The temperature profile from feed zone to nozzle was set as 30/190/190/190/190/200 °C, respectively. The tensile specimen is type I model, according to ASTM D638. The

specimens for impact resistance testing were molded to the dimension, following ASTM D256

Figure 3.2 Twin Screw Extruder (LTE-26-44, Labtech Scientific)

Figure 3.3 Cutting Machine (Labtech Scientific)

Figure 3.4 Hopper Dryer (SHINI Plastic Technologies)

Figure 3.5 Injection molding machine (NEX80, Nissei, USA)

3.8 Characterizations

3.8.1 Virgin Cellulose Fibril and Modified Cellulose Fibril Properties

3.8.1.1 Water Retention Value (WRV)

To identify the water content held in virgin CF, the water retention value was measured. A certain amount of CF was dispersed in deionized water in a centrifuge tube for 24 h at ambient temperature, followed by centrifugation at 30 Hz for 20 min using a centrifuge machine (TD5M-WS, Senova, China). Then, the sample was dried at 105 °C for 24 h. The WRV value was calculated following the equation:

$$WRV = \frac{W_w - W_d}{W_d} \times 100$$

Where W_w is the weight of wet sample and W_d is the weight of dried sample [134].

3.8.1.2 Morphology

A field emission scanning electron microscope (FE-SEM, Hitachi S-4800, Japan) with a conducting layer of carbon (thickness: ca. 5 nm) was used to investigate the morphology of virgin CF. A transmission electron microscope (TEM, TECNAI T20 G2, FEI, Netherlands) was employed to confirm the web-like morphology of CF. A drop of 10 µl of re-dispersed CF in water was added onto a carbon-coated electron microscopy grid and the excess water was absorbed by a filter paper. The sample was negatively stained with 2% of uranyl acetate. In case of modified CF, the morphology was

investigated by a scanning electron microscope (JSM 6460 LV, JeOl, Japan) with an acceleration voltage of 15 kV. The sample was coated with gold to prevent the electrical discharge prior to characterization.

Figure 3.6 Field emission scanning electron microscope (FE-SEM, Hitachi S-4800)

Figure 3.7 Transmission electron microscope (TEM, TECNAI T20 G2, FEI)

Figure 3.8 Scanning electron microscope (JSM 6460 LV, JeOl)

3.8.1.3 Functional Groups

The functional groups of virgin CF and modified CF were analyzed by a Fourier transform infrared spectrometer (Nicolet 6700, Thermo Electron Corporation) using a transmission mode and KBr disk sample.

Figure 3.9 FT-IR spectrometer (Nicolet 6700, Thermo Electron Corporation)

3.8.1.4 Particle Size Distribution

The particle size distribution of virgin CF and modified CF was measured by dynamic light scattering technique using a particle size analyzer (Brookhaven Instrument Corp., USA). Virgin CF was dispersed in water and dropped into a quartz cuvette before measurement whereas toluene was used as a medium for modified CF.

Figure 3.10 Particle size analyzer (Brookhaven Instrument Corp.)

3.8.1.5 Crystal Morphology

An X-ray diffractometer (D8 Advance, Bruker, Germany) was employed to investigate the crystallinity of virgin CF and modified CF using a Cu Kα target at 40 kV and the diffraction angle ranging from 5-40°.

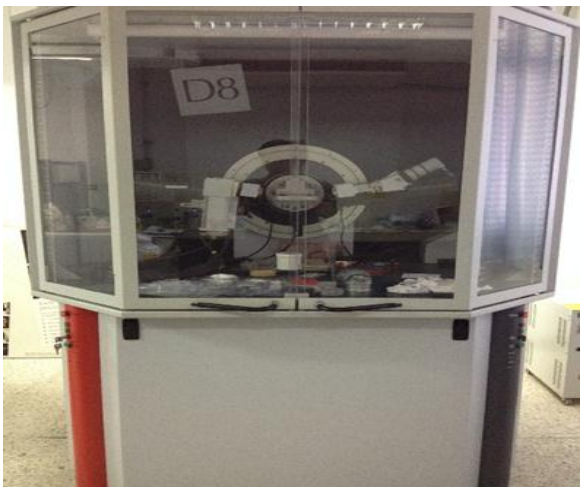

Figure 3.11 X-ray diffractometer (D8 Advance, Bruker)

3.8.2 Effect of Oil-g-CF and Silane-g-CF on Polypropylene Properties

3.8.2.1 Dispersibility of Modified CF in PP

The dispersion of modified CF in the hydrophobic polymer was studied using a polarized optical microscope (CX31, Olympus, Japan) under a transmittance light. The composite films from section 3.6 were put on a glass slide and covered by a coverslip before investigation.

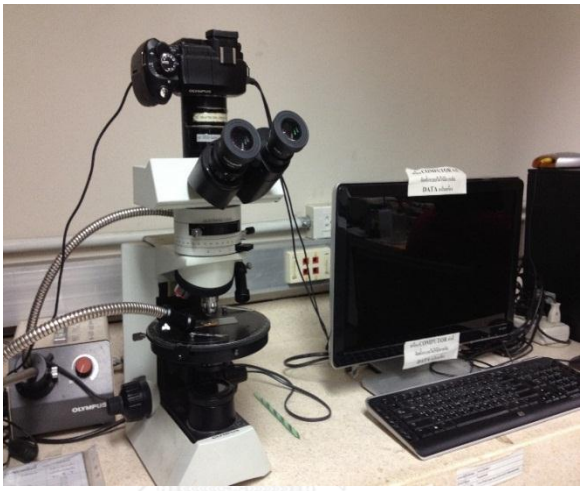

Figure 3.12 Polarized optical microscope (CX31, Olympus)

3.8.2.2 Crystalline Morphology by Etching

Neat PP, Oil-g-CF, and Silane-g-CF/PP films were chemically etched in an etchant solution. The etchant solution containing 1% of potassium permanganate in a solution of 10:4:1 (v/v) of 98% sulfuric acid, 85% orthophosphoric acid, and distilled water was prepared following the method of Olley and Bassett [135] to remove the amorphous part of the sample. The crystalline structure, size and number were analyzed by SEM.

3.8.2.3 Nonisothermal Crystallization Behavior

The effect of modified CF on the crystallization behavior of PP was investigated by a polarized optical microscope (DMR, Leica, Germany) equipped with a hotstage (Mettler Toledo, USA) using a cross-polarized mode under nonisothermal condition. Firstly, the composite film was placed between the glass slide and the coverslip in the hotstage. The sample was heated from 30 to 210 °C with a heating rate of 20 °C/min

and held for 5 min to remove the thermal history. Then, the sample was cooled from 210 to 30 °C with the cooling rate of 10 °C/min. The crystallization behavior during cooling was recorded by a digital camera in every 10 seconds.

Figure 3.13 Polarized optical microscope (DMR, Leica)

Figure 3.14 Hotstage (Mettler Toledo)

3.8.2.4 Thermal Stability

The thermal stability of virgin CF, Oil-g-MFC, Silane-g-CF, neat PP film and composite films were characterized by a thermogravimetric analyzer (TGA/STDA851, Mettler Toledo, USA). About 5.0 mg of sample was heated from 50 to 600 °C at a heating rate of 10 °C /min under nitrogen atmosphere with a gas flow rate of 20 ml/min.

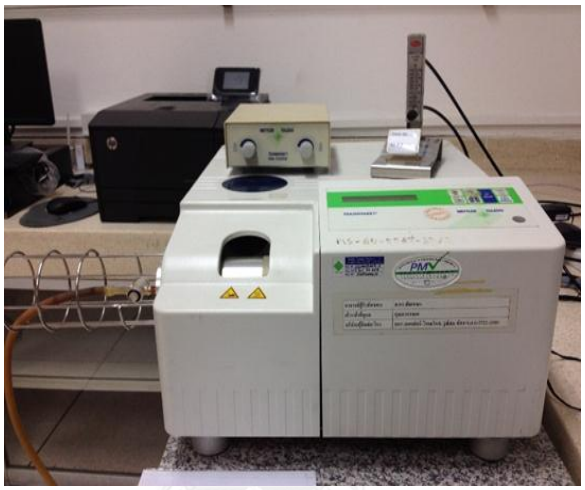

Figure 3.15 Thermogravimetric analyzer (TGA/STDA851, Mettler Toledo)

3.8.2.5 Thermal Properties

The thermal properties were analyzed using a DSC1 (Mettler Toledo, USA). About 1.0-2.0 mg of sample was characterized within the temperature range of 0-220 °C at a heating rate of 10 °C/min under nitrogen atmosphere with the gas flow rate of 50 ml/min. The sample was held at 220 °C for 3 min to remove the previous thermal history before cooling down. Then, the sample was cooled down to 0 °C at a cooling rate of 10 °C/min. The sample was tested by 4 scans of 1st heating, 1st cooling, 2nd heating and 2nd cooling using the same heating and cooling rate. The thermal properties of composites including melting temperature (T_m), crystallization temperature (T_c) and enthalpy (ΔH) were considered from the second heating and second cooling scan. The degree of crystallinity (X_c) was calculated as follows:

$$X_c = \frac{\Delta H_m}{\Delta H_m^{\circ} * f} \times 100$$

Where f is the weight fraction of PP in composite, ΔH_m is the enthalpy of melting (J/g) and ΔH°_m (the enthalpy of melting for 100% crystalline PP) is taken as 209.0 J/g [136]

Figure 3.16 Differential scanning calorimeter (DSC1, Mettler Toledo)

3.8.3 Properties of Organosilane Modified Cellulose Fibril/Polypropylene Composites

3.8.3.1 Thermal Stability

The thermal stability of PP composites with various content of Silane-g-CF was investigated by TGA. About 5-10 mg of the composite pellet was heated from 50 to 600 °C at a heating rate of 10 °C/min under N_2 atmosphere with the gas flow rate of 20 ml/min.

3.8.3.2 Thermal Properties

The thermal properties of neat PP and PP composites were characterized by DSC. The approximate 5 mg of sample was studied under a non-isothermal condition with the temperature ranging from 0-220 °C. The sample was tested by 4 scans of 1st heating, 1st cooling, 2nd heating and 2nd cooling, respectively at the heating and cooling rate of 10 °C/min. The sample was held at 220 °C for 3 min to remove the previous thermal history. The experiment was performed under nitrogen atmosphere with the gas flow rate of 50 ml/min. The thermal properties of composites such as melting

temperature (T_m), crystallization temperature (T_c) and enthalpy (ΔH) were determined from the second heating and the second cooling scan. The degree of crystallinity (X_c) was calculated using the equation in section 3.8.2.5.

3.8.3.3 Fracture Surface Morphology

The cryo-fractured morphologies of neat PP and CF/PP composites were investigated by SEM at the accelerating voltage of 15 kV. The fractured specimens were prepared by breaking the dumbbell-shaped samples which were immersed in liquid nitrogen. The surface of sample was coated with gold to prevent the electrical discharge.

3.8.3.4 Crystal Morphology

The crystal morphology of neat PP and CF/PP composites was characterized by the X-ray diffractometer using the Cu Kα target at 40 kV and the diffraction angle ranging from 5-40°.

3.8.3.5 Mechanical Properties

3.8.3.5.1 Tensile Properties

The tensile properties of neat PP and composites were determined by a universal testing machine (LLOYD, LR100K, UK), according to ASTM D638. The average sample dimension was 165.0 mm long, 12.85 mm wide and 3.20 mm thick. The sample with the distance between grips of 115 mm was tested under a load cell of 10 KN and a crosshead speed of 50 mm/min.

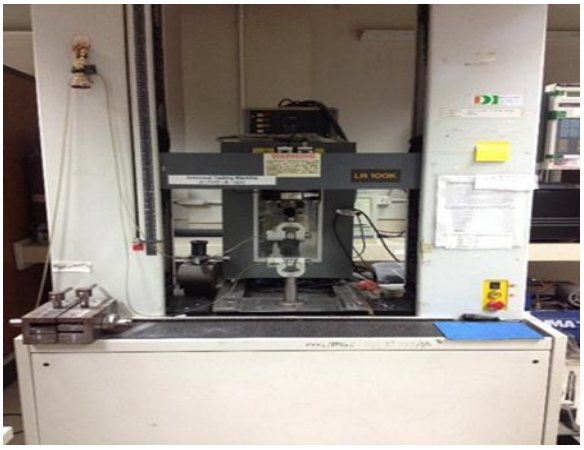

Figure 3.17 Universal testing machine (LLOYD, LR100K)

3.8.3.5.2 Impact Resistance

The impact resistance was measured according to ASTM D256 using an impact testing machine (GT-7045-MD, GOTECH, Taiwan) with a 1.00 J hammer. The notched samples were prepared before testing. The average dimension of the specimen was 3.30 mm wide, 8.50 mm depth under notch and 6.00 mm long. The impact resistance (KJ/m^2) was obtained by dividing the breaking energy with the cross-sectional area (width x depth under notch).

Figure 3.18 Impact testing machine (GT-7045-MD, GOTECH)

3.8.4 Properties of Organosilane Modified Cellulose Fibril/Polylactic acid Composites

3.8.4.1 Thermal Stability

The effect of Silane-g-CF on the thermal stability of PLA was characterized by TGA. About 5-10 mg of the composite pellet was heated from 50 to 600 °C at the heating rate of 10 °C/min. The experiment was performed under nitrogen atmosphere with the gas flow rate of 20 ml/min.

3.8.4.2 Thermal Properties

The DSC was employed to study the thermal properties of Silane-g-CF/PLA composites. The approximate 5 mg of sample was studied under the non-isothermal condition with the temperature ranging from 25-200 °C under nitrogen atmosphere

with the gas flow rate of 50 ml/min. The experiment was done by 4 scans of 1st heating, 1st cooling, 2nd heating, and 2nd cooling using the heating and cooling rate of 5 °C/min. The sample was held at 200 °C for 3 min to eliminate the thermal history before cooling down. The thermal properties including glass transition temperature (T_g), cold crystallization temperature (T_{cc}), melting temperature (T_m) and enthalpy (ΔH) were studied using the data from the second heating scan. The degree of crystallinity (X_c) was calculated following the equation:

$$X_c = \frac{\Delta H_m - \Delta H_{cc}}{\Delta H^{\circ}_{m} * f} \times 100$$

Where f is the weight fraction of PLA in composite, ΔH_m is the enthalpy of melting, ΔH_{cc} is the enthalpy of crystallization during heating scan (cold crystallization) and ΔH°_{m} is the enthalpy of melting of 100% crystalline PLA taken as 93.0 J/g [137]

Moreover, the effect of slow cooling rate on the thermal properties of composites was also investigated using the heating rate of 10 °C/min and the cooling rate of 1 °C/min.

3.8.4.3 Fracture Surface Morphology

The cryo-fractured surface morphologies of neat PLA and PLA composites were investigated by SEM using the accelerating voltage of 15 kV. The dumbbell-shaped sample was quenched in the liquid nitrogen and then broken. The fractured surface was coated with gold to prevent the electrical discharge.

3.8.4.4 Crystal Morphology

The crystal morphology of neat PLA and PLA composites was characterized by the X-ray diffractometer using the Cu Kα target at 40 kV and the diffraction angle ranging from 5-40°.

3.8.4.5 Mechanical Properties

3.8.4.5.1 Tensile Properties

The tensile properties of neat PLA and PLA composites were characterized by the universal testing machine following ASTM D638. The average sample dimension

was 165.0 mm long, 12.85 mm wide and 3.20 mm thick. The sample with the distance between grips of 115 mm was tested under the load cell of 10 KN and the crosshead speed of 5 mm/min.

3.8.4.5.2 Impact Resistance

The impact resistance was measured according to ASTM D256 using the impact testing machine with the 1.00 J hammer. The samples were notched before testing. The average dimension of the specimen was 3.30 mm wide, 8.50 mm depth under notch and 6.00 mm long. The impact resistance (KJ/m^2) was obtained by dividing the breaking energy with the cross-sectional area (width x depth under notch).

CHAPTER IV
RESULTS AND DISCUSSION

4.1 Properties of Virgin Cellulose Fibril and Modified Cellulose Fibril

4.1.1 Water Retention Value (WRV) of Virgin Cellulose Fibril

Water retention value (WRV) was measured to investigate the degree of homogenization or microfibrillation of cellulosic materials, corresponding to fibril or microfibril surface and volumetric phenomena [138]. As shown in Figure 4.1, water retention value of microcrystalline cellulose (MCC), regenerated MCC and cellulose fibril (CF) are 222%, 1740%, and 2022%, respectively. The increasing of WRV arises from the increasing of fibrils surface area due to the small size of cellulose fibrils [91]. Therefore, the result indicates that the size of CF is smallest, followed by regenerated MCC and MCC, respectively. The smallest size of CF is achieved from the anti-coagulation effect of starch which acts as a dispersing agent and prevents the agglomeration of cellulose fibrils during the precipitation step, resulting in the significantly high WRV when compared to regenerated MCC and MCC. The larger surface area of CF leads to the plentiful portions of the free hydroxyl groups which can form hydrogen bonds with water [139], resulting in the cellulose gel form which is not observed in case of regenerated MCC as shown in Figure 4.2.

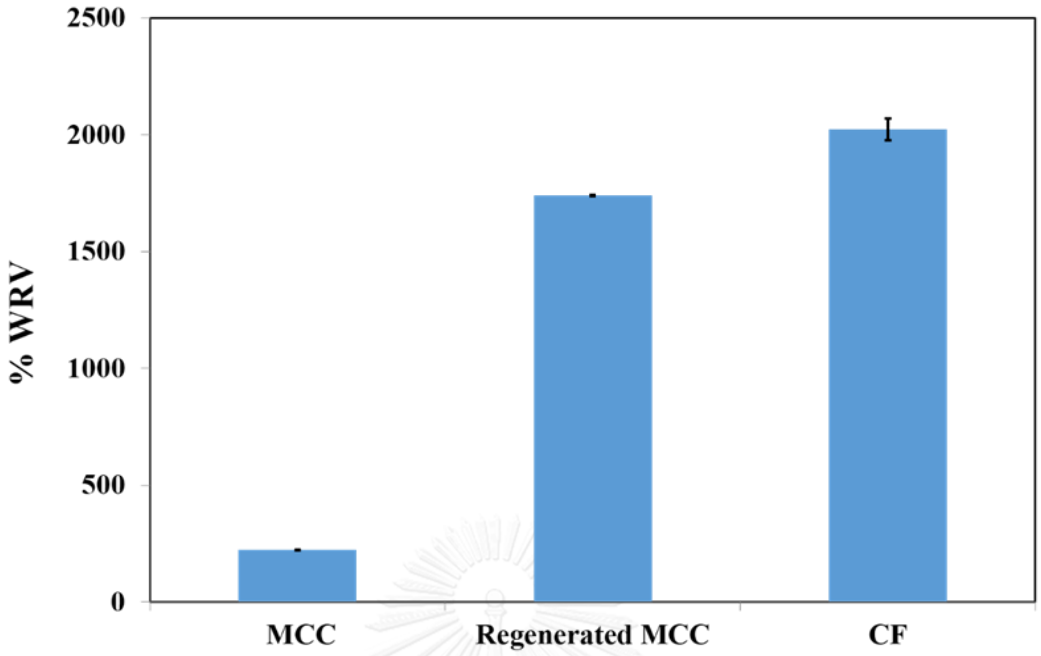

Figure 4.1 Water retention value (%) of MCC, regenerated MCC and cellulose fibril (CF)

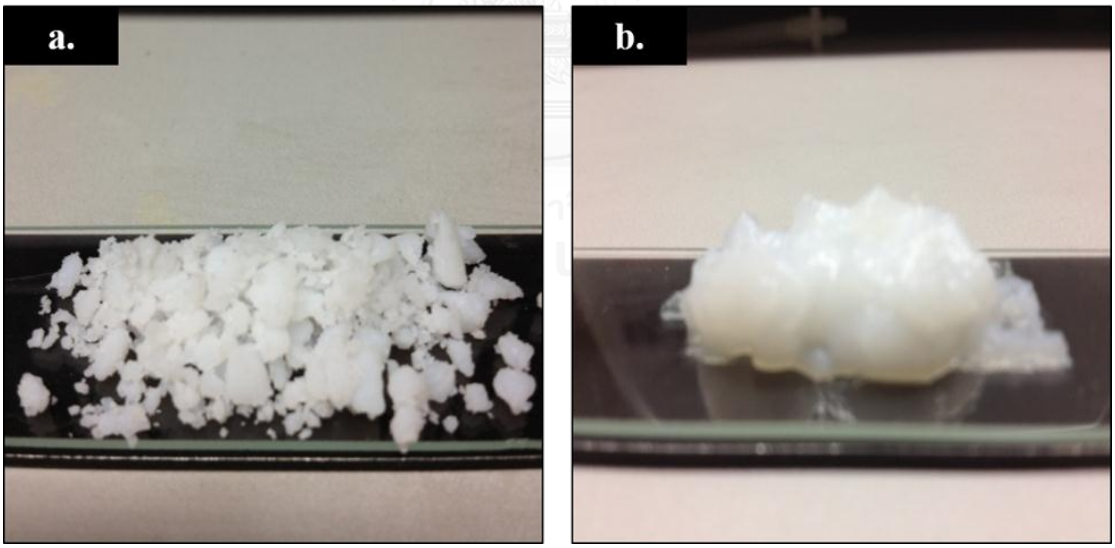

Figure 4.2 Physical appearance of a.) regenerated MCC and b.) cellulose fibril

4.1.2 Morphology of Cellulose Fibril and Modified Cellulose Fibril

The morphology of CF was investigated by FE-SEM and TEM. The micrographs are shown in Figure 4.3 (a.) and (b.). The web-like morphology of CF is obtained from the anti-coagulation effect of starch which helps to prevent the agglomeration of cellulose fibrils during the precipitation step in the HCl solution, resulting in the tiny cellulose fibrils with high surface area. The diameter of CF is found in the range of 10-40 nm and the length is more than 500 nm. It is noticed that some fibrils agglomeration can be observed [140].

However, the morphological images of soybean oil modified cellulose fibril (Oil-g-CF) and organosilane modified cellulose fibril (Silane-g-CF) are totally different from the unmodified CF. As shown in Figure 4.4 (a.), Oil-g-CF exhibits the large agglomerate due to the surface hydrophobicity characteristic. In a similar manner, the morphology of Silane-g-CF also shows the form of agglomerate particles. Interestingly, the both types of modified CF particles exhibit the loosely packing of the particles agglomeration, evidenced by the high swelling in nonpolar solvents such as toluene whereas the virgin CF stayed intact in toluene indicating the harder aggregation characteristic which results from cellulose hydrophilicity. Therefore, the modification of CF using the malenized soybean oil and the organosilane were expected to enhance the dispersion and compatibility of CF in a hydrophobic polymer matrix such as polypropylene and polylactic acid when it was compounded by melt extrusion [133].

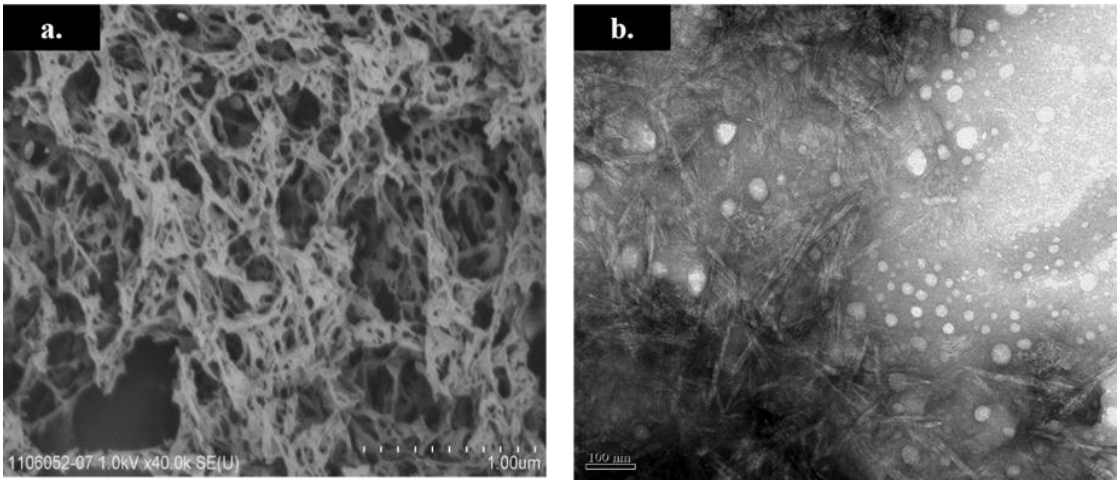

Figure 4.3 a.) FE-SEM and b.) TEM micrographs of cellulose fibril

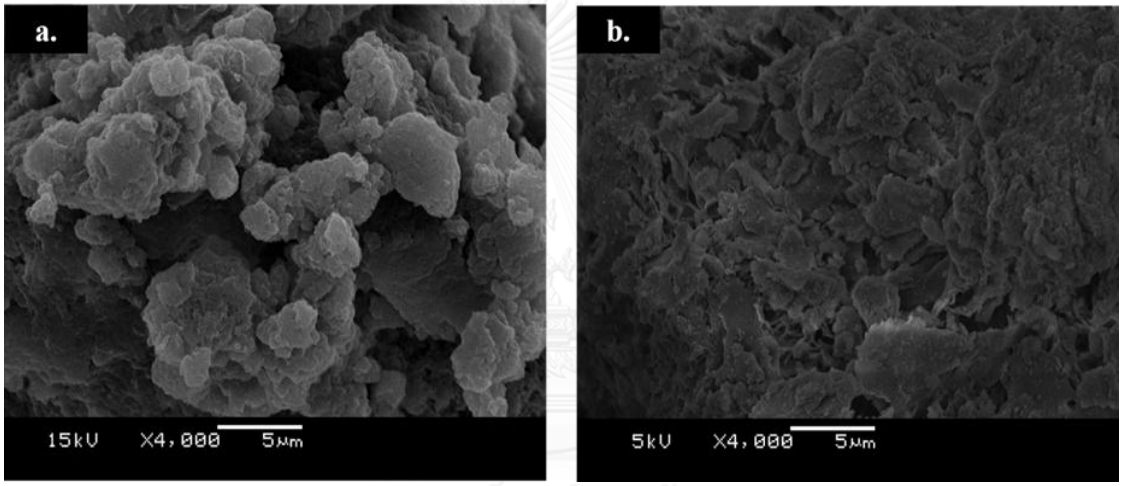

Figure 4.4 SEM micrographs of modified cellulose fibril a.) Oil-g-CF and b.) Silane-g-CF

4.1.3 Functional Groups of Virgin Cellulose Fibril and Modified Cellulose Fibril

The FT-IR spectrums of virgin CF, Oil-g-CF, and Silane-g-CF are presented in Figure 4.5. The spectrum of CF presents the characteristic absorption bands of typical cellulose with the broad O-H stretching band between 3200 and 3600 cm^{-1} while the C-H stretching band shows up at 2871 cm^{-1}. The absorption band at 1640 cm^{-1} corresponds to the characteristic IR absorption band of bound water, indicating the extremely high water content which presents in CF network. The absorption vibrations at 1153 cm^{-1}, 1041 cm^{-1}, and 899 cm^{-1} belong to the C-O stretching of cellulose, the vibration of C-O-C pyranose ring skeleton, and the characteristic of β-glucosidic linkages of glucose units, respectively [141] In case of Oil-g-CF spectrum, the disappearance of O-H band at 3400 cm^{-1} reveals that the surface treatment of CF was modified successfully and the hydrophobic cellulose was obtained. The two absorption bands corresponding to the symmetric and asymmetric stretching vibration of CH_2 groups show up at 2911 cm^{-1} and 2846 cm^{-1}, respectively. The absorption band at 1750 cm^{-1} which attributes to the carbonyl vibration arising from malenized soybean oil is found, obviously [142]. As seen in the spectrum of Silane-g-CF, the strong absorption bands at 2911 cm^{-1} and 2846 cm^{-1} are responsible for the symmetric and asymmetric vibrations of silane CH_2 moieties. The absorption bands at 3100 cm^{-1} to 3500 cm^{-1} and 1650 cm^{-1} correspond to the presence of partially free silica silanol (Si-OH) group. The rocking and symmetric stretching of SiO_2 intertetrahedral oxygen atoms exhibit at 450 cm^{-1} and 800 cm^{-1}, respectively while the asymmetric stretching of SiO_2 intertetrahedral oxygen atoms at 1080 cm^{-1} and the absorption band of Si-O-C between 1000 cm^{-1} and 1150 cm^{-1} are overlapped with the primary and secondary alcohol groups of cellulose [143]. The functional groups with the wave number of each sample are summarized in Table 4.1.

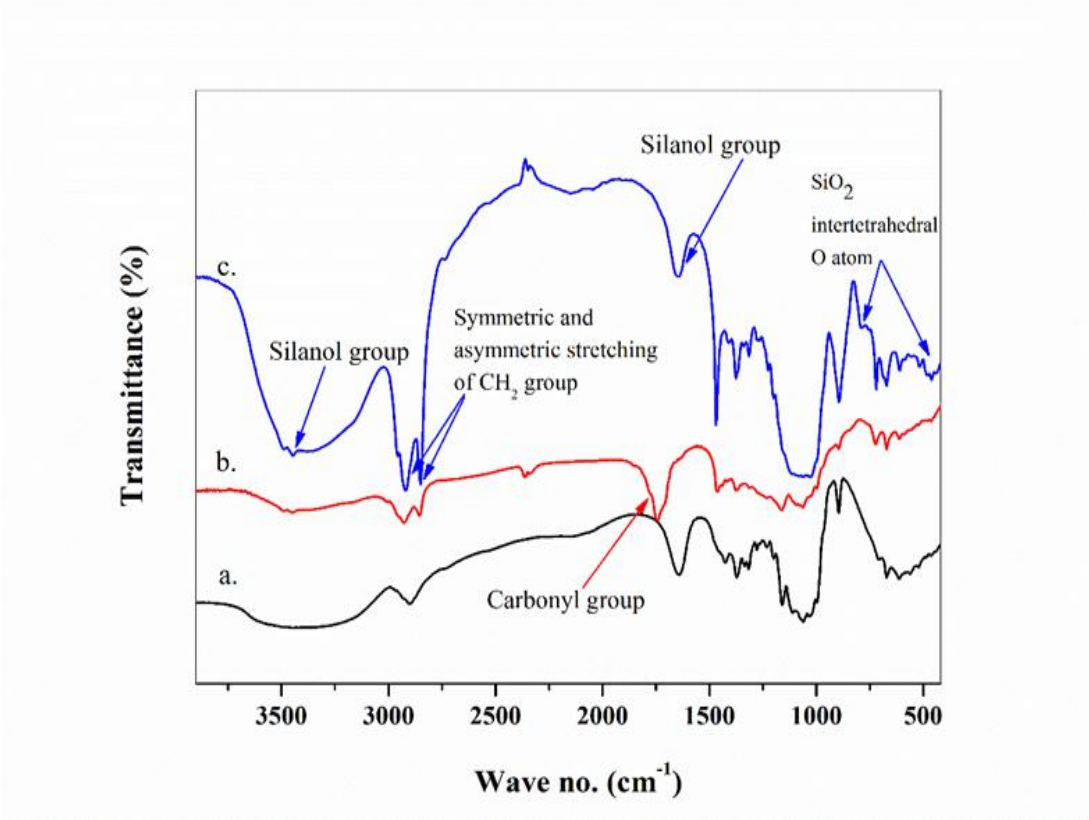

Figure 4.5 FT-IR spectra of a) virgin CF, b) Oil-g-CF and c) Silane-g-CF

Table 4.1 Functional groups and wave number of virgin CF, Oil-g-CF, and Silane-g-CF

Sample	Wave no. (cm^{-1})	Functional Group
Virgin CF	3600-3200	O-H stretching
	2871	C-H stretching
	1640	Bending of absorbed water
	1153	C-O stretching
	1041	Vibration of C-O-C pyranose ring
	899	β-glucosidic linkage of glucose unit
Oil-g-CF	2911	Symmetric stretching vibration of CH_2
	2846	Asymmetric stretching vibration of CH_2
	1750	-C=O vibration

Sample	Wave no. (cm^{-1})	Functional Group
Silane-g-CF	3500-3100	O-H stretching (Silanol group, Si-OH)
	2911	Symmetric stretching vibration of Silane CH_2
	2846	Asymmetric stretching vibration of Silane CH_2
	1650	Bending of absorbed water
	800	Symmetric stretching of SiO_2 intertetrahedral oxygen atoms
	450	Rocking of SiO_2 intertetrahedral oxygen atoms

4.1.4 Particle Size Distribution of Virgin Cellulose Fibril and Modified Cellulose Fibril

The particle size distributions of CF, Oil-g-CF, and Silane-g-CF are shown in Figure 4.6. According to the hydrophilicity of cellulose, distilled water was employed as a medium for virgin CF whereas toluene was employed as a medium for Oil-g-CF and Silane-g-CF. The particle size distributions of virgin CF reveals an average diameter around 560 nm while the average diameters of Oil-g-CF and Silane-g-CF are 1700 nm and 850 nm, respectively. The increasing of average particles diameter attributes to the agglomeration of modified CF particles. However, the agglomeration of particles exhibits the soft agglomeration characteristic which can be observed from the swellability of surface treated CF in nonpolar solvents [144].

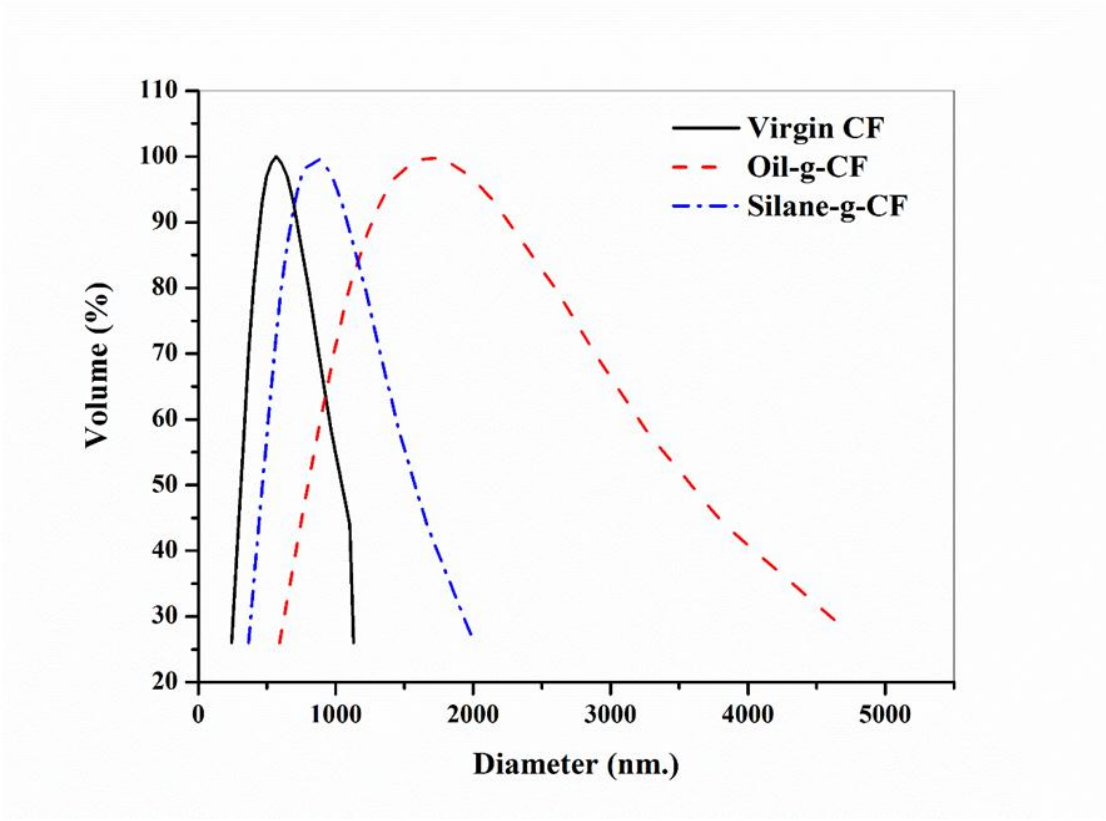

Figure 4.6 Particle size distribution of virgin CF, Oil-g-CF, and Silane-g-CF

4.1.5 Crystal Morphology of Virgin Cellulose Fibril and Modified Cellulose Fibril

The XRD patterns of cotton fabric waste MCC, regenerated MCC and CF are shown in Figure 4.7. The characteristic peaks of Cellulose I crystal at 2θ = 15.0°, 16.3°, 22.9° and 34.1° [144] are found in MCC whereas the shift of 2θ peak from 15-16° to 19.8° as well as the decreasing of the peak intensity due to the transformation of Cellulose I crystal to Cellulose II crystal [129] are observed in case of regenerated MCC. The XRD pattern of CF shows the characteristic of the amorphous cellulose structure. Generally, amorphous cellulose is obtained by several methods such as cellulose-ball milling, deacetylation of cellulose acetate in nonaqueous alkali condition and regeneration of cellulose solution into nonaqueous or aqueous media [145]. Therefore, the regeneration of MCC solution and the anti-coagulating effect caused by the starch molecules that obstruct the packing of cellulose molecules during the precipitation step result in the amorphous structure of CF [140]. Kadokawa et al. [146] prepared cellulose-starch composite gel obtained by keeping the homogeneous mixture of 10 wt% cellulose and 5 wt% starch in 1-butyl-3-methylimidazolium chloride (BMIMCl) for several days at room temperature. The XRD pattern of the composite gel also revealed the amorphous structure which might attribute to the disruption of most of crystalline regions of cellulose and starch in the gel probably due to the compatibility of the two polysaccharides.

Interestingly, the XRD patterns of modified CF in Figure 4.8 exhibit the change of the amorphous structure to the Cellulose II crystal structure, evidenced by the rising of 2θ peak at 20° and 21.5°. Moreover, Silane-g-CF shows the higher peak intensity than Oil-g-CF. The change of crystallinity from amorphous to crystal structure can be explained by its crystalline characteristic by nature which prefers to self-orientation under the suitable condition [140].

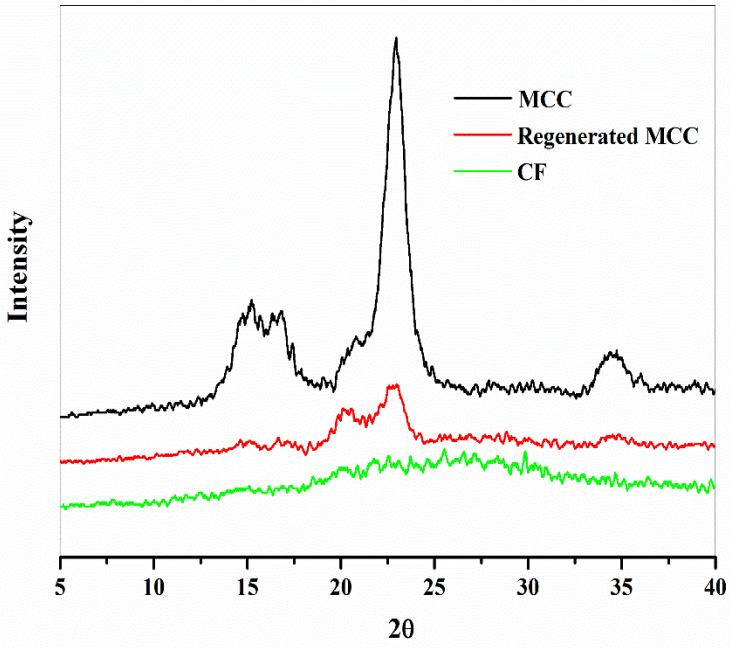

Figure 4.7 The XRD patterns of MCC, regenerated MCC and CF

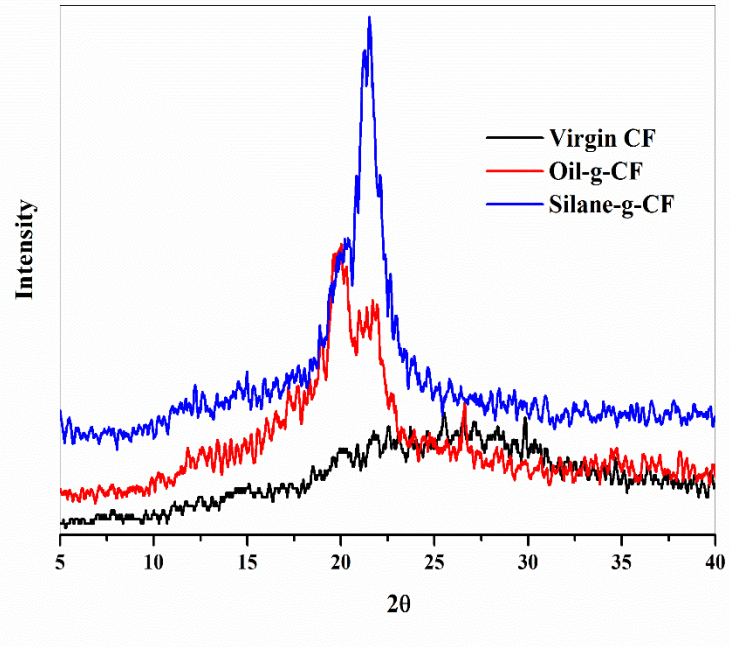

Figure 4.8 The XRD patterns of virgin CF, Oil-g-CF, and Silane-g-CF

4.1.6 Thermal Stability of Virgin CF and Modified CF

The mechanism of cellulose thermal degradation by Brodino and Shafizadeh is presented in Figure 4.9. [147]. The first step of degradation is the formation of active cellulose by depolymerization without the mass loss due to the scission of glycosidic bonds caused by transglycosylation [148]. The second step consists of the dehydration of pyranose ring and forming of anhydrocellulose, resulting in the loss of mass. The further degradation of pyranose produces CO_2, volatile gases and unsaturated cyclic compounds [149].

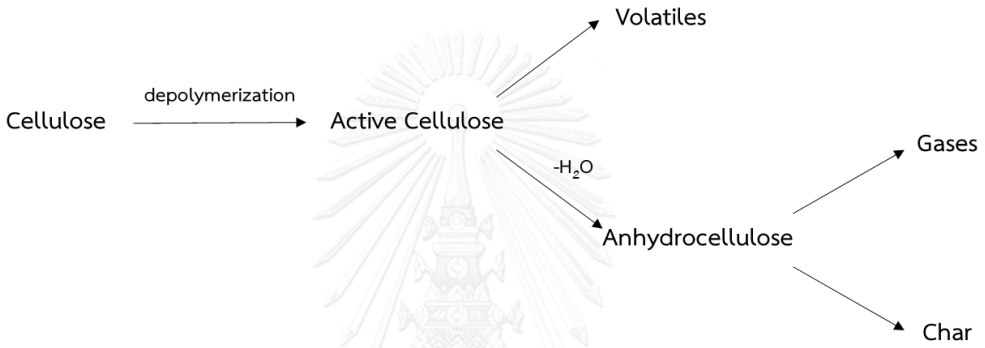

Figure 4.9 The mechanism of cellulose thermal degradation from Brodino and Shafizadeh [147]

As seen in the TG thermograms in Figure 4.10, virgin CF shows a weight loss around 60–100 °C due to the evaporation of water [143], indicating its hydrophilic characteristics. Afterwards, CF starts to degrade at 270 °C (T_{onset}) which is significantly lower than those of modified CF. The relatively low degradation temperature of CF is associated with the presence of moisture which accelerates the thermal degradation of cellulose by hydrolysis reaction. In comparison with unmodified CF, the modification of cellulose fibril by malenized soybean oil enhances the T_{onset} to 325 °C, indicating the better thermal stability due to the lack of bound moisture as well as the increasing of crystallinity. The organosilane modified cellulose fibril exhibits two degradation steps at 300 °C and at 450 °C. The first degradation of Silane-g-CF corresponds to the degradation of cellulose, followed by the second degradation which attributes to the decomposition of grafted silane [150, 151]. The DTG thermograms of all cellulosic materials are presented in Figure 4.11. The DTG curve of CF shows the small peak

around 60 °C according to the evaporation of the absorbed water [152] while the maximum degradation temperature (T_{max}) caused by the decomposition of cellulose shows up at 338 °C [153]. In case of Oil-g-CF, the DTG curve exhibits a monomodal shape with two separate maximum degradation temperatures at 369 °C and 424 °C as a result of cellulose decomposition, followed by the decomposition of the grafted malenized soybean oil. The DTG curve of Silane-g-CF shows a bimodal shape with two different maximum degradation temperatures. The first DTG peak occurs at 335 °C corresponding to the decomposition of cellulose while the second DTG peak caused by the decomposition of grafted silane is found at 490 °C. The TGA results of unmodified CF and modified CF are summarized in Table 4.2.

Table 4.2 Thermal stability of virgin CF, Oil-g-CF and Silane-g-CF

Sample	T_{onset} (°C)	T_{max1} (°C)	T_{max2}(°C)
virgin CF	270	338	-
Oil-g-CF	325	369	424
Silane-g-CF	300	335	490

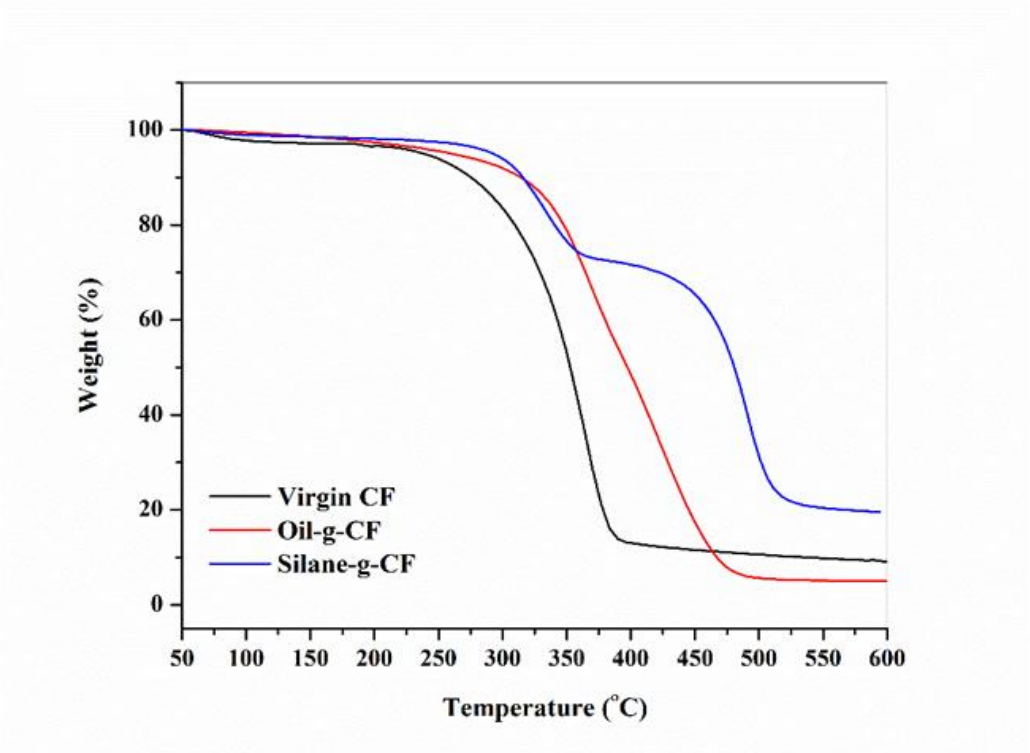

Figure 4.10 TG thermograms of virgin CF, Oil-g-CF, and Silane-g-CF

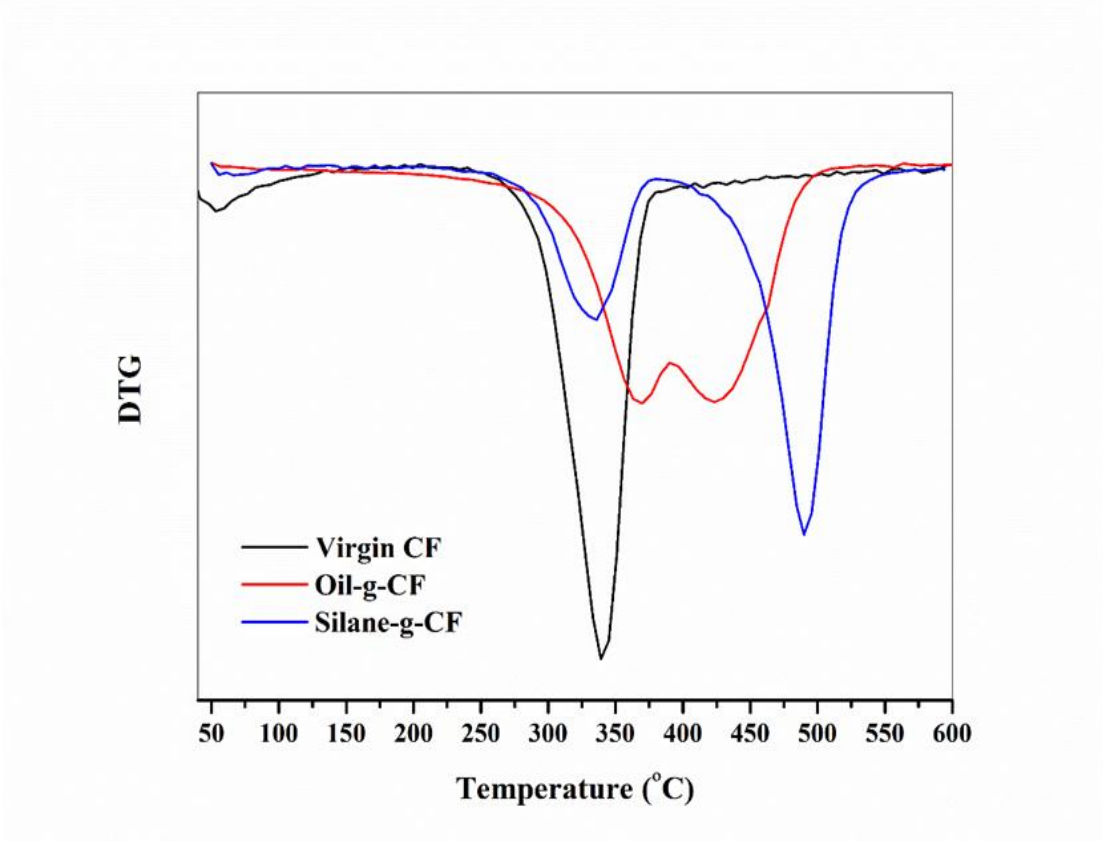

Figure 4.11 DTG thermograms of virgin CF, Oil-g-CF, and Silane-g-CF

4.2 The Properties Comparison between Soybean Oil Modified Cellulose Fibril (Oil-g-CF) and Organosilane Modified Cellulose Fibril (Silane-g-CF) Filled Polypropylene

4.2.1 Dispersibility of Modified Cellulose Fibril in Polypropylene

The optical micrographs of neat PP film and PP composite films filled with 4.0 wt% of Oil-g-CF and Silane-g-CF are shown in Figure 4.12. (a.-c.). Neat PP film shows the clear transparency under the transmitted light. In case of Oil-g-CF filled PP, the particles are found scatter in the agglomerate form with the particle size ranging from 70-200 μm which is significantly larger than the original size obtained by the particle size analyzer in section 4.1.4. The larger agglomerates of Oil-g-CF indicate that cohesive force among particles is stronger than the adhesion force between Oil-g-CF and PP. In a similar manner, Silane-g-CF particle exhibits the particles size range between 40-80 μm when it was compounded with PP. Changing of the particle size reflects that modified CF exhibits meltability characteristic which plays a key role in wetting plastics, consequently resulting in filler particles with the good compatibility and dispersibility [133].

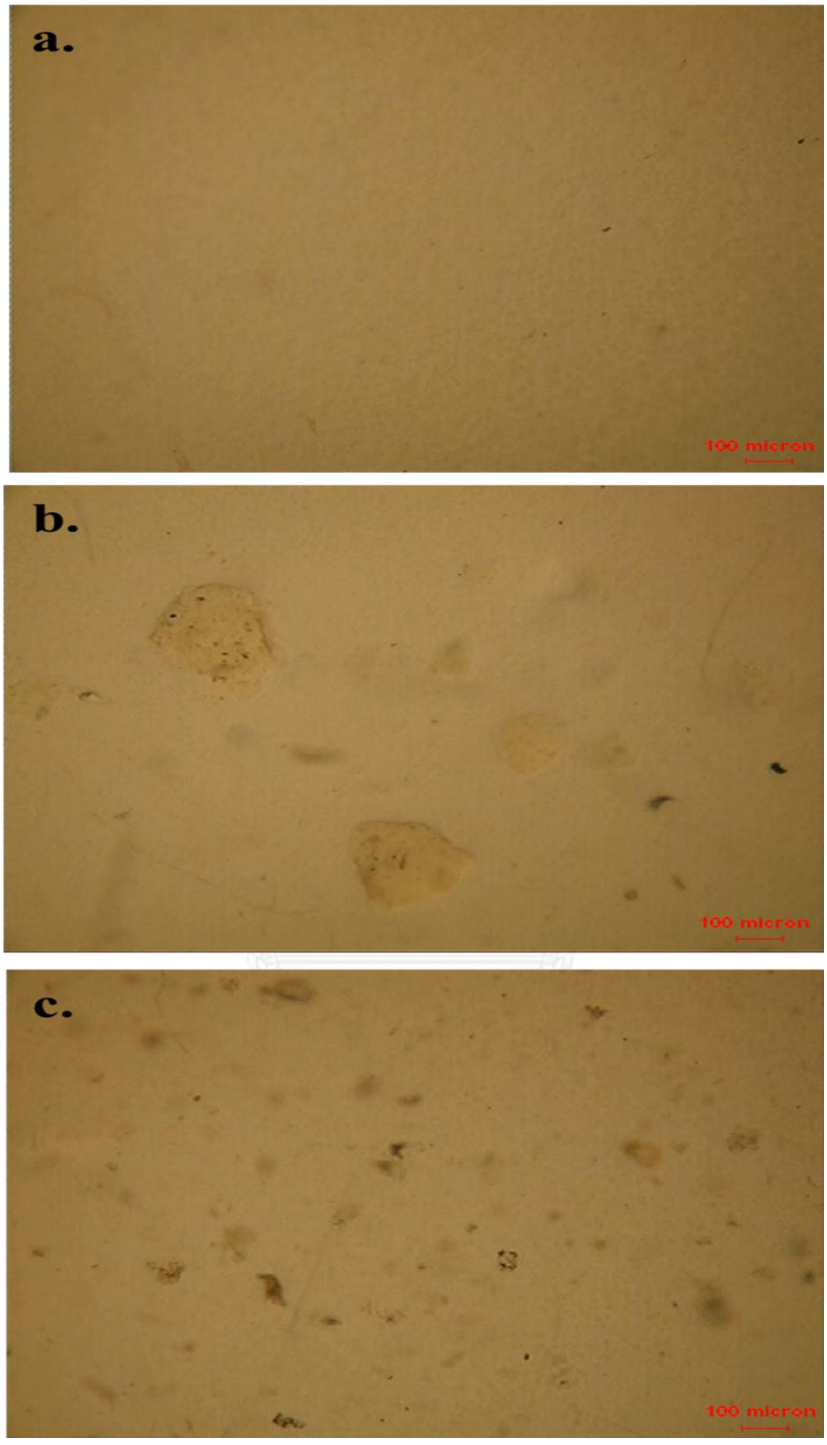

Figure 4.12 Optical micrographs (transmission mode) of a.) neat PP, b.) Oil-g-CF/PP composite and c.) Silane-g-CF/PP composite with 4.0 wt% filler loading (scale bar 100 μm)

4.2.2 Crystal Morphology of Neat PP and Modified Cellulose Fibril/PP Composites

The remaining crystalline morphologies of samples after removal of the amorphous region by chemical etching are displayed in Figure 4.13. The spherulite crystals are obviously seen in all cases. Neat PP shows the common spherulite structure with an average diameter of 28 μm. The crystalline morphology of both Oil-g-CF and Silane-g-CF filled PP reveals an increase in spherulite number while the spherulite size is decreased when compared to neat PP. The average spherulite diameter of Oil-g-CF/PP composite and Silane-g-CF/PP composite is 17 and 23 μm, respectively. The increasing of spherulite number and the decreasing of spherulite size as found in PP composites indicate the nucleation effect caused by the addition of modified CF [154]. The nucleation effect accelerates the crystallization process, leading to the small spherulite size due to the high nucleation density [155, 156].

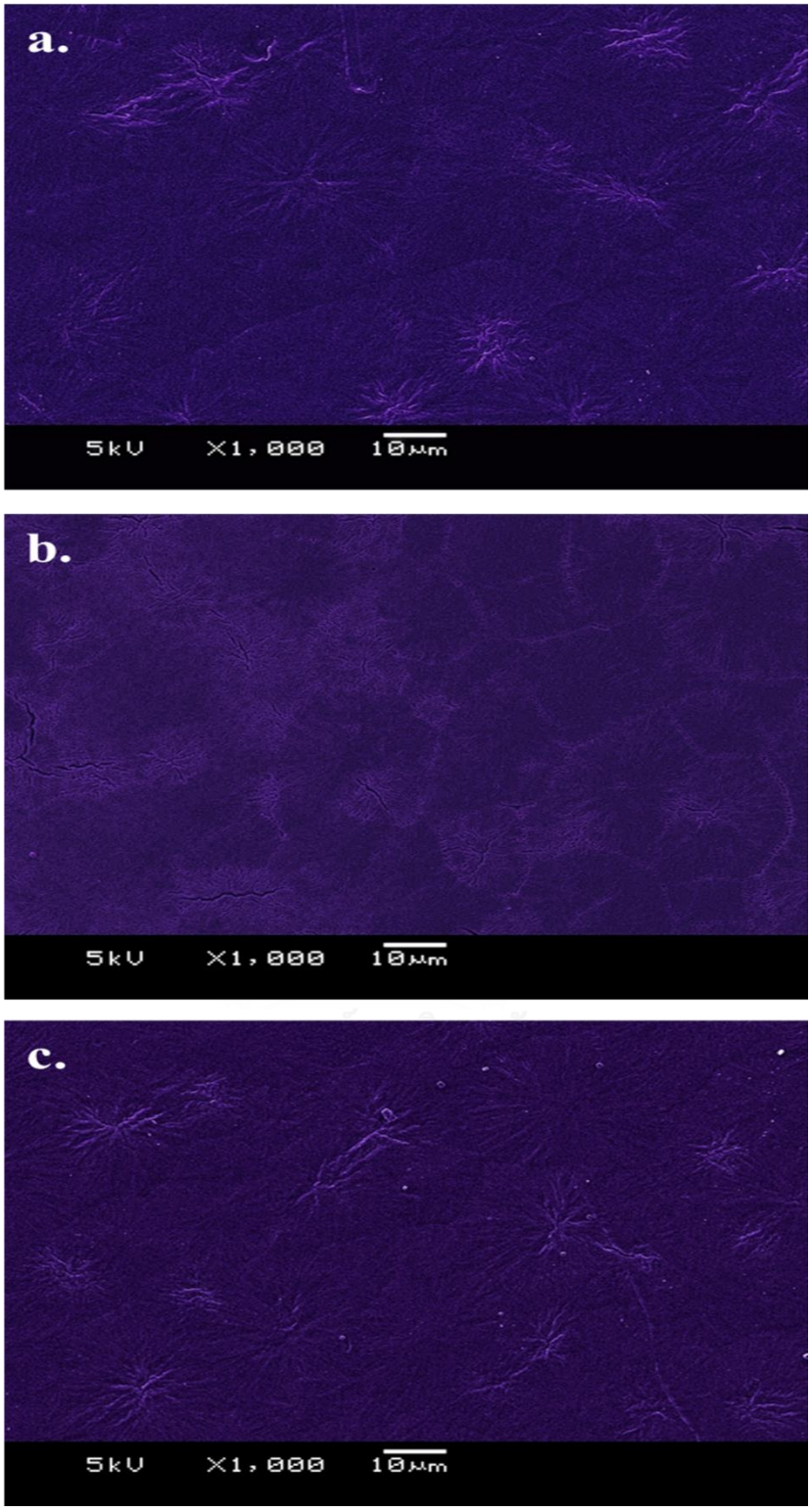

Figure 4.13 SEM images of the etched films a.) neat PP, b.) Oil-g-CF/PP composite and c.) Silane-g-CF/PP composite with 4.0 wt% filler loading (scale bar 10 μm)

4.2.3 Crystallization Behavior of Neat PP and Modified Cellulose Fibril/PP Composites

The non-isothermal crystallization behavior at 125, 120 and 115 °C of neat PP and composites are presented in Figure 4.14. Neat PP is still in the molten state at 125 °C and then the existence of spherulites is found at 120 °C, followed by the continuous growth of spherulites when the temperature was cooled down to 115 °C. When compared to neat PP, both composites start nucleation earlier observed by the presence of small spherulites at 125 °C. At 120 °C, composites exhibit the faster crystallization rate than neat PP judged by the higher spherulite number and spherulite growth. The crystallization process of both composites is complete at 115 °C while neat PP still continues to crystallize. These results indicate that both Oil-g-CF and Silane-g-CF are able to be a nucleating agent for PP due to its faster crystallization performance [157, 158]. The nucleation ability of both particles attributes to a number of tiny particle sizes of fillers which facilitate nucleation sites for spherulite growth due to the large surface area whereas neat PP contains the absence of nucleating site, resulting in slower nucleation process.

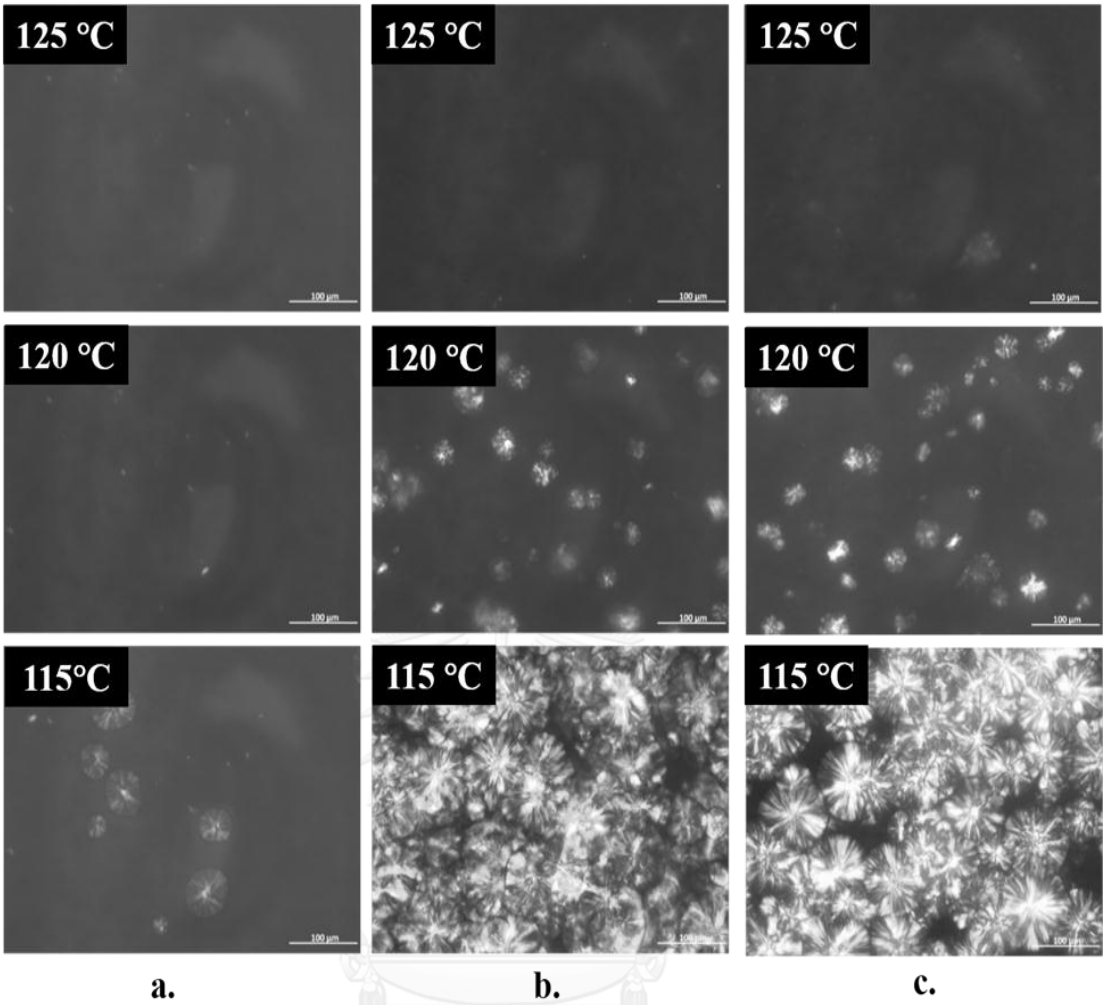

Figure 4.14 Optical micrographs of the crystallization process of a.) neat PP, b.) Oil-g-CF/PP composite and c.) Silane-g-CF/PP composite (scale bar 100 μm)

4.2.4 Thermal Stability

Figure 4.15 shows the thermal degradation mechanism of PP which occurs above 250 °C through a radical chain process propagated by carbon-centered radical caused by carbon-carbon bond scission to volatile products [159].

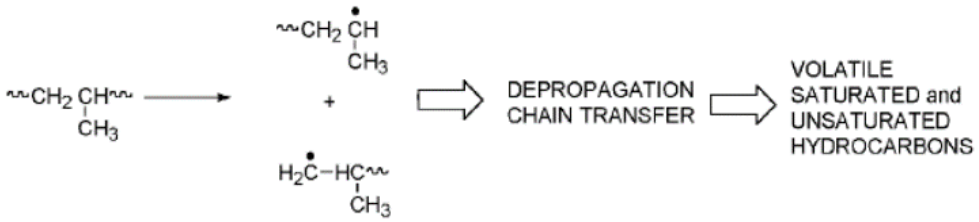

Figure 4.15 Thermal degradation of polypropylene [159]

The TG and DTG thermograms of neat PP and modified CF filled PP composites are presented in Figure 4.16 and 4.17. The onset degradation of PP film begins at 422 °C whereas Oil-g-CF/PP film and Silane-g-CF/PP film show the delayed onset degradation temperature up to 20 °C. As seen in the DTG curves, the maximum degradation of neat PP occurs at 455 °C while the addition of both modified CF shifts the maximum degradation of PP up to 10 °C, approximately. Therefore, both modified CF help improve the thermal stability of PP, judged by the increasing of T_{onset} and T_{max}, corresponding to the improved interaction between CF and PP obtained by cellulose surface modification [160]. The TGA results of modified CF reinforced PP are shown in Tale 4.3.

Table 4.3 Thermal stability of neat PP, Oil-g-CF/PP composite and Silane-g-CF/PP composite

Sample	T_{onset} (°C)	T_{max} (°C)
Neat PP	422.0	454.5
4.0 wt% Oil-g-CF/PP	441.8	464.9
4.0 wt% Silane-g-CF/PP	441.8	461.8

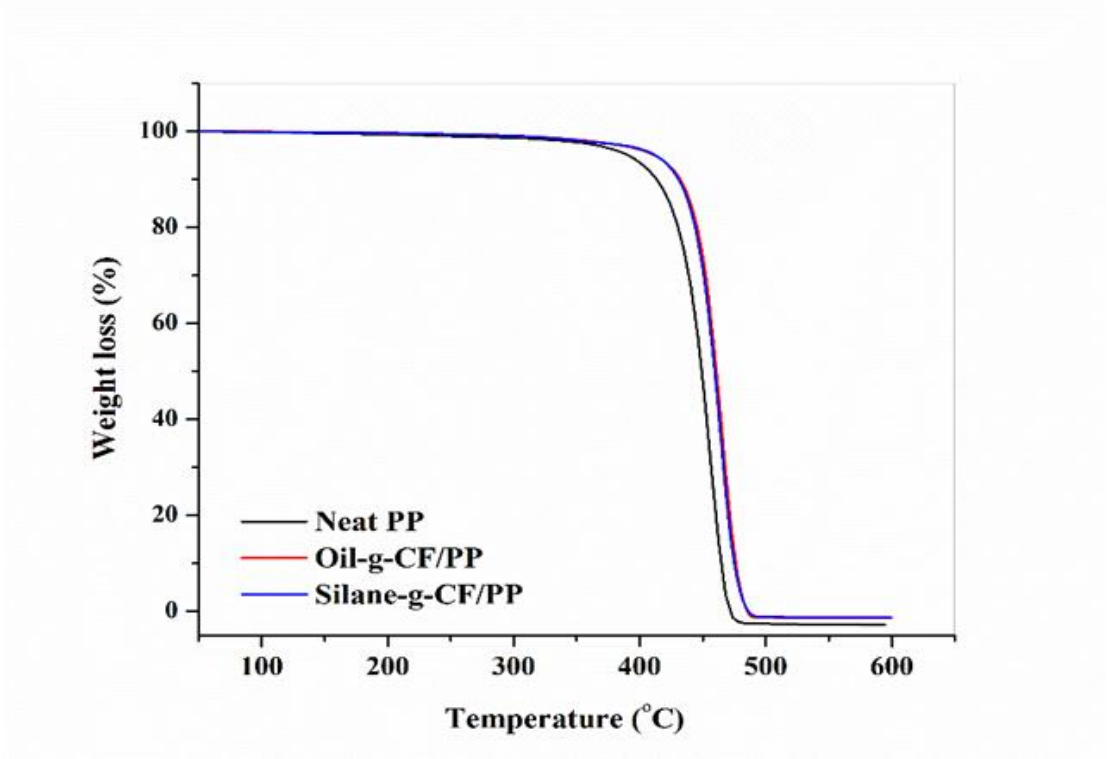

Figure 4.16 TG thermograms of neat PP, Oil-g-CF/PP composite, and Silane-g-CF/PP composite

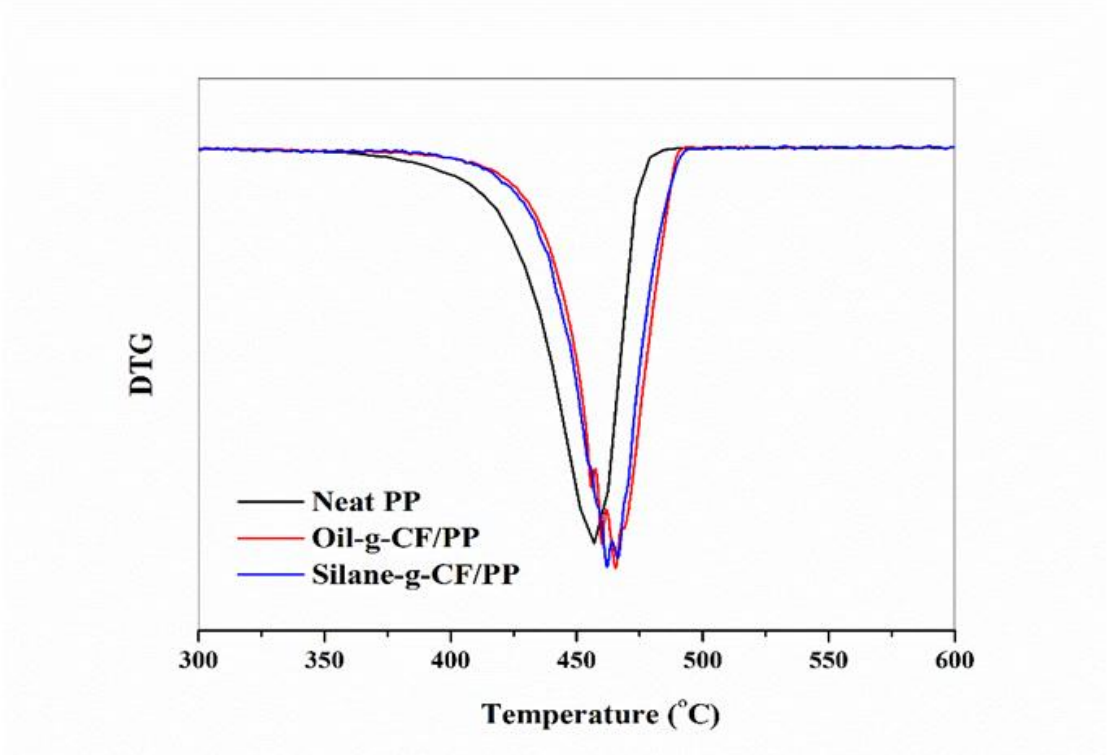

Figure 4.17 DTG thermograms of neat PP, Oil-g-CF/PP composite, and Silane-g-CF/PP composite

4.2.5 Thermal Properties

As shown in Figure 4.18 (a.), the DSC heating curves of all samples exhibit only a single melting peak of α-form crystals [161, 162]. The melting peak (T_m) of neat PP is found at 155.4 °C along with a small shoulder in front of the peak, attributing to the recrystallization or reorganization of crystals initially formed during non-isothermal crystallization [163]. The addition of Oil-g-CF into PP raises the melting temperature by 4 °C, approximately whereas the addition of Silane-g-CF shows the prominent increasing of melting temperature up to 6 °C. As seen in Table 4.4, the addition of Oil-g-CF and Silane-g-CF also increase the degree of crystallinity (X_c) of PP up to 6 and 11%, respectively. The rising of melting temperature can be explained by the increasing of crystallinity due to the nucleation effect of modified CF particles which provide nucleation sites for the crystallization and the partial crystal growth of PP as well as the better compatibility and interaction between CF and PP after surface modification [152].

The DSC cooling curves in Figure 4.18 (b.) reveals the greater nucleation performance of Silane-g-CF than Oil-g-CF judged by the shift of crystallization temperature (T_c) of PP [164] from 114.7 °C to 118.4 °C in case of Silane-g-CF/PP composite whereas T_c of Oil-g-CF/PP composite is similar as neat PP (115.0 °C). The rising of T_c corresponds to the faster crystallization process which is accelerated by Silane-g-CF due to its better compatibility and stronger interaction with PP [165]. When compared to organosilane modified CF, Oil-g-CF exhibits the inferior performance as the nucleating agent for PP attributing to the plasticization effect caused by the molecular structure of malenized soybean oil [133]. The thermal properties of neat PP and composites are summarized in Table 4.4.

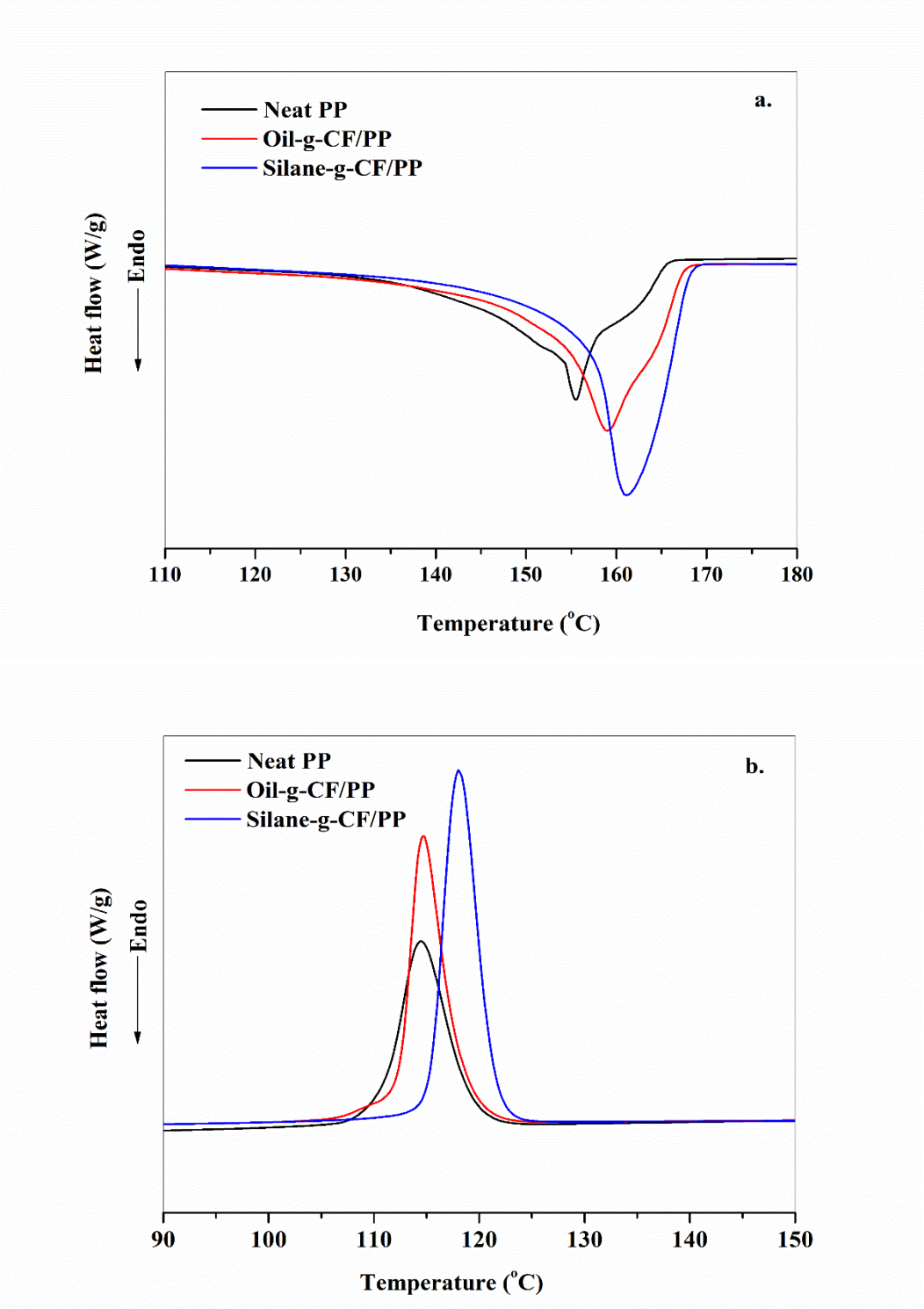

Figure 4.18 DSC thermograms of neat PP, Oil-g-CF composite, and Silane-g-CF/PP composite a.) Second endothermic curve and b.) Second exothermic curve

Table 4.4 Thermal properties of neat PP, Oil-g-CF/PP composite, and Silane-g-CF/PP composite obtained from the second heating and the second cooling scan

Sample	T_m (°C)	ΔH_m (J/g)	X_c (%)	T_c (°C)	ΔH_c (J/g)
Neat PP	155.4	69.9	33.4	114.7	73.7
4.0 wt% Oil-g-CF/PP	158.9	79.0	39.4	115.0	87.3
4.0 wt% Silane-g-CF/PP	161.0	89.3	44.5	118.4	97.9

4.3 Properties of Organosilane Modified Cellulose Fibril/Polypropylene Composites

4.3.1 Thermal Stability

The TG thermograms of neat PP and Silane-g-CF filled PP composites are shown in Figure 4.19. Neat PP exhibits a single step of thermal degradation due to a random chain scission and a radical chain mechanism [153]. The onset degradation temperature (T_{onset}) of neat PP shows at 420 °C as similar as 0.5 wt% Silane-g-CF/PP composite while the addition of 1.0, 3.0 and 5.0 wt% of Silane-g-CF increases the T_{onset} of PP to 436.8, 438.0 and 437.8 °C, respectively. The addition of virgin CF also improves the T_{onset} of PP up to 14 °C but it is slightly lower than the addition of 1.0 wt% of organosilane modified CF around 3 °C, indicating the weak interaction between filler and matrix [160] due to the hydrophilic-hydrophobic nature of cellulose-PP. The DTG thermograms of neat PP and composites in Figure 4.20 show a single maximum thermal degradation temperature (T_{max}) in all case. The shift of maximum thermal degradation temperature of PP from 449 °C to the higher temperature is observed in both Silane-g-CF/PP composites and virgin CF/PP composite. The addition of 0.5, 1.0, 3.0 and 5.0 wt% increases the maximum thermal degradation temperature to 451.7, 458.3, 460.5 and 462.1, respectively. However, the maximum thermal degradation of virgin CF filled PP is similar as modified CF at the same filler content (1.0 wt%), indicating that the influence of filler loading is greater than filler-matrix interaction in this case.

The increasing of T_{onset} and T_{max} which is found in CF/PP composites indicates that the thermal stability of PP is improved. Generally, the increasing of thermal stability is attributed to the hindered diffusion of volatile products from the decomposition of polymer composites [166]. Therefore, the diffusion of volatile products from carbon-carbon bond scission of PP matrix is hindered by cellulose particles, resulting in the delayed or higher thermal degradation temperature of CF/PP composites when compared to neat PP [153, 166]. In addition, the hindered diffusion of volatile products relates to the filler content, evidenced by the small increment of onset degradation temperature and maximum thermal degradation temperature when

the small amount of Silane-g-CF was added (0.5 wt%). The TGA results are summarized in Table 4.5.

Table 4.5 Thermal stability of neat PP, Silane-g-CF/PP composites, and virgin CF/PP composite

Sample	T_{onset} (°C)	T_{max} (°C)
Neat PP	420.3	449.0
0.5 wt% Silane-g-CF/PP	420.5	451.7
1.0 wt% Silane-g-CF/PP	436.8	458.3
3.0 wt% Silane-g-CF/PP	438.0	460.5
5.0 wt% Silane-g-CF/PP	437.8	462.1
1.0 wt% virgin CF/PP	434.3	459.6

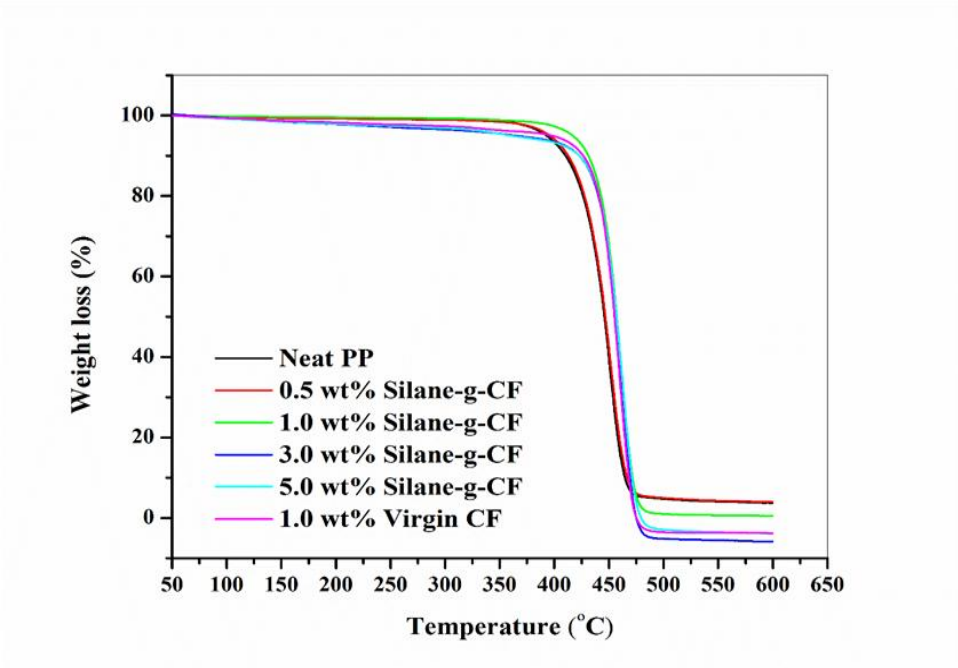

Figure 4.19 TG Thermograms of neat PP, Silane-g-CF/PP composites, and virgin CF/PP composite

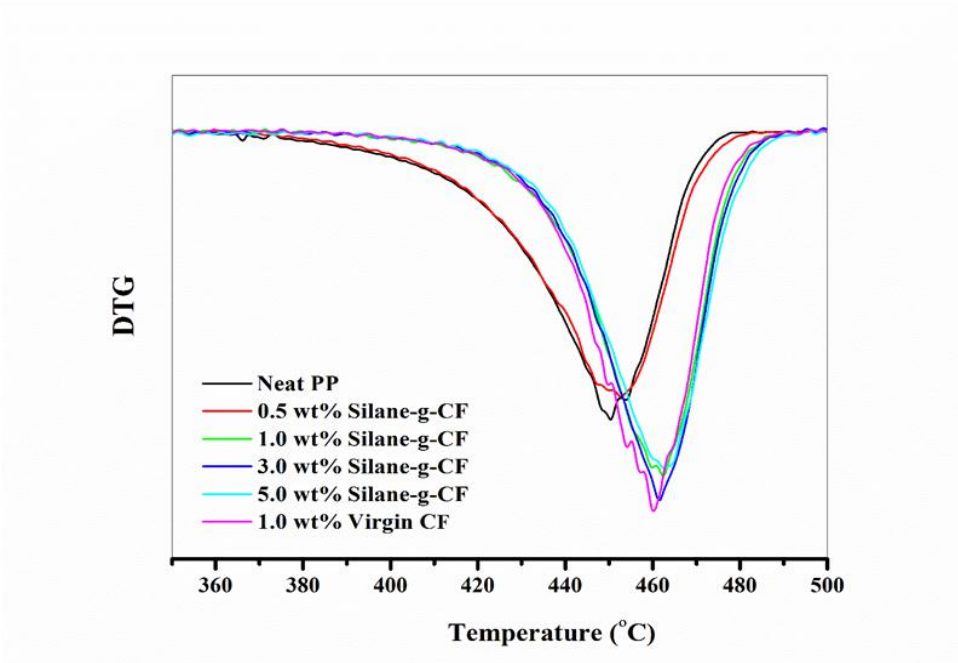

Figure 4.20 DTG thermograms of neat PP, Silane-g-CF/PP composites, and virgin CF/PP composite

4.3.2 Thermal Properties

As seen in Figure 4.21, the DSC heating curves of all samples display a single melting peak, indicating that only α (monoclinic) crystalline polymorph of PP is formed [147]. The melting peak of neat PP is found at 160 °C with a small shoulder around 165 °C. The two steps melting can be explained by the melt recrystallization of slow heating rate, the secondary nucleation of crystals in PP caused by the impurities or the annealing of lamella within crystals [167]. The addition of 0.5, 1.0, 3.0 and 5.0 wt% of Silane-g-CF slightly increases the melting temperature of PP around 1 °C as well as the addition of virgin CF. The degree of crystallinity of Silane-g-CF/PP composites is higher than neat PP up to 5% at 1.0 wt% filler loading, then gradually decreased around 2.5 to 3.5% when Silane-g-CF loading is increased whereas the addition of virgin CF remains unchanged in the degree of crystallinity of PP.

The crystallization exotherms in Figure 4.22 reveal the ability of Silane-g-CF as a nucleating agent for PP observed by the shift of crystallization peak of PP filled with Silane-g-CF to the higher temperature. The addition of Silane-g-CF at 0.5, 1.0, 3.0 and 5.0 wt% raises the crystallization temperature of PP from 114 °C to 115.4, 116.7, 118.6 and 117.8 °C, respectively. The rising of T_c indicates the faster crystallization process which relates to the increasing of nucleation sites when the higher amount of filler was added [147, 152]. When compared to Silane-g-CF, virgin CF does not act as a nucleating agent for PP proved by the unchanged crystallization temperature and degree of crystallinity. These results indicate the effect of organosilane surface treatment on the nucleating performance, attributing to the improved dispersion, compatibility as well as interaction with PP matrix. The all thermal properties of neat PP and composites are summarized in Table 4.6.

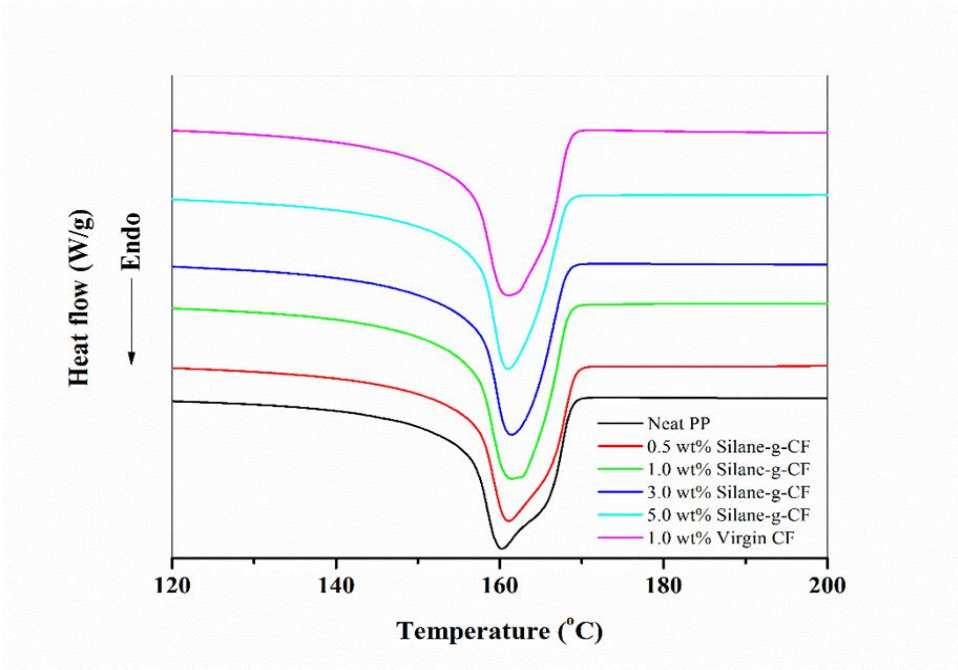

Figure 4.21 DSC second heating thermograms of neat PP, Silane-g-CF/PP composites, and virgin CF/PP composite

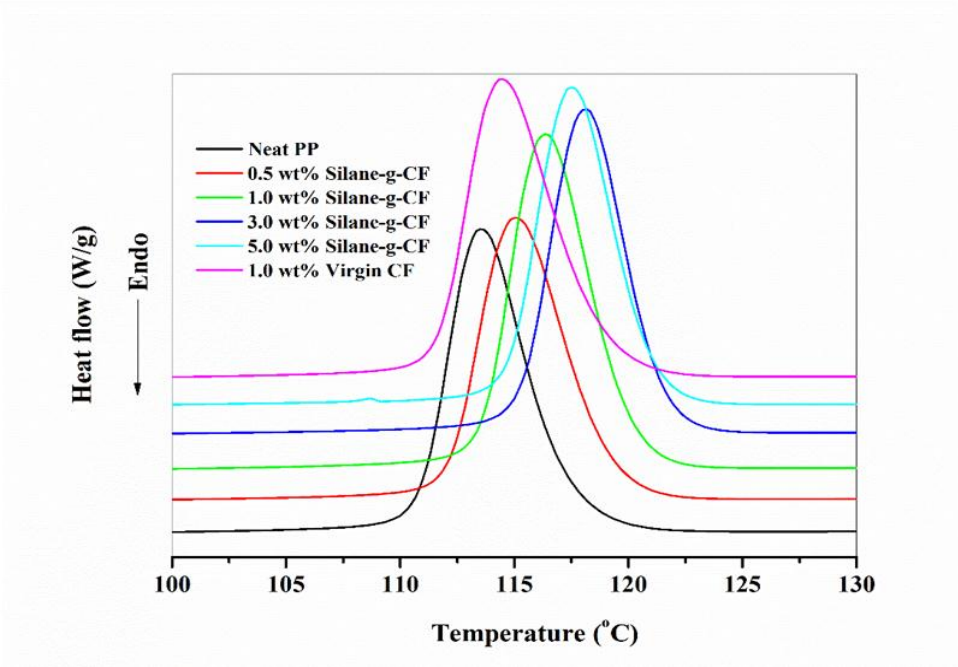

Figure 4.22 DSC second cooling thermograms of neat PP, Silane-g-CF/PP composites, and virgin CF/PP composite

Table 4.6 Thermal properties of neat PP, Silane-g-CF/PP composites, and virgin CF/PP composite

Sample	T_m (°C)	ΔH_m (J/g)	X_c(%)	T_c (°C)	ΔH_m (J/g)
Neat PP	160.2	90.5	43.3	114.0	91.2
0.5 wt% Silane-g-CF/PP	161.0	87.6	42.0	115.4	90.4
1.0 wt% Silane-g-CF/PP	161.3	98.4	47.5	116.7	99.1
3.0 wt% Silane-g-CF/PP	161.3	89.1	44.0	118.6	91.9
5.0 wt% Silane-g-CF/PP	160.8	90.6	45.6	117.8	90.7
1.0 wt% virgin CF/PP	161.0	89.1	43.1	114.9	97.0

4.3.3 Fracture Surface Morphology

The SEM micrographs in Figure 4.23 display the cryo-fractured surface of neat PP and PP composites filled with organosilane modified CF and unmodified CF. Obviously, the fracture surface of neat PP (Figure 4.23 (a.)) exhibits the smoother surface when compared to Silane-g-CF/PP composites (Figure 4.23 (b.-e.)). The smooth fracture surface of neat PP indicates the brittle nature [76] and the weak resistance to crack propagation [168] whereas the rough surface of composites indicates the high energy requirement to break the specimen [169], corresponding to the good interfacial adhesion between Silane-g-CF and PP matrix caused by organosilane surface treatment. Silane-g-CF appears as a white particle which is surrounded by matrix without voids, indicating the good adhesion between Silane-g-CF and PP [170]. However, some partially covered or uncovered particles which may attribute to the incompletely modified CF are observed also. Yang et al. [171] explained the rough fracture surface of cellulose nanofibril/PP composites as a result of the very hard crack initiation at the interface of reinforcement and matrix. As seen in the Figure 4.23 (f.), the fracture surface of untreated CF filled PP exhibits the smoother surface when compared to the treated CF, indicating the weaker crack resistance due to the poor interfacial adhesion between filler and matrix which results in the easy crack propagation and the smaller energy dissipation at the interfacial area. Figure 4.24 shows the fracture surface of neat PP and composites at higher magnification. As seen in Figure 4.24 (b.-e.), Silane-g-CF exhibits both fully and partially covered surface by PP while the virgin CF exhibits the debonding interface due to the lack of compatibility between filler and matrix. However, the agglomeration of Silane-g-CF to the larger particle with less surface area is observed at higher filler loading which may diminish the mechanical properties of materials.

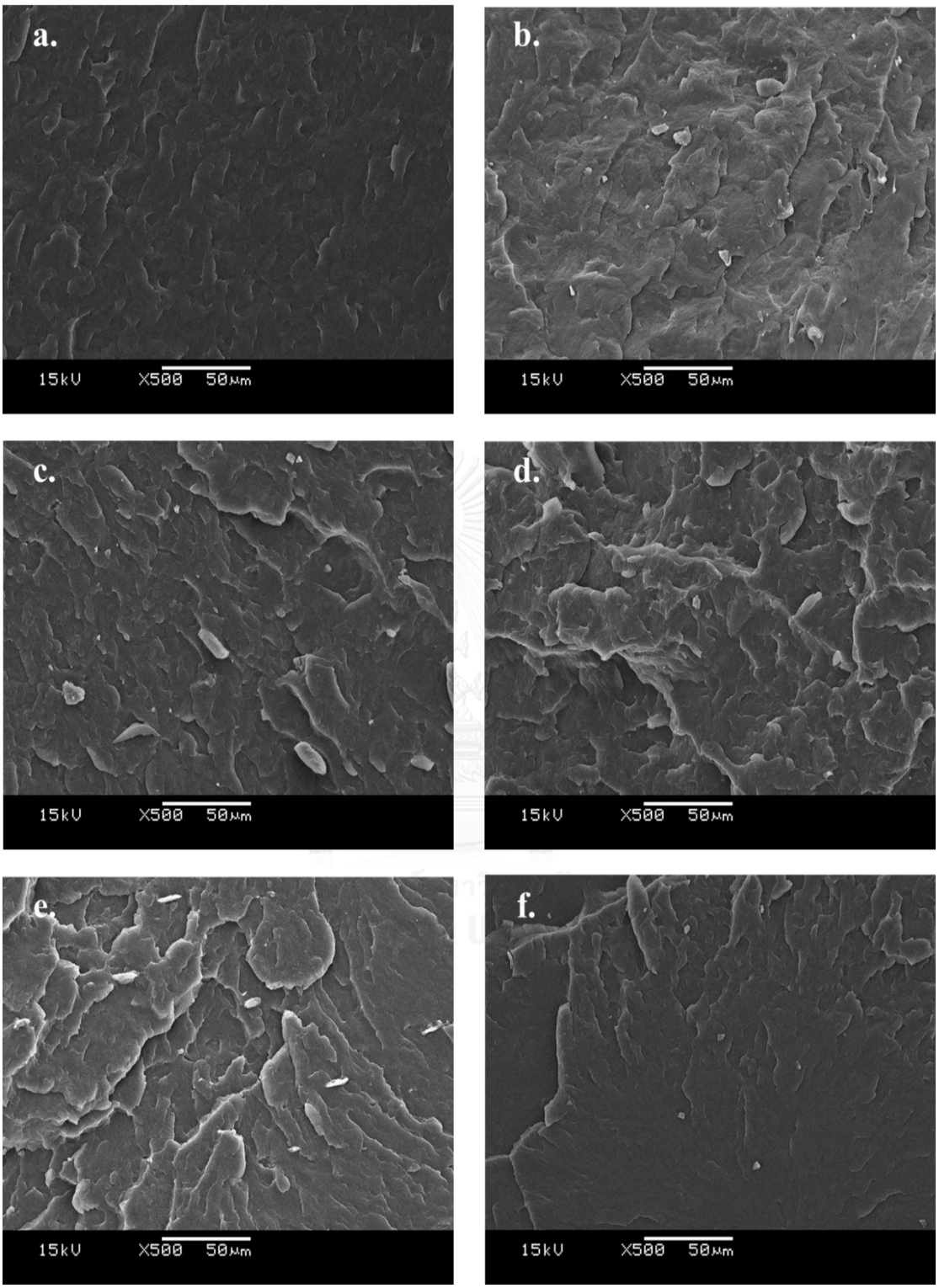

Figure 4.23 SEM micrographs (500x magnification) of cryo-fractured surface of (a.) neat PP, (b.) 0.5 wt% Silane-g-CF/PP composite, (c.) 1.0 wt% Silane-g-CF/PP composite, (d.) 3.0 wt% Silane-g-CF/PP composite, (e.) 5.0 wt% Silane-g-CF/PP composite and (f.) 1.0 wt% virgin CF composite

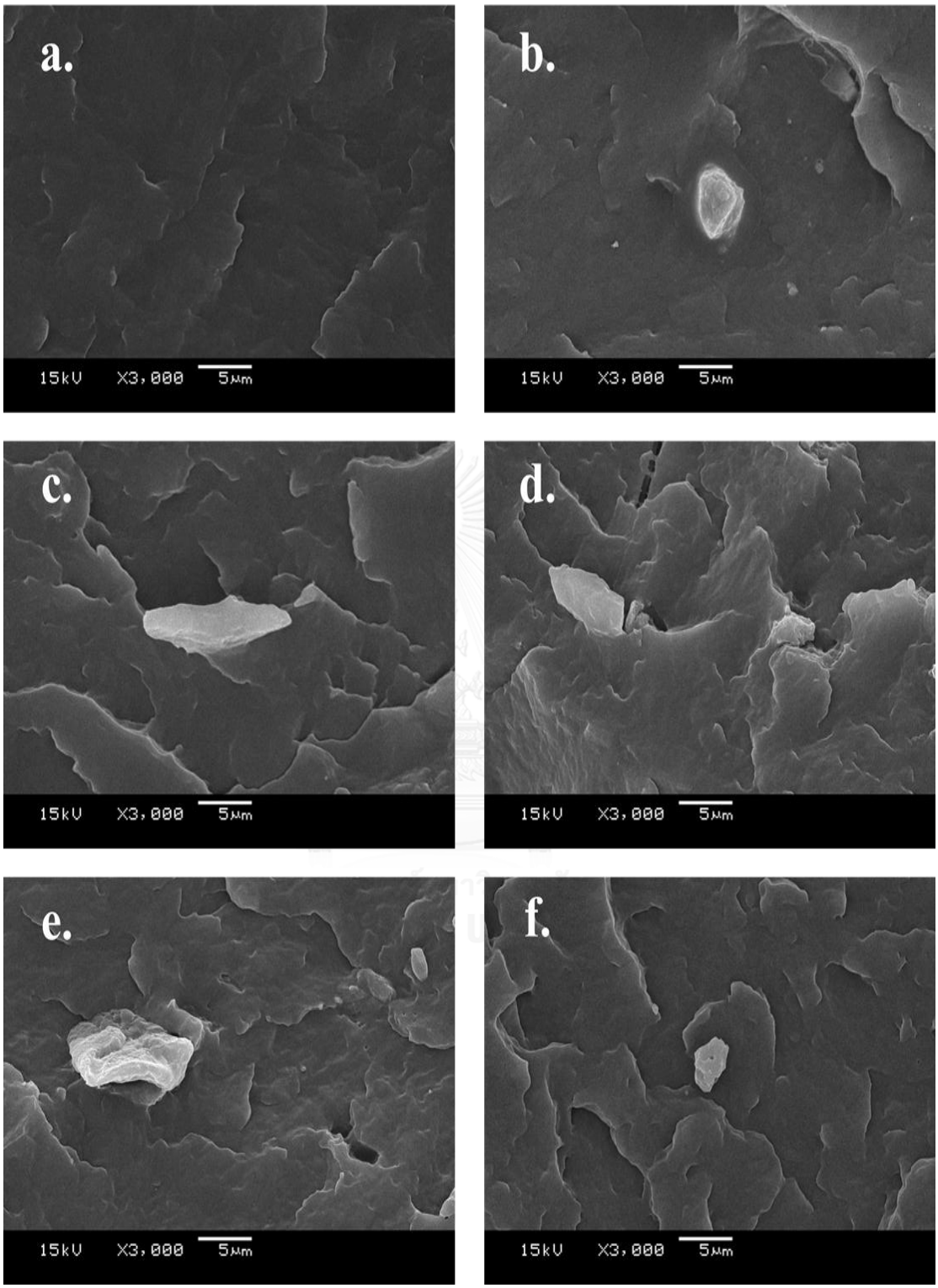

Figure 4.24 SEM micrographs (3000x magnification) of cryo-fractured surface of (a.) neat PP, (b.) 0.5 wt% Silane-g-CF/PP composite, (c.) 1.0 wt% Silane-g-CF/PP composite, (d.) 3.0 wt% Silane-g-CF/PP composite, (e.) 5.0 wt% Silane-g-CF/PP composite and (f.) 1.0 wt% virgin CF composite

4.3.4 Crystal Morphology

The XRD pattern of neat PP and CF/PP composites are shown in Figure 4.25. All samples exhibit the 2θ peak at 14.3°, 17.1°, 18.5°, 22.0°, 25.5° and 28.7°, corresponding to the 110, 130, 111, 041, 060 and 220 diffraction planes of the α-form PP crystals, respectively [172, 173]. As seen in Table 4.7, the incorporation of Silane-g-CF into PP at low filler content (0.5 and 1.0 wt%) does not affect the increase in crystallinity but the rising of crystallinity is observed when the filler content is increased to 3.0 and 5.0 wt%. Obviously, the decreasing of crystallinity is found in 1.0 wt% virgin CF/PP composite indicating the poor nucleation performance of the untreated cellulose which attributes to the nonhomogeneous dispersion and incompatibility with PP.

Table 4.7 Effect of Silane-g-CF and virgin CF on the crystallinity of PP

Sample	Crystallinity (%)
Neat PP	44.2
0.5 wt% Silane-g-CF/PP	43.5
1.0 wt% Silane-g-CF/PP	43.8
3.0 wt% Silane-g-CF/PP	45.9
5.0 wt% Silane-g-CF/PP	46.7
1.0 wt% virgin CF/PP	41.0

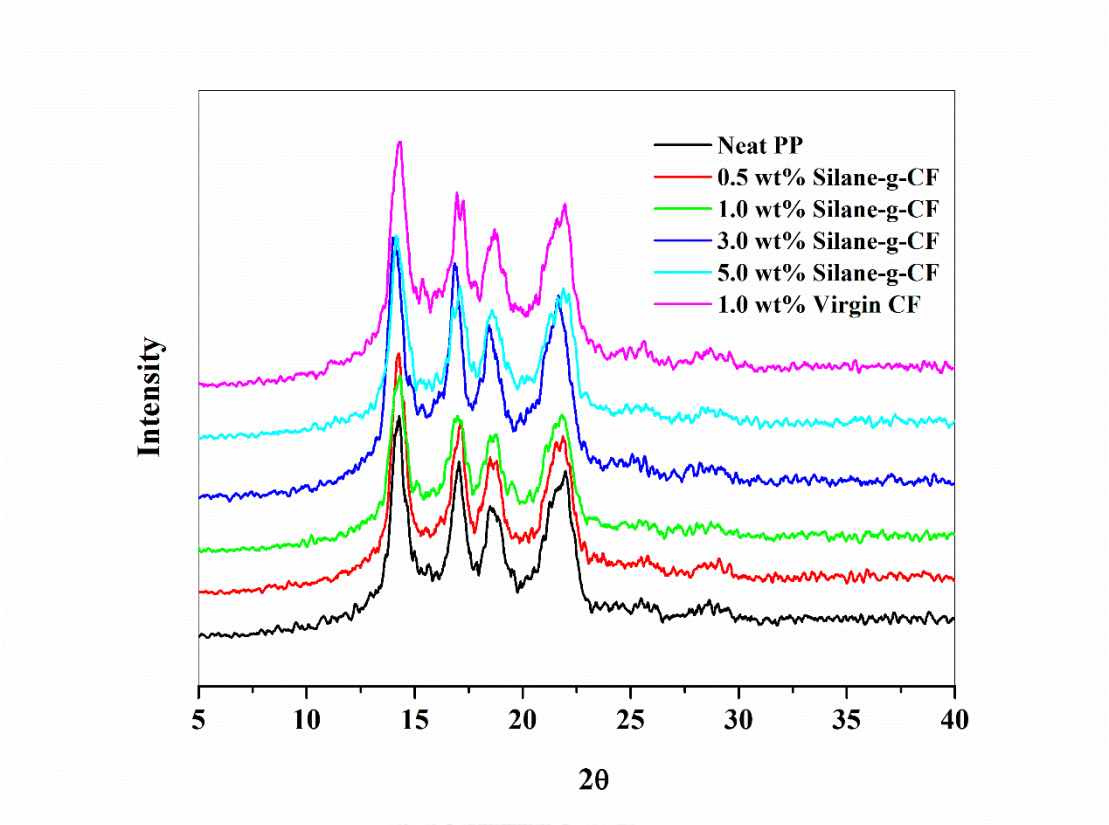

Figure 4.25 The XRD patterns of neat PP, Silane-g-CF/PP composites, and virgin CF/PP composite

4.3.5 Mechanical Properties

4.3.5.1 Tensile Properties

The effects of untreated and organosilane treated cellulose fibril on tensile properties of PP are investigated and shown in Figure 4.26, the results are summarized in Table 4.8. As seen in Figure 4.26 (a.), the addition of small amount of Silane-g-CF loading (0.5 wt%) slightly increases the tensile strength of PP but the addition of higher filler loading gradually decreases the tensile strength. The decreasing of tensile strength at higher filler loading may attribute to the effect of particle agglomeration which leads to the decreasing of mechanical properties. The addition of unmodified CF also slightly improves the tensile strength of PP, indicating the effect of cellulose fibril rigidity due to the hydrogen bonding interaction between cellulose molecules, in spite of the inhomogeneous distribution of CF in PP but the effect of CF-CF interaction could not be ignored [174]. The Young's modulus of PP is increased up to 10% by the incorporation with Silane-g-CF depending on the filler loading, corresponding to the good dispersion and the improved interfacial adhesion between CF and PP caused by the surface modification. In case of virgin CF, the addition of 1.0 wt% unmodified cellulose shows the higher Young's modulus than neat PP, attributing to the effect of hydrogen bonding network among cellulose molecules as mention earlier.

Obviously, the strain at break of PP drops dramatically when cellulose fibril was added. In case of organosilane modified cellulose fibril, the rapid decreasing of strain at break caused by the surface treatment of cellulose fibril via silanization. The silanization by hexadecyltrimethoxysilane disturbs the hydrogen bonding network between cellulose molecules, resulting in the embrittle Silane-g-CF due to the weaker cohesion force among celluloses. The embrittlement behavior of Silane-g-CF causes the decrease in strain at break which can be explained in term of the increase in interface strength [175, 176]. In case of virgin CF filled PP, the decreasing of strain at break corresponds to the incompatibility and the poor interfacial adhesion due to the hydrophilic nature of cellulose and hydrophobic nature of PP.

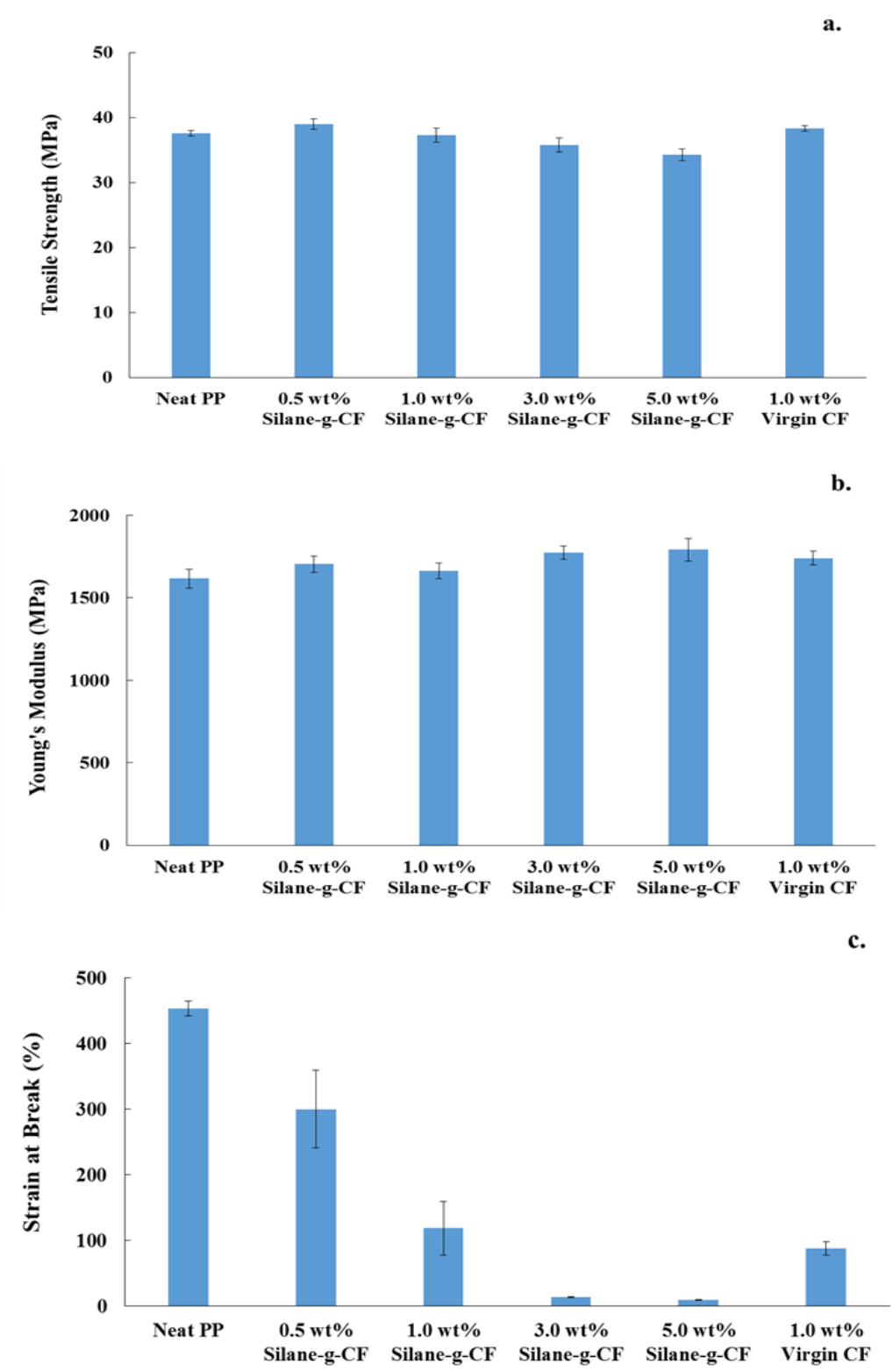

Figure 4.26 a) Tensile strength, b) Young's modulus and c.) Strain at break of neat PP Silane-g-CF/PP composites and virgin CF/PP composite

Table 4.8 Tensile properties of neat PP, Silane-g-CF/PP composites, and virgin CF/PP composite

Sample	Tensile Strength (MPa)	Young's Modulus (MPa)	Strain at Break (%)
Neat PP	37.6 ± 0.4	1616.0 ± 57.9	452.9 ± 11.3
0.5 wt% Silane-g-CF/PP	39.0 + 0.8	1704.1 ± 50.5	300.1 ± 59.4
1.0 wt% Silane-g-CF/PP	37.3 ± 1.1	1663.9 ± 46.5	118.6 ± 41.2
3.0 wt% Silane-g-CF/PP	35.8 ± 1.1	1774.2 ± 40.0	13.5 ± 0.5
5.0 wt% Silane-g-CF/PP	34.2 ± 0.9	1791.1 ± 68.3	9.7 ± 0.2
1.0 wt% virgin CF/PP	38.3 ± 0.4	1739.9 ± 41.6	87.6 ± 10.3

4.3.5.2 Impact Resistance

The impact strength reflects the toughness of materials. The toughness of fiber reinforced composites is affected by many factors such as the intrinsic properties of matrix, the volume fraction of fiber, interfacial bond strength and the test conditions such as test temperature or test speed [177, 178]. Figure 4.26 reveals the trend of impact resistance of neat PP and CF/PP composites. The addition of 0.5, 1.0, 3.0 and 5.0 wt% of Silane-g-CF increases the impact resistance of PP up to 12, 17, 20 and 19%, respectively, indicating the good interfacial adhesion between cellulose fibril and PP caused by the chemical surface treatment using the long alkyl chain organosilane. The good interfacial adhesion requires more energy to initiate the fracture when the impact loading is applied and contributes the energy dissipation [171]. Therefore, the inferior impact strength is observed in case of unmodified CF filled PP. The addition of 1.0 wt% virgin CF dramatically decreases the impact resistance of PP up to 20% caused by the low energy dissipation at the interfacial area and non-uniform stress transfer due to the poor adhesion among untreated CF and PP, resulting in the easy crack initiation and propagation.

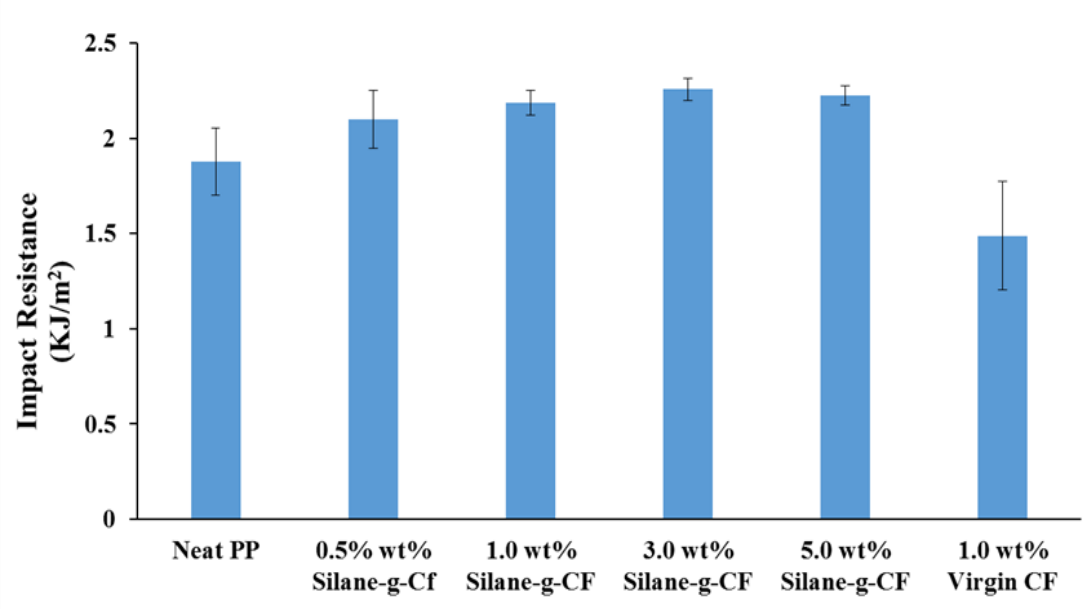

Figure 4.27 Impact resistance of neat PP, Silane-g-CF/PP composites, and virgin CF/PP composite

Table 4.9 Impact resistance of neat PP, Silane-g-CF/PP composites, and virgin CF/PP composite

Sample	Impact Resistance (KJ/m^2)
Neat PP	1.9 ± 0.2
0.5 wt% Silane-g-CF/PP	2.1 ± 0.2
1.0 wt% Silane-g-CF/PP	2.2 ± 0.1
3.0 wt% Silane-g-CF/PP	2.3 ± 0.1
5.0 wt% Silane-g-CF/PP	2.2 ± 0.1
1.0 wt% virgin CF/PP	1.5 ± 0.3

4.4 Properties of Organosilane Modified Cellulose Fibril/Polylactic acid Composites

4.4.1 Thermal Stability

The thermal decomposition of PLA is an intramolecular transesterification of polylactide, resulting in the formation of cyclic oligomers. In addition, CO, CO_2, acetaldehyde and possible H_2O from fragmentation reactions can be identified as a result of primary pyrolysis also [179]. As seen in the TG thermograms in Figure 4.28, neat PLA starts to degrade at 350 °C while the addition of Silane-g-CF into PLA just slightly increases the onset degradation temperature around 3 °C. The minor change on T_{onset} can be explained by the thermal degradation of filler. As mentioned earlier in section 4.1.6, Silane-g-CF exhibits the two degradation steps at 300 °C and 450 °C which occur in the same range of neat PLA thermal degradation. Therefore, when it was compounded with PLA, the thermal stability is slightly improved. When compared to Silane-g-CF, the addition of virgin CF remains unchanged T_{onset}, attributing to the thermal decomposition behavior of cellulose fibril which occurs before PLA around 80 °C. The small increase in thermal stability of Silane-g-CF/PLA composites can indicate the better compatibility and interfacial adhesion between organosilane modified CF and PLA when compared to unmodified CF [180]. Consequently, Silane-g-CF can be considered as a suitable processing aid for PLA. The DTG thermograms in Figure 4.29 also exhibits the little increment in maximum degradation temperature of PLA composites, indicating the effect of both unmodified and modified CF on the improvement of PLA thermal stability. The TGA data are summarized in Table 4.10.

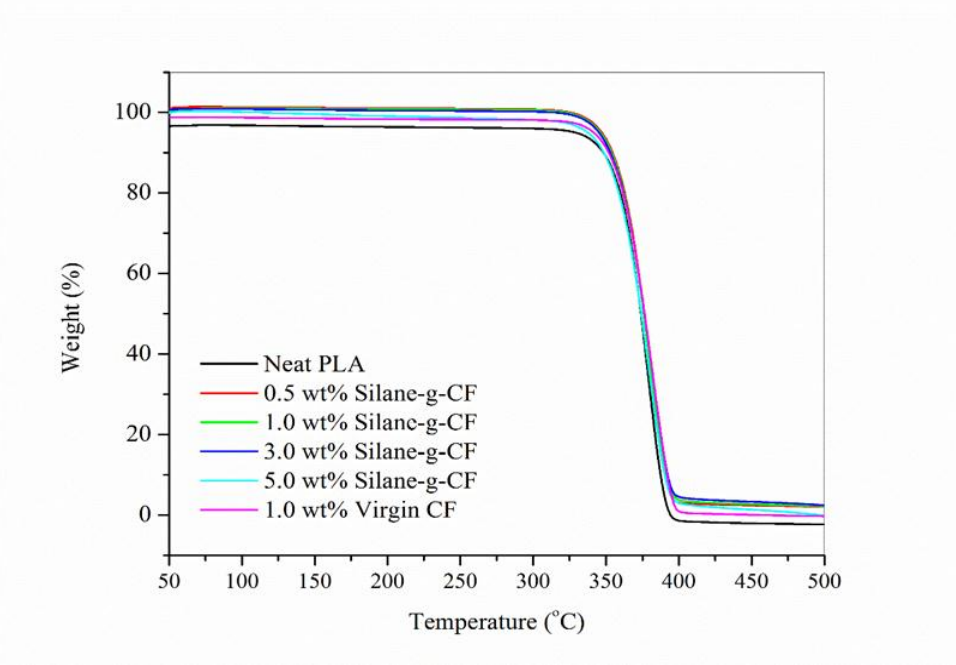

Figure 4.28 TG Thermogram of neat PLA, Silane-g-CF/PLA composites, and virgin CF/PLA composite

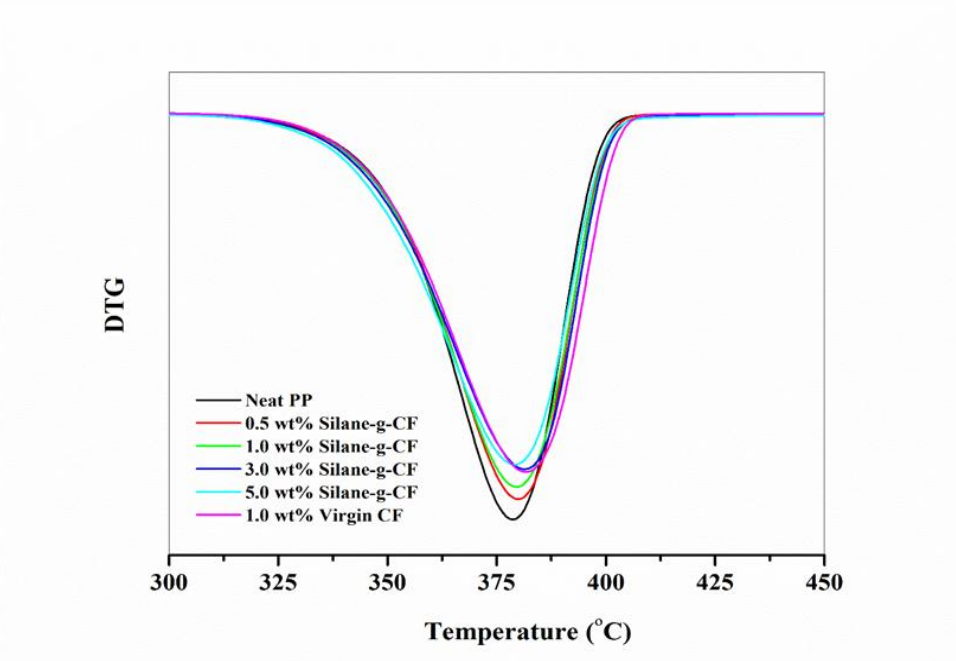

Figure 4.29 DTG Thermogram of neat PLA, Silane-g-CF/PLA composites, and virgin CF/PLA composite

Table 4.10 TGA results of neat PLA, Silane-g-CF/PLA composites, and virgin CF/PLA composite

Sample	T_{onset} (°C)	T_{max} (°C)
Neat PLA	350.5	376.0
0.5 wt% Silane-g-CF/PLA	353.3	378.7
1.0 wt% Silane-g-CF/PLA	353.8	377.9
3.0 wt% Silane-g-CF/PLA	352.8	379.0
5.0 wt% Silane-g-CF/PLA	353.1	377.1
1.0 wt% virgin CF/PLA	350.9	380.3

4.4.2 Thermal Properties

Figure 4.30 shows the second DSC heating thermograms of PLA and composites at the heating rate of 5 °C/min, which consist of glass transition temperature (T_g), cold crystallization temperature (T_{cc}) and melting temperature (T_m) indicating a characteristic of the typical semi-crystalline polymer [181]. The thermal properties obtained by DSC are summarized in Table 4.11. The heating thermograms reveal a little change in T_g of 5.0 wt% Silane-g-CF/PLA composite which is lower than neat PP. It is known that T_g is a complex phenomenon depending on several factors including intermolecular interaction, steric effects, chain flexibility, molecular weight, branching as well as crosslinking density. In this case, the decreasing of T_g at high Silane-g-CF loading probably attributes to the steric effect of filler particles that obstructs polymer chains orientation. This effect leads to an increasing of polymer matrix free volume, resulting in the decreasing of T_g [182, 183]. The T_{cc} of neat PLA is observed at 104 °C whereas PLA composites show the lower T_{cc} by 2-4 °C, approximately depending on the filler loading. This result indicates that both Silane-g-CF and virgin CF can induce the faster crystallization by acting as a nucleating agent. Cellulose fibril can promote heterogeneous nucleation mechanism which induces a decrease in free energy barrier and triggers crystallization [184].

As seen in the heating thermograms, all samples exhibit two melting peaks. Neat PLA shows the lower melting peak (T_{m1}) at 146 °C and the higher melting peak (T_{m2}) at 156 °C. This phenomenon can be explained by a large tendency of PLA crystals that can reorganize into more stable structures via continuously partial melting-recrystallization-perfection mechanism during heating scan [185]. T_{m1} relates to the melting of less perfect or small crystalline structures while T_{m2} attributes to the melting of perfectly crystalline structures [186]. In case of Silane-g-CF/PP composites, T_{m1} shifts to the lower temperature when compared to neat PLA and virgin CF filled PLA while T_{m2} remains unchanged. The shift of T_{m1} is associated with the decrease in T_{cc} which is caused by the restriction of chain segment mobility. The decrease in chain mobility is unfavorable with respect to the growth of lamellae, resulting in the smaller lamellae with lower melting temperature. When the primary lamellae melted, the chain

segments still maintained an ordered structure and then the recrystallization occurred. Since the recrystallization occurred at almost the same temperature, the newly formed lamellae had a similar thickness leading to the similar T_{m2} of all composites [187]. The effect of filler on the crystallinity of PLA is hindered by the influence of the rapid cooling rate which was employed during the cooling scan, resulting in the low degree of crystallinity due to the limited crystallization time of PLA molecular chains to orientate themselves into the crystalline morphology. Consequently, all samples become amorphous evidenced by the absence of crystallization temperature (T_c) when the cooling rate of 5 °C/min was applied as shown in Figure 4.31. In addition, Silane-g-CF can play a role as the better nucleating agent than virgin CF proved by the lower T_{cc} and the higher degree of crystallinity.

Table 4.11 Thermal properties of neat PLA, Silane-g-CF/PLA composites and virgin CF/PLA composite obtained from the second heating scan using heating rate of 5 °C /min

Filler loading	T_g (°C)	T_{cc} (°C)	ΔH_{cc} (J/g)	T_{m1} (°C)	T_{m2} (°C)	ΔH_m (J/g)	X_c (%)
Neat PLA	55.8	103.8	29.5	146.3	156.2	31.5	2.2
0.5 wt% Silane-g-CF	55.0	102.0	29.1	145.4	156.1	32.2	3.4
1.0 wt% Silane-g-CF	55.2	100.0	27.6	144.7	156.1	31.4	4.1
3.0 wt % Silane-g-CF	55.4	101.1	27.0	145.0	156.0	31.5	5.0
5.0 wt% Silane-g-CF	53.5	100.3	27.3	144.5	155.7	28.7	1.6
1.0 wt% virgin CF	55.3	102.0	28.0	146.1	156.0	31.0	3.3

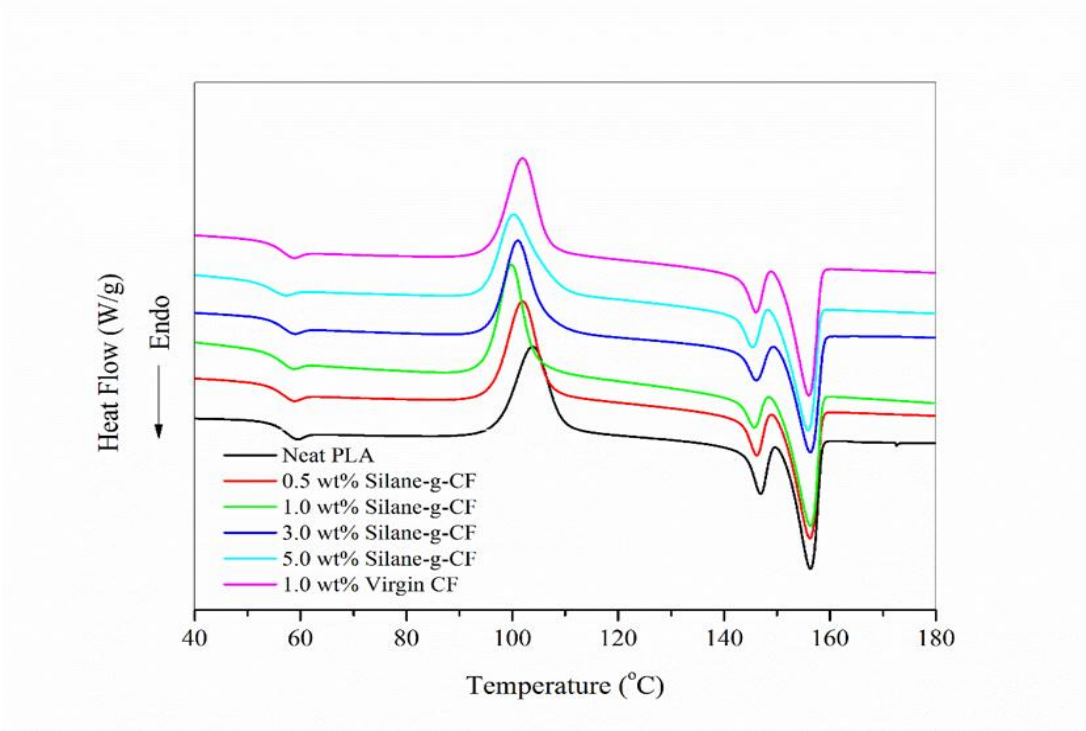

Figure 4.30 DSC second heating thermograms of neat PLA, Silane-g-CF/PLA composites, and virgin CF/PLA composite at heating rate of 5 °C/min

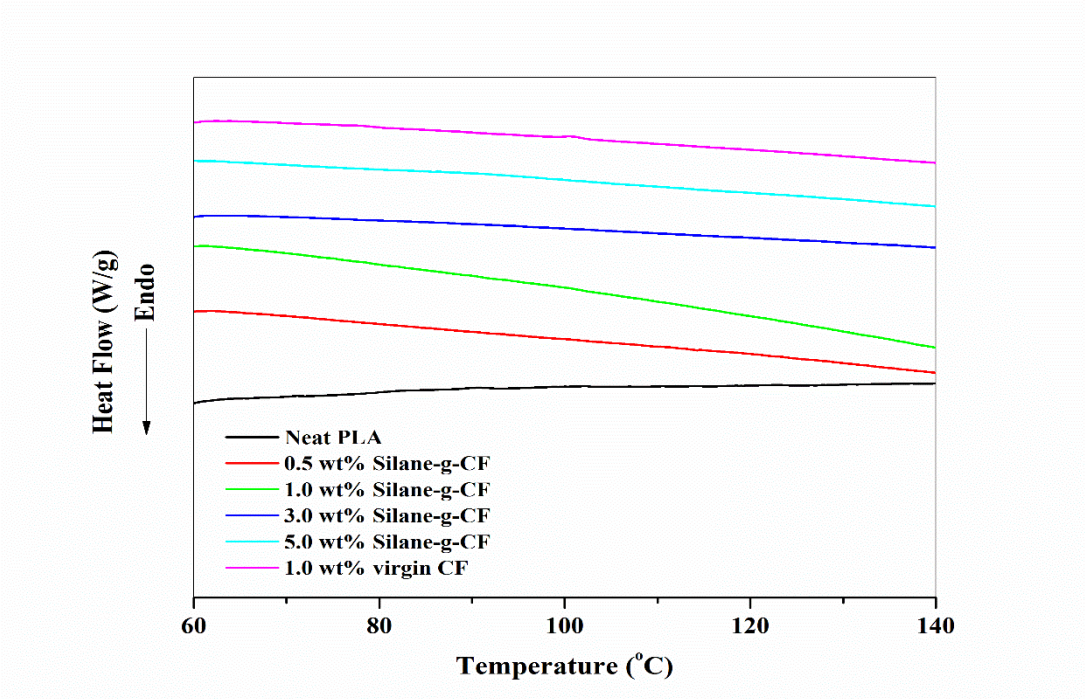

Figure 4.31 DSC second cooling thermograms of neat PLA, Silane-g-CF/PLA composites, and virgin CF/PLA composite at cooling rate of 5 °C/min

According to the effect of fast cooling rate as mentioned earlier, the thermal properties of PLA and composites were investigated again under non-isothermal condition using the slow cooling rate as 1 °C/min and a heating rate of 10 °C/min. The DSC thermograms of the second heating scan and the second cooling scan are presented in Figure 4.32 and 4.33, respectively.

The DSC endotherms of PLA and composites using the heating rate of 10 °C/min also show T_g, T_{cc} and T_m, as similar as the using of the heating rate at 5 °C/min. However, the dominant influence of the steric effect caused by filler particles is clearly observed in this case, resulting in the increasing of polymer matrix free volume. Therefore, the drastic decrease in T_g is seen when the filler content is higher. Interestingly, the T_g of PLA filled with 5.0 wt% Silane-g-CF is almost absence, indicating that the composite becomes more crystalline. The virgin CF/PLA composite still exhibits the dominant peak of T_g when compared to Silane-g-CF/PLA composites, attributing to the amorphous behavior. The addition of 0.5 wt% and 1.0 wt% Silane-g-CF into PLA composites shows the drop of cold crystallization temperature (T_{cc}) up to 7 °C. The shift of T_{cc} to lower temperature indicates that Silane-g-CF can induce the faster crystallization and enhance the crystallinity by acting as the nucleating agent. Silane-g-CF can promote the heterogeneous nucleation mechanism which induces the decrease in free energy barrier and triggers crystallization [184]. The nucleating effect of Silane-g-CF is clearly observed at higher filler loading evidenced by the absence of T_g and T_{cc}, indicating that the composites become more highly crystalline [188]. In comparison with Silane-g-CF, virgin CF also exhibits the decreasing of T_{cc} but the heat capacity of cold crystallization is higher, attributing to the poor self-nucleation of PLA. In the similar melting behavior, the two melting peaks are observed in all cases also. Neat PLA shows the lower melting peak (T_{m1}) at 147.5 °C and the higher melting peak (T_{m2}) at 155.7 °C. As mentioned earlier, T_{m1} of composites shifts to the lower temperature when compared to neat PLA, corresponding to the decreasing of T_{cc} while T_{m2} remains unchanged due to the melting behavior of the small or imperfect PLA crystals.

Figure 4.33 reveals the crystallization peak (T_c) of neat PLA and composites which cannot be found when the cooling rate of 5 °C/min was employed. The small crystallization peak of neat PLA is found at 95.6 °C whereas T_c of Silane-g-CF/PLA composites shifts to the higher temperature due to the nucleation effect of organosilane modified CF. In case of unmodified CF, the addition of 1.0 wt% virgin CF into PLA suppresses T_c to 94 °C, indicating its poorer nucleating ability when compared to Silane-g-CF. Obviously, the results confirm that Silane-g-CF performs the good nucleating ability for PLA. The addition of Silane-g-CF enhances the degree of crystallinity up to 20-29% depending on the filler content whereas virgin CF just slightly increases the degree of crystallinity around 9%. Table 4.12 presents all thermal properties of neat PLA and composites investigated under slow cooling rate.

Table 4.12 Thermal properties of neat PLA, Silane-g-CF/PLA composites, and virgin CF/PLA composite obtained from the second heating and the second cooling scan using heating rate of 10 °C /min and cooling rate of 1 °C /min.

Filler loading	T_g (°C)	T_{cc} (°C)	ΔH_{cc} (J/g)	T_{m1} (°C)	T_{m2} (°C)	ΔH_m (J/g)	T_c (°C)	X_c (%)
Neat PLA	56.0	112.1	22.6	147.5	155.7	34.8	95.6	13.1
0.5 wt% Silane-g-CF	54.3	105.3	6.0	144.8	154.8	38.7	96.7	35.3
1.0 wt% Silane-g-CF	54.5	107.2	6.6	145.1	154.8	37.3	97.1	33.3
3.0 wt% Silane-g-CF	55.0	-	-	144.6	154.8	35.4	98.7	39.2
5.0 wt% Silane-g-CF	53.7	-	-	145.0	155.0	37.0	100.7	41.9
1.0 wt% virgin CF	54.3	105.5	17.1	145.7	155.0	37.8	94.2	22.5

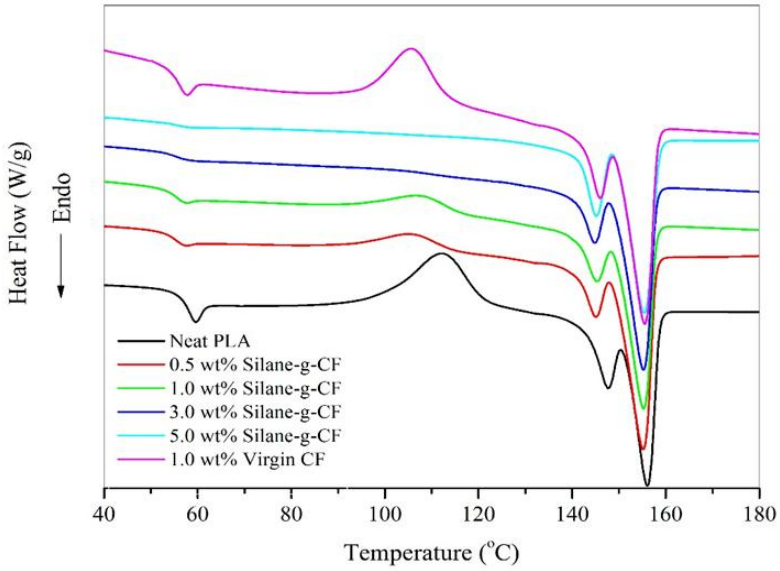

Figure 4.32 DSC second heating thermogram of neat PLA, Silane-g-CF/PLA composites, and virgin CF/PLA composite at heating rate of 10 °C/min

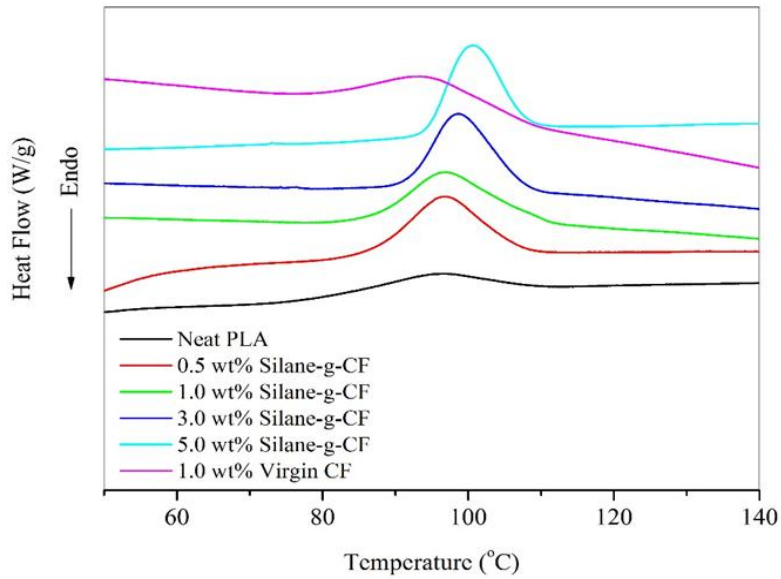

Figure 4.33 DSC second cooling thermogram of neat PLA, Silane-g-CF/PLA composites, and virgin CF/PLA composite at cooling rate of 1 °C/min

4.4.3 Fracture Surface Morphology

The cryo-fractured surface images of neat PLA, Silane-g-CF/PLA composites and virgin CF/PLA composite are presented in Figure 4.34. The brittleness characteristic is revealed by the smooth fracture surface as seen in case of neat PLA (Figure 4.34 (a.)) due to the weak resistance to crack propagation as explained earlier in section 4.3.3. On the other hand, the rougher fracture surface is observed in case of Silane-g-CF/PLA composites (Figure 4.34 (b.-e.)), depending on the increasing of filler loading. The rough surface corresponds to the high energy requirement to fracture the specimen due to the good interfacial adhesion between filler and matrix [169]. Wang et al. [189] prepared cellulose nanofiber (CNF)/PLA composites by a solvent evaporation technique, followed by a compression molding to obtain sheet specimens. The SEM micrographs of fracture surfaces also showed the smooth surface of neat PLA indicating a typical characteristic of brittle materials while the composite had very rough surface. This significant deformation reveals that the addition of Silane-g-CF is capable of enhancing PLA toughness via the energy absorption-dissipation mechanism as found in case of nanosized rigid particles such as SiO_2, TiO_2, $CaSiO_3$, Al_2O_3, carbon nanotubes and nanoclays reinforced plastics [187]. The effect of surface modification on the compatibility and interfacial adhesion between CF and PLA is confirmed by the rougher fracture surface of Silane-g-CF/PLA composites when compared to virgin CF/PLA composite (Figure 4.34 (f.)). Figure 4.35 shows the SEM micrographs of neat PLA and composites at higher magnification. Figure 4.35 (b.-e.) reveals that the Silane-g-CF is embedded in PLA while the virgin CF (Figure 4.35 (f.)) shows the debonding interface due to the incompatibility, resulting from its hydrophilic nature.

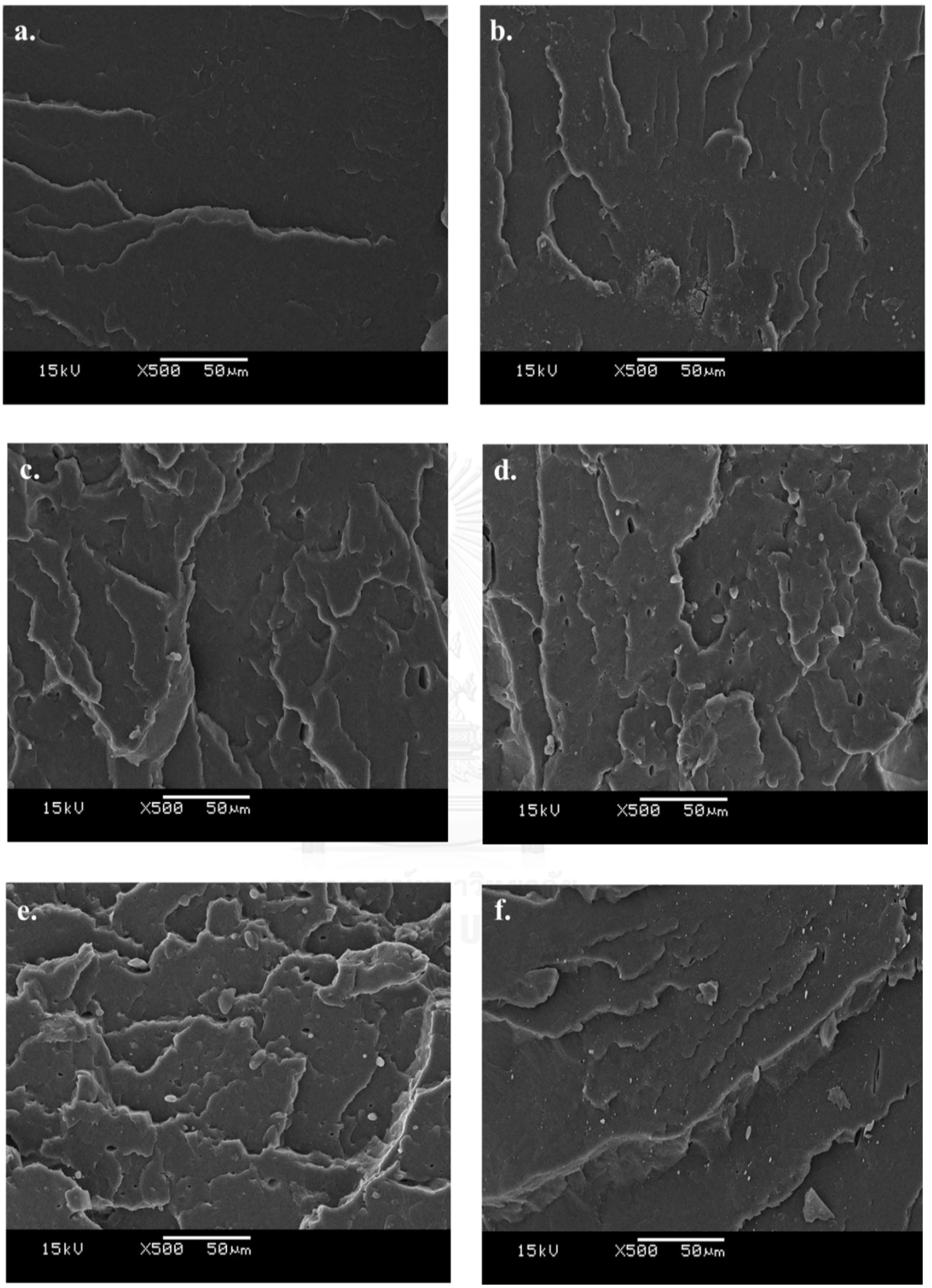

Figure 4.34 SEM micrographs (500x magnification) of cryo-fractured surface of (a.) neat PLA, (b.) 0.5 wt% Silane-g-CF/PLA composite, (c.) 1.0 wt% Silane-g-CF/PLA composite, (d.) 3.0 wt% Silane-g-CF/PLA composite, (e.) 5.0 wt% Silane-g-CF/PLA composite and (f.) 1.0 wt% virgin CF/PLA composite

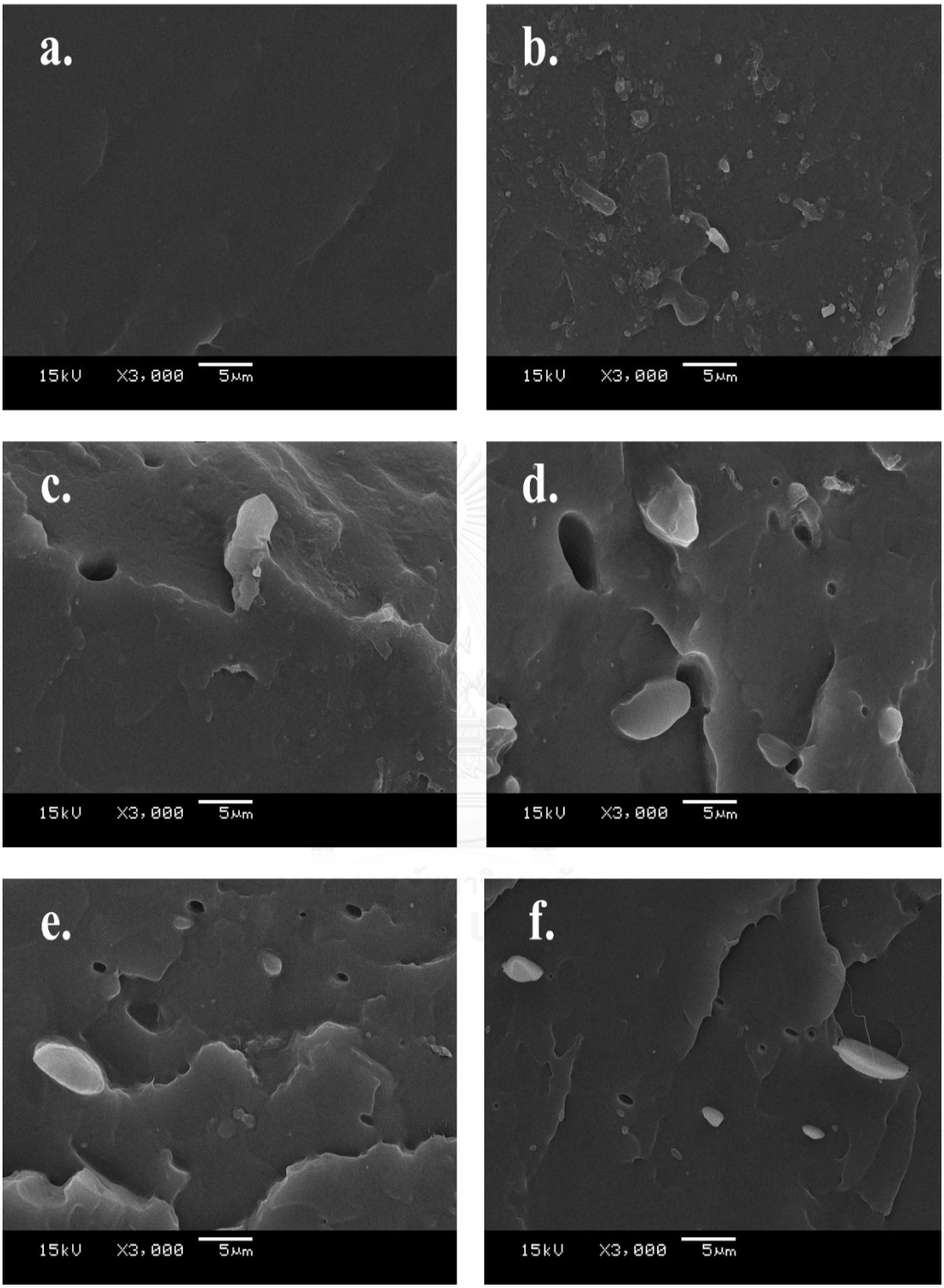

Figure 4.35 SEM micrographs (3000x magnification) of cryo-fractured surface of (a.) neat PLA, (b.) 0.5 wt% Silane-g-CF/PLA composite, (c.) 1.0 wt% Silane-g-CF/PLA composite, (d.) 3.0 wt% Silane-g-CF/PLA composite, (e.) 5.0 wt% Silane-g-CF/PLA composite and (f.) 1.0 wt% virgin CF/PLA composite

4.4.4 Crystal Morphology

Normally, the XRD pattern of neat PLA exhibits the sharp and intense diffraction peak at 2θ peak = 16.7° and 19.0°, indicating the crystalline structure of PLA [181]. The peak at 2θ = 16.7° corresponds to the reflection of 110 and 200 crystal plane of PLA while the peak at 2θ = 19.0° attributes to the 203 crystal plane [187]. However, the XRD patterns in Figure 4.36 indicate that neat PLA and all composites are in the amorphous state. This result can be explained by the effect of processing condition that leads to the lower crystallinity of materials due to the rapid cooling or demolding process [190]. In this research, the compound was cooled rapidly in the water bath during melt extrusion, resulting in the amorphous sample. The effect of rapid cooling during processing step on the crystallinity agrees with the result obtained from DSC when the fast cooling rate was employed in section 4.4.2.

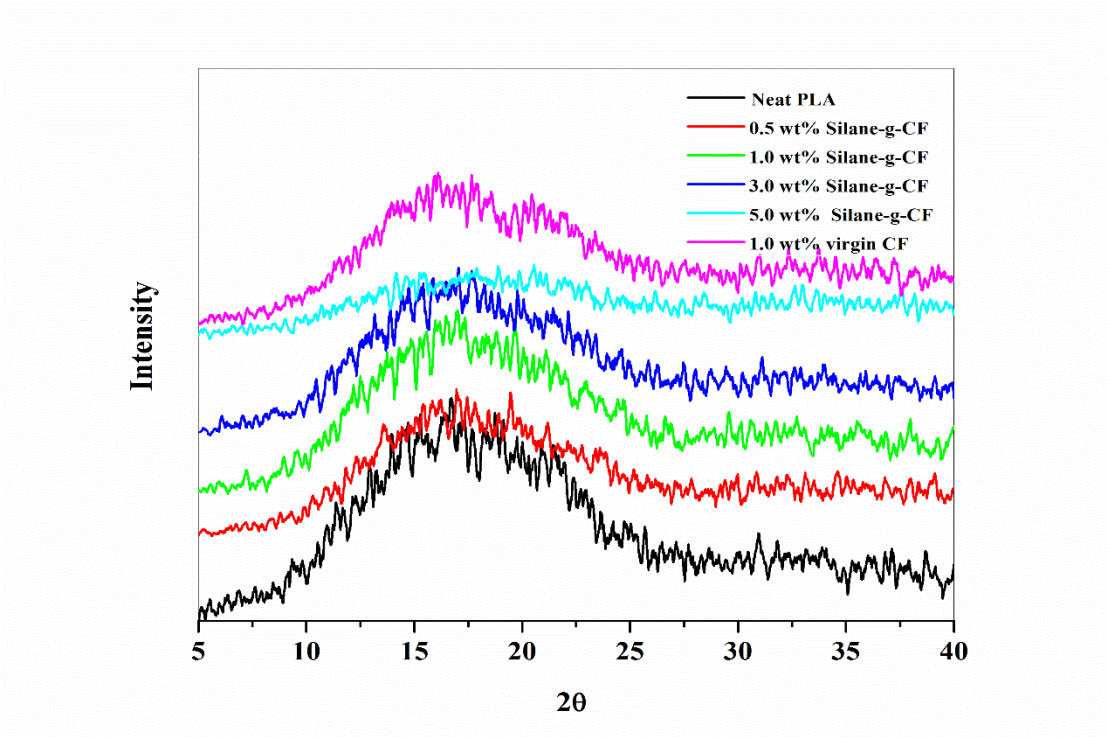

Figure 4.36 XRD patterns of neat PLA, Silane-g-CF/PLA composites, and virgin CF/PLA composite

4.4.5 Mechanical Properties

4.4.5.1 Tensile Properties

The tensile properties of neat PLA and composites are shown in Figure 4.37 and summarized in Table 4.13. Obviously, the addition of Silane-g-CF decreases both tensile strength and Young's modulus of PLA when filler loading is increased. However, the improvement of tensile properties is found in 0.5 wt% Silane-g-CF/PLA composite that the elongation at break is increased up to 50%, approximately and then slightly decreased when filler loading is higher. These results can be explained by the plasticization effect caused by the silanization of cellulose using a long alkyl chain organosilane. Therefore, Silane-g-CF can act as a plasticizer for PLA by decreasing the extensive intermolecular forces among PLA chains but increasing the mobility of PLA chain, resulting in more flexible specimens [191]. Several types of plasticizers such as citrate ester [192], poly(ethylene glycol), glucose monoesters [193, 194] and oligomeric lactic acid [195] have been used to enhance the flexibility and resilience of PLA. Consequently, plasticized PLA exhibits the increase in elongation at break with the decrease in tensile strength and Young's modulus. However, the agglomeration of Silane-g-CF when the filler loading is higher (>1.0 wt%) decreases all tensile properties of PLA. Moreover, the plasticization effect caused by the surface modification can be confirmed when compared to the tensile properties of unmodified CF filled PLA. The addition of 1.0 wt% virgin CF remains unchanged tensile properties of PLA.

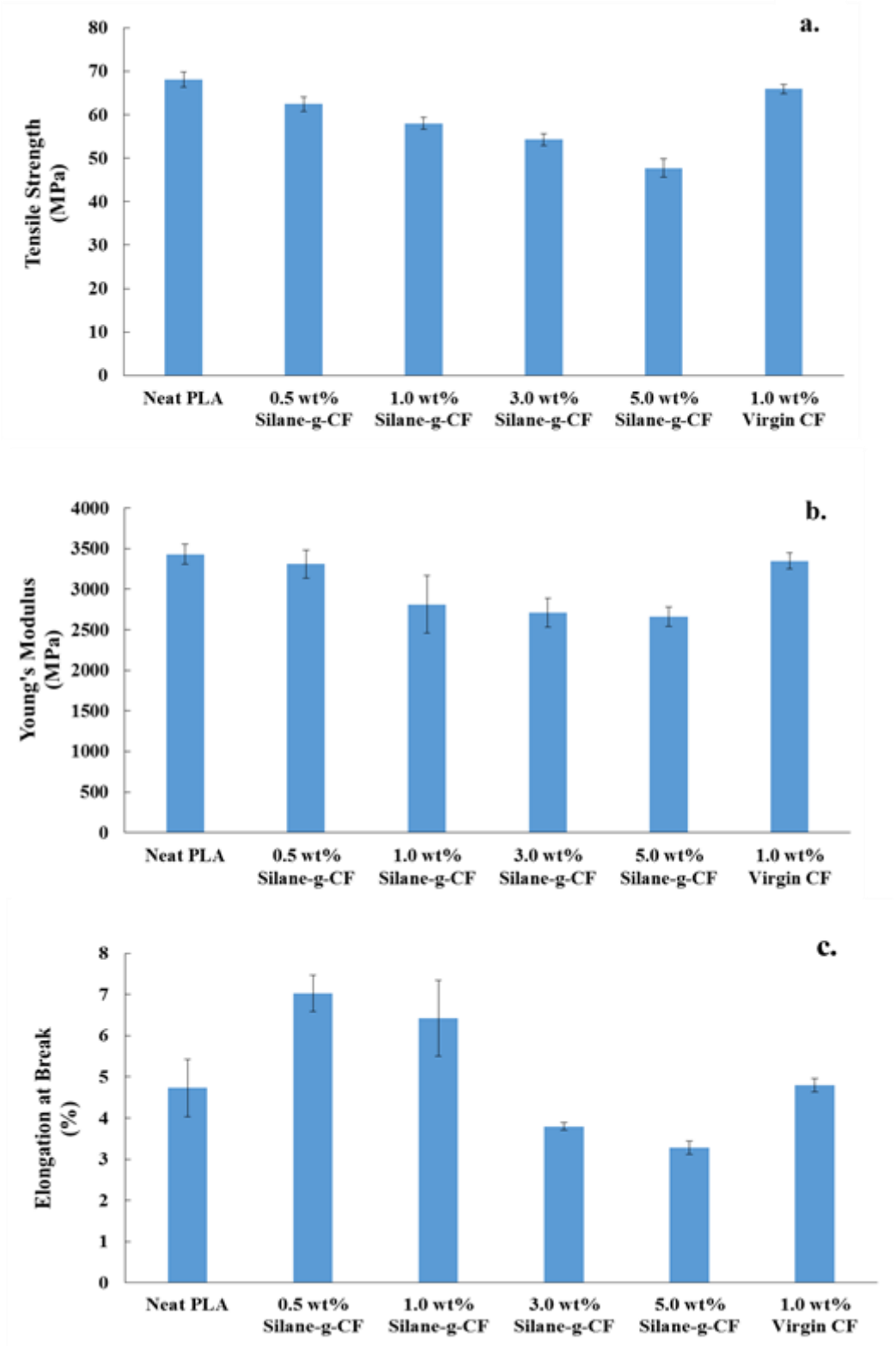

Figure 4.37 a) Tensile strength, b) Young's modulus and c.) Elongation at break of neat PLA, Silane-g-CF/PLA composites and virgin CF/PLA composite

Table 4.13 Tensile properties of neat PLA, Silane-g-CF/PLA composites and virgin CF/PLA composite

Sample	Tensile Strength (MPa)	Young's Modulus (MPa)	Elongation at Break (%)
Neat PLA	68.0 ± 1.8	3430.2 ± 126.3	4.7 ± 0.7
0.5 wt% Silane-g-CF/PLA	62.5 ± 1.7	3308.8 ± 170.9	7.0 ± 0.4
1.0 wt% Silane-g-CF/PLA	58.0 ± 1.4	2809.9 ± 354.3	6.4 ± 0.9
3.0 wt% Silane-g-CF/PLA	54.3 ± 1.3	2708.9 ± 174.2	3.8 ± 0.1
5.0 wt% Silane-g-CF/PLA	47.7 ± 2.2	2664.5 ± 119.5	3.3 ± 0.2
1.0 wt% virgin CF/PLA	65.9 ± 1.0	3345.6 ± 99.1	4.8 ± 0.2

The SEM micrographs of fracture surfaces obtained from tensile testing are shown in Figure 4.38. The fracture morphology of neat PLA exhibits smoother surface than Silane-g-CF/PLA composites which are rougher depending on the increasing of filler loadings. The rough surface reveals the better interfacial adhesion between filler and matrix, which is expected to help improve energy absorption and energy dissipation, resulting in the decreasing of brittleness while the toughness is increased. The virgin CF/PLA composite also shows the smoother fracture surface compared to Silane-g-CF/PLA composites, indicating the poor interfacial adhesion as well as the incompatibility between virgin CF and PLA that are the factors to diminish the mechanical properties of materials. However, the agglomeration of Silane-g-CF can be observed at 3.0 and 5.0 wt% filler loading, resulting in the adverse effect on mechanical properties.

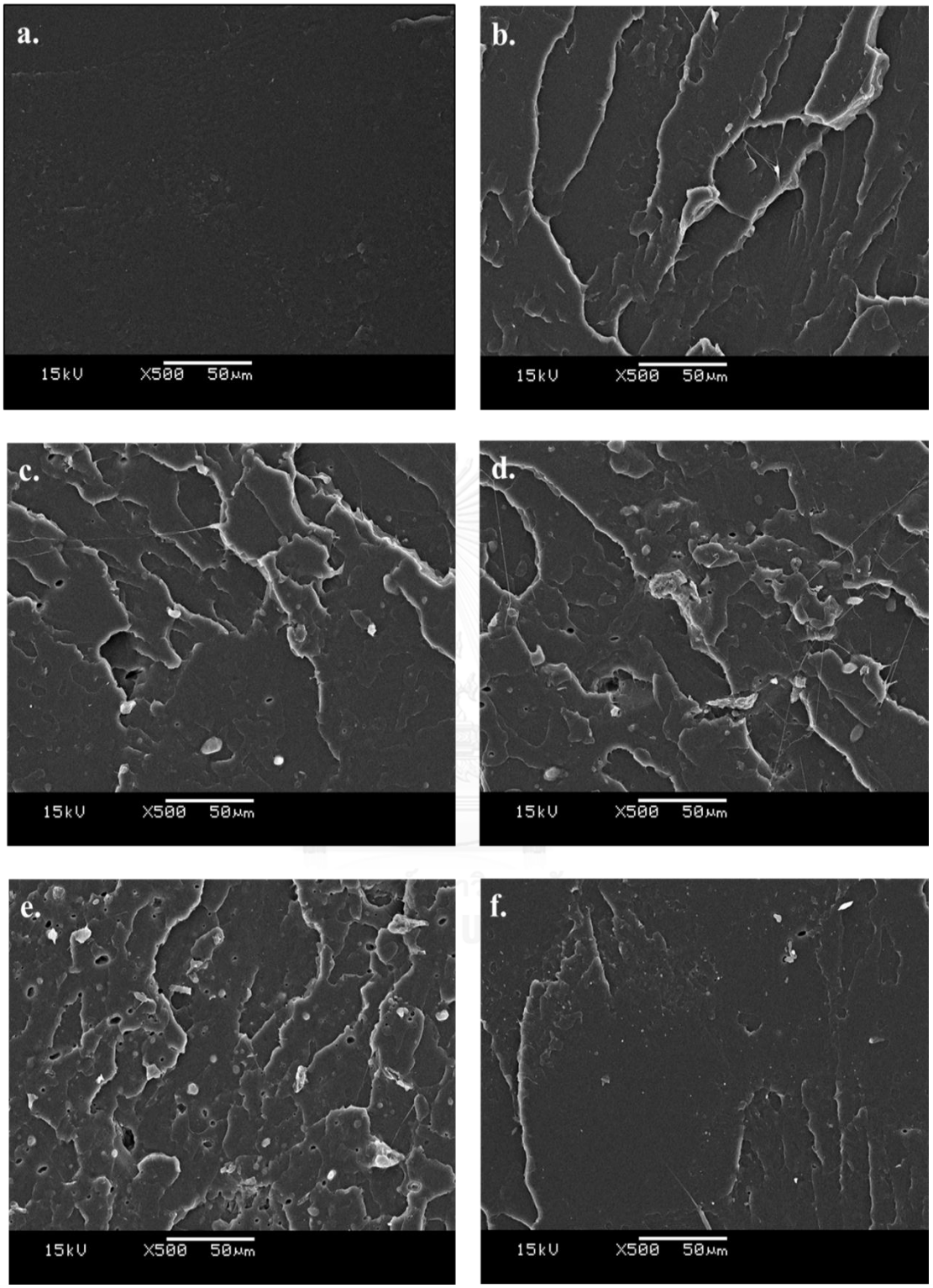

Figure 4.38 SEM micrographs of fracture morphology obtained from tensile testing of (a.) neat PLA, (b.) 0.5 wt% Silane-g-CF/PLA composite, (c.) 1.0 wt% Silane-g-CF/PLA composite, (d.) 3.0 wt% Silane-g-CF/PLA composite, (e.) 5.0 wt% Silane-g-CF/PLA composite and (f.) 1.0 wt% virgin CF/PLA composite

4.4.5.2 Impact Resistance

Figure 4.39 shows the impact resistance neat PLA and composites. The addition of 0.5, 1.0, 3.0, and 5.0 wt% of Silane-g-CF increases the impact resistance of PLA up to 10, 20, 30, and 12%, respectively. The drop of impact resistance at high filler loading corresponds to the effect of filler agglomeration. The improvement in impact resistance is indicative of the compatibility between filler and matrix. This means that Silane-g-CF plays a role in improving the properties of composite materials [196]. In this research, the surface modification of CF via silanization leads to the higher hydrophobicity of cellulose which exhibits the better compatibility as well as the interfacial adhesion between filler and matrix. Therefore, the impact resistance is improved due to the enhancement of the energy absorption and the energy dissipation, resulting in the higher toughness [197]. Obviously, the virgin CF fails to improve the brittleness of PLA and the impact resistance dramatically drops approximately by 30%. This result is caused by the poor interfacial adhesion as well as the incompatibility between cellulose and the hydrophobic polymer matrix.

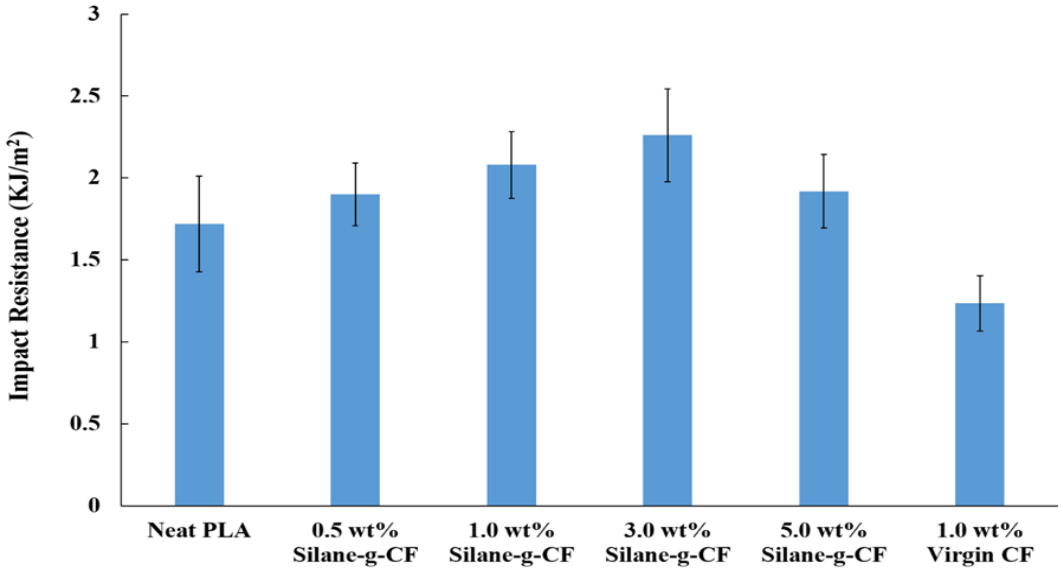

Figure 4.39 Impact resistance of neat PLA, Silane-g-CF/PLA composites and virgin CF/PLA composite

Table 4.14 Impact resistance of neat PLA, Silane-g-CF/PLA composites and virgin CF/PLA composite

Sample	Impact Resistance (KJ/m^2)
Neat PLA	1.7 $\pm$ 0.3
0.5 wt% Silane-g-CF/PLA	1.9 $\pm$ 0.2
1.0 wt% Silane-g-CF/PLA	2.1 $\pm$ 0.2
3.0 wt% Silane-g-CF/PLA	2.3 $\pm$ 0.3
5.0 wt% Silane-g-CF/PLA	1.9 $\pm$ 0.2
1.0 wt% virgin CF/PLA	1.2 $\pm$ 0.2

CHAPTER V
CONCLUSIONS

The preparation of cellulose fibril (CF) was succeeded by the new innovative technique based on the dissolution and precipitation of cellulose. Microcrystalline cellulose (MCC) obtained from the acid hydrolysis of cotton fabric waste was completely dissolved in NaOH/urea/distilled water solution (7:12:81 by weight) at -5 °C. The starch solution was added into MCC solution. The mixed solution was precipitated in HCl solution, followed by washing with distilled water and filtration. Then, cellulose fibril was obtained and investigated. The results show that:

i. The water retention value of CF is higher than MCC by 1800%, indicating the larger surface area of CF due to the small size caused by the anti-coagulating effect of starch molecules that prevents the agglomeration of cellulose fibril during the precipitation step.

ii. Cellulose fibril exhibits the web-like morphology with the diameter range of 10-40 nm and the length more than 500 nm.

iii. The FT-IR spectrum of CF presents the characteristic absorption bands of typical cellulose with the broad O-H stretching band between 3200 to 3600 cm^{-1} along with the absorption band at 1640 cm^{-1} which corresponds to the absorption band of bound water, indicating the extremely high water content which presents in CF network.

iv. The XRD pattern of CF reveals the amorphous structure due to the regeneration of MCC solution and the anti-coagulating effect of starch solution.

The surface of CF was modified by the two modifying agents including malenized soybean oil and hexadecyltrimethoxysilane to obtain malenized soybean oil modified CF (Oil-g-CF) and hexadecyltrimethoxysilane modified CF (Silane-g-CF). The properties of two modified cellulose fibrils indicate that:

i. The surface modification of CF was successful via two methods proved by the disappearance of O-H band at 3400 cm^{-1} and the existence of the two absorption bands of symmetric and asymmetric stretching vibration of CH_2 groups as well as the absorption band of the carbonyl vibration in case of Oil-g-CF while Silane-g-CF shows the strong absorption bands of the symmetric and asymmetric vibrations of silane CH_2 moieties and the absorption bands of the partially free silica silanol (Si-OH) groups along with the rocking and symmetric stretching of SiO_2 intertetrahedral oxygen atoms at 450 cm^{-1} and 800 cm^{-1}.

ii. The morphology of modified CF exhibits the large agglomerate caused by the surface hydrophobicity characteristic. However, the particles pack loosely together, evidenced by the high swelling in toluene. The average particle size diameter of Silane-g-CF and Oil-g-CF is 850 and 1700 nm, respectively.

iii. The XRD patterns of both modified cellulose fibril show the rising of crystallinity from the amorphous structure to Cellulose II crystal structure caused by its crystalline characteristic by nature that prefers self-orientation under the suitable condition.

iv. The onset degradation temperature of modified CF is higher than unmodified CF indicating the better thermal stability.

The properties of Oil-g-CF/PP composites and Silane-g-CF/PP composites were studied to find out the most efficient modified filler. The PP composites filled with 4.0 wt% filler loading were prepared by the simple melt mixing method. The properties of composites were investigated and can be concluded as follows:

i. Silane-g-CF shows the better dispersion in PP than Oil-g-CF. However, the agglomeration was found in both types, resulting in the larger particle size than the original.

ii. The crystalline morphology of Oil-g-CF/PP composite and Silane-g-CF/PP composite exhibits the higher spherulite density and smaller spherulite size compared to neat PP, indicating the ability as a nucleating agent for PP.

iii. The addition of Oil-g-CF and Silane-g-CF in PP can enhance the thermal stability of PP judged by the increasing of the onset degradation temperature and the maximum degradation temperature up to 20°C.

iv. Silane-g-CF performs as the more efficient nucleating agent for PP than Oil-g-CF evidenced by the rising of melting temperature up to 6 °C, the increasing of degree of crystallinity by 11% as well as the increasing of crystallization temperature around 4 °C, indicating the better compatibility and interaction between Silane-g-CF and PP whereas the nucleation effect of Oil-g-CF is hindered by the plasticization effect caused by the bulky molecular structure of malenized soybean oil, resulting in the small increment of melting temperature, crystallization temperature, and degree of crystallinity.

According to the better properties of Silane-g-CF, Silane-g-CF reinforced PP composites with the filler content of 0.5, 1.0, 3.0 and 5.0 wt% was prepared by the twin screw extrusion, followed by the injection molding. The properties of composites show that:

i. Silane-g-CF/PP composites exhibit the better thermal stability than neat PP depending on the amount of filler. The good dispersion and interaction of Silane-g-CF in PP hinders the diffusion of volatile compounds during the decomposition, resulting in the delayed onset degradation temperature.

ii. Silane-g-CF plays a role as the nucleating agent for PP by increasing the degree of crystallinity and raising the crystallization temperature up to 5 °C, corresponding to the increasing of the nucleation sites.

iii. The rougher fracture surface of Silane-g-CF/PP composites is observed clearly when compared to neat PP and virgin CF/PP composite, indicating the improvement of interfacial adhesion between CF and PP due to the silanization surface treatment.

iv. The XRD patterns of Silane-g-CF/PP composites confirms the ability of Silane-g-CF as the nucleating agent judged by the raising of PP crystallinity.

v. The addition of Silane-g-CF improves the Young's modulus of PP up to 10% due to the good compatibility and interfacial adhesion between two phases while the increasing of tensile strength is found when the small amount of Silane-g-CF was added. However, the elongation at break is decreased due to the embrittlement of Silane-g-CF.

vi. The impact resistance of PP is increased up to 20% by the addition of Silane-g-CF, reflecting the enhancement of material toughness caused by the better interfacial adhesion between Silane-g-CF and PP.

To prepare the fully bio-based material, Silane-g-CF was used as the reinforcement of polylactic acid composites. The composites were prepared following the same method as Silane-g-CF/PP composites. The properties of composites indicate that:

i. The addition of Silane-g-CF just slightly improves the thermal stability of PLA, attributing to the nearby thermal degradation temperature of filler and matrix.

ii. The effect of Silane-g-CF as the nucleating agent is clearly observed by DSC using the slow cooling rate of 1 $^{\circ}$C/min. The absence of glass transition temperature and cold crystallization temperature of PLA can be seen at high filler loading, indicating the more crystallinity of composites that increases up to 30%. Silane-g-CF also accelerates the crystallization process of PLA, evidenced by the raising of crystallization temperature around 5 $^{\circ}$C.

iii. The rough fracture surface of Silane-g-CF/PLA composites confirms the good interfacial adhesion between filler and matrix, attributing to the enhancement of material toughness.

iv. As seen in the XRD patterns, not only neat PLA but also CF/PLA composites exhibits the amorphous structure due to the effect of processing condition when the sample was cooled rapidly.

v. The plasticization effect of Silane-g-CF caused by the long alkyl chain of organosilane leads to the decreasing of the extensive intermolecular forces

among PLA chains while the mobility of PLA chain is increased, resulting in the more flexible specimens. The elongation at break of Silane-g-CF/PLA composites is higher than neat PLA and virgin CF/PLA composite up to 50% at 0.5 wt% filler loading in contrast with the decreasing of tensile strength and Young's modulus. However, the decreasing of all tensile properties can be found when filler loading is higher.

vi. The addition of Silane-g-CF can increase the impact resistance of PLA up to 30% due to the ability to absorb and dissipate energy caused by the good interfacial adhesion between filler and matrix, resulting in the increasing of PLA toughness.

REFERENCES

1. Lavoine, N., Desloges, I., Dufresne, A., and Bras, J., *Microfibrillated cellulose-its barrier properties and applications in cellulosic materials: a review.* Carbohydr Polym, 2012. **90**(2): p. 735-64.
2. Samir, M. A. S. A., Alloin, F., Paillet, M., and Dufresne, A., *Tangling effect in fibrillated cellulose reinforced nanocomposites.* Macromolecules, 2004. **37**(11): p. 4313-4316.
3. Simon, J., Miller, H. P., Koch, R., and Miiller, V., *Thermoplastic and biodegradable polymers of cellulose.* Polymer Degradation and Stability, 1998. **59**(1-3): p. 107-115.
4. Heinze, T. and Liebert, T., *Unconventional methods in cellulose functionalization.* Progress in Polymer Science, 2001. **26**(9): p. 1689-1762.
5. Aulin, C., Ahola, S., Josefsson, P., Nishino, T., Hirose, Y., Osterberg, M., and Wagberg, L., *Nanoscale cellulose films with different crystallinities and mesostructures;Their surface properties and interaction with water.* Langmuir, 2009. **25**(13): p. 7675-7585.
6. Siqueira, G., Bras, J., and Dufresne, A., *Cellulosic bionanocomposites: A review of preparation, properties and applications.* Polymers, 2010. **2**(4): p. 728-765.
7. Credou, J. and Berthelot, T., *Cellulose: from biocompatible to bioactive material.* Journal of Materials Chemistry B, 2014. **2**: p. 4767-4788.
8. Klemm, D., Schmauder, H., and Heinze, T., *Cellulose*, in *Biopolymers Online*, A. Steinbüchel, Editor. 2005, Wiley-VCH Verlag GmbH & Co. KGaA. p. 275-312.
9. Heinze, T., *Cellulose: Structure and properties*, in *Cellulose Chemistry and Properties: Fibers, Nanocelluloses and Advanced Materials*, O.J. Rojas, Editor. 2015, Springer: Switzerland. p. 1-52.
10. Habibi, Y., Lucia, L. A., and Rojas, O. J., *Cellulose nanocrystals: Chemistry, self-Assembly, and applications.* Chemical Reviews, 2010. **110**(63479-3500): p. 3479-3500.

11. Miao, C. and Hamad, W. Y., *Cellulose reinforced polymer composites and nanocomposites: a critical review.* Cellulose, 2013. **20**(5): p. 2221-2262.
12. Thoorens, G., Krier, F., Leclercq, B., Carlin, B., and Evrard, B., *Microcrystalline cellulose, a direct compression binder in a quality by design environment—A review.* International Journal of Pharmaceutics, 2014. **473**(1-2): p. 64-72.
13. Mathew, A. P., Oksman, K., and Sain, M., *Mechanical properties of biodegradable composites from polylactic acid (PLA) and microcrystalline cellulose (MCC).* Journal of Applied Polymer Science, 2005. **97**(5): p. 2014-2025.
14. Dong, X. M., Revol, J. F., and Gray, D. G., *Effect of microcrystallite preparation conditions on the formation of colloid crystals of cellulose.* Cellulose, 1998. **5**(1): p. 19-32.
15. Samir, M. A. S. A., Alloin, F., Sanchez, J. Y., Kissi, N. E., and Dufresne, A., *Preparation of cellulose whiskers reinforced nanocomposites from an organic medium suspension.* Macromolecules, 2004. **37**(4): p. 1386-1393.
16. Helbert, W., Cavaillé, J. Y., and Dufresne, A., *Thermoplastic nanocomposites filled with wheat straw cellulose whiskers. Part I: Processing and mechanical behavior.* Polymer Composites, 1996. **17**(4): p. 604-611.
17. Dinand, E., Chanzy, H., and Vignon, R. M., *Suspensions of cellulose microfibrils from sugar beet pulp.* Food Hydrocolloids, 1999. **13**(3): p. 275-283.
18. Chen, D., Lawton, D., Thompson, M. R., and Liu, Q., *Biocomposites reinforced with cellulose nanocrystals derived from potato peel waste.* Carbohydrate Polymers, 2012. **90**(1): p. 709-716.
19. Araki, J., Wada, M., Kuga, S., and Okano, T., *Influence of surface charge on viscosity behavior of cellulose microcrystal suspension.* Journal of Wood Science, 1999. **45**(3): p. 258-261.
20. Sakurada, I., Nukushina, Y., and Ito, T., *Experimental determination of the elastic modulus of crystalline regions in oriented polymers.* Journal of Polymer Science Part A: Polymer Chemistry, 1962. **57**(165): p. 651-660.
21. Zimmermann, T., Pohler, E., and Geiger, T., *Cellulose fibrils for polymer reinforcement.* Advanced Engineering Materials, 2004. **6**(9): p. 756-761.

22. Carlmark, A., Larsson, E., and Malmström, E., *Grafting of cellulose by ring-opening polymerisation – A review.* European Polymer Journal, 2012. **48**(10): p. 1646–1659.

23. Abdul Khalil, H. P. S., Bhat, A. H., and Ireana Yusra, A. F., *Green composites from sustainable cellulose nanofibrils: A review.* Carbohydrate Polymers, 2012. **87**(2): p. 963-979.

24. Siró, I. and Plackett, D., *Microfibrillated cellulose and new nanocomposite materials: a review.* Cellulose, 2010. **17**(3): p. 459-494.

25. Bhatnagar, A. and Sain, M., *Processing of cellulose nanofiber-reinforced composites.* Journal of Reinforced Plastic & Composites, 2005. **24**(12): p. 1259-1268.

26. Alila, S., Besbes, I., Vilar, M. R., Mutjé, P., and Bouf, S., *Non-woody plants as raw materials for production of microfibrillated cellulose (MFC): A comparative study.* Industrial Crops and Products, 2013. **41**: p. 250-259.

27. Spence, K. L., Venditti, R. A., Habibi, Y., Rojas, O. J., and Pawlak, J. J., *The effect of chemical composition on microfibrillar cellulose films from wood pulps: Mechanical processing and physical properties.* Bioresource Technology, 2010. **101**(15): p. 5961-5968.

28. Pääkkö, M., Ankerfors, M., Kosonen, H., Nykänen, A., Ahola, S., Österberg, M., Ruokolainen, J., Laine, J., Larsson, P. T., Ikkala, O., and Lindström, T., *Enzymatic hydrolysis combined with mechanical shearing and high-pressure homogenization for nanoscale cellulose fibrils and strong gels.* Biomacromolecules, 2007. **8**(6): p. 1934-1941.

29. Anonymous, in *Kirk-Othmer Encyclopedia of Chemical Technology*, Arza Seidel and Mickey Bickford, Editors. 2004, Wiley-Interscience.

30. Nakagaito, A. N., Iwamoto, S., and Yano, H., *Bacterial cellulose: the ultimate nano-scalar cellulose morphology for the production of high-strength composites.* Applied Physics A, 2005. **80**(1): p. 93-97.

31. Czaja, W., Krystynowicz, A., Kawecki, M., Wysota, K., Sakiel, S., Wróblewski, P., Glik, J., Nowak, M., and Bielecki, S., *Cellulose: Molecular and structural biology*.

Biomedical Applications of Microbial Cellulose in Burn Wound Recovery. 2007: Springer Netherlands.

32. Juntaro, J., Pommet, M., Kalinka, G., Mantalaris, A., Shaffer, M. S. P., and Bismarck, A., *Creating hierarchical structures in renewable composites by attaching bacterial cellulose onto sisal fibers.* Advanced Materials, 2008. **20**(16): p. 3122-3126.
33. Shah, J. and Brown Jr., R. M., *Towards electronic paper displays made from microbial cellulose.* Applied Microbiology and Biotechnology, 2005. **66**(4): p. 352-355.
34. Evans, B. R., O'Neill, H. M., Malyvanh, V. P., Lee, I., and Woodward, J., *Palladium-bacterial cellulose membranes for fuel cells.* Biosensors and Bioelectronics, 2003. **18**(7): p. 917–923.
35. Vilay, V., Mariatti, M., Taib, R. M., and Todo, M., *Effect of fiber surface treatment and fiber loading on the properties of bagasse fiber–reinforced unsaturated polyester composites.* Composites Science and Technology, 2008. **68**(3-4): p. 631-638.
36. Zárate, C. N., Aranguren, M. I., and Reboredo, M. M., *Thermal degradation of a phenolic resin, vegetable fibers, and derived composites.* Journal of Applied Polymer Science, 2008. **107**(5): p. 2977-2985.
37. Zhou, Y., Pervin, F., Rangari, V. K., and Jeelani, S., *Fabrication and evaluation of carbon nano fiber filled carbon/epoxy composite.* Materials Science and Engineering: A, 2006. **426**(1-2): p. 221-228.
38. Setua, D. K. and De, S. K., *Short silk fibre reinforced nitrile rubber composites.* Journal of Materials Science, 1984. **19**(3): p. 983-999.
39. Rezaei, F., Yunus, R., Ibrahim, N. A., and Mahdi, E. S., *Development of short-carbon-fiber-reinforced polypropylene composite for car bonnet.* Polymer-Plastics Technology and Engineering, 2008. **47**(4).
40. Lu, W., Lin, H., and Chen, G., *Voltage-induced resistivity relaxation in a high-density polyethylene/graphite nanosheet composite.* Journal of Polymer Science Part B: Polymer Physics, 2007. **45**(7): p. 860-863.

41. Chazeau, L., Cavaille, J. Y., Canova, G., Dendievel, R., and Boutherin, B., *Viscoelastic properties of plasticized PVC reinforced with cellulose whiskers.* Journal of Applied Polymer Science, 1999. **71**(11): p. 1797-1808.

42. Chen, J. and Tsubokawa, N., *Electric properties of conducting composite from poly(ethylene oxide) and poly(ethylene oxide)-grafted carbon black in solvent vapor.* Polymer Journal, 2000. **32**: p. 729-736.

43. Bondeson, D. and Oksman, K., *Dispersion and characteristics of surfactant modified cellulose whiskers nanocomposites.* Composite Interfaces, 2007. **14**(7-9): p. 617-630.

44. Singh, S., Mohanty, A. K., Sugie, T., Takai, Y., and Hamada, H., *Renewable resource based biocomposites from natural fiber and polyhydroxybutyrate-co-valerate (PHBV) bioplastic.* Composites Part A: Applied Science and Manufacturing, 2008. **39**(5): p. 875–886.

45. Dufresne, A., *Dynamic mechanical analysis of the interphase in bacterial polyester/cellulose whiskers natural composites.* Composite Interfaces, 2000. **7**(1): p. 53-67.

46. Kvien, I., Sugiyama, J., Votrubec, M., and Oksman, K., *Characterization of starch based nanocomposites.* Journal of Materials Science, 2007. **42**(19): p. 8163-8171.

47. Gindl, W. and Keckes, J., *All-cellulose nanocomposite.* Polymer Composites, 2005. **46**(23): p. 10221–10225.

48. Saheb, D. N. and Jog, J. P., *Natural fiber polymer composites: A review.* Advances in Polymer Technology, 1999. **18**(4): p. 351-363.

49. John, M. J. and Thomas, S., *Biofibres and biocomposites.* Carbohydrate Polymers, 2008. **71**: p. 343-364.

50. Mohanty, A. K., Misra, M., and Drzal, L. T., *Sustainable bio-composites from renewable resources: Opportunities and challenges in the green materials world.* Journal of Polymers and the Environment, 2002. **10**(1): p. 19-26.

51. Anonymous. *Technologies and products of natural fibre composites*. CIP-EIP-Eco-Innovation-2008: Pilot and market replication projects - ID: ECO/10/277331

2008 [cited 2016 June 3]; Available from: http://www.celluwood.com/LinkClick.aspx?fileticket=F6U7DtrDqow=.

52. Jayaraman, K., *Manufacturing sisal–polypropylene composites with minimum fibre degradation.* Composites Science and Technology, 2003. **63**(3-4): p. 367–374.

53. Satyanarayana, K. G., Ravikumar, K. K., Sukumaran, K., Mukherjee, P. S., Pillai, S. G. K., and Kulkarni, A. G., *Structure and properties of some vegetable fibres.* Journal of Materials Science, 1986. **21**(1): p. 57-63.

54. Suddell, B. C. and Evans, W. J., *Natural fiber composites in automotive applications*, in *Natural Fibers, Biopolymers, and Biocomposites*, Amar K. Mohanty, Manjusri Misra, and Lawrence T. Drzal, Editors. 2005, CRC Press USA.

55. Tingaut, P., Zimmermann, T., and Lopez-Suevos, F., *Synthesis and characterization of bionanocomposites with tunable properties from poly(lactic acid) and acetylated microfibrillated cellulose.* Biomacromolecules, 2010. **11**(2): p. 454-464.

56. Bulota, M., Kreitsmann, K., Hughes, M., and Paltakari, J., *Acetylated microfibrillated cellulose as a toughening agent in poly(lactic acid).* Journal of Applied Polymer Science, 2012. **126**(S1): p. E449–E458.

57. Goussé, C., Chanzy, H., Cerrada, M. L., and Fleury, E., *Surface silylation of cellulose microfibrils: preparation and rheological properties.* Polymer, 2004. **45**(5): p. 1569–1575.

58. Plueddemann, E. P., *Silane coupling agents*. 2 ed. 1991, USA: Springer US.

59. Papirer, E. and Balard, H., *Influence of surface chemistry and surface morphology on the acid-base interaction capacities of glass fibers and silicas.* Journal of Adhesion Science and Technology, 1990. **4**(8): p. 653.

60. Chu, C. W., Kirby, D. P., and Murphy, P. D., *Interactions of aminosilane with alumina and silica substrates deposited from nonaqueous and aqueous media.* Journal of Adhesion Science and Technology, 1993. **7**(5): p. 417-433.

61. Sabata, A., Van Ooij, W. J., Koch, R. J., and Adhesion, J., *The interphase in painted metals pretreated by functional silanes.* Journal of Adhesion Science and Technology, 1993. **7**(11): p. 1153-1170.

62. Weaver, K. D., Stoffer, J. O., and Day, D. E., *Interfacial bonding and optical transmission for transparent fiberglass/poly(methyl methacrylate) composites.* Polymer Composites, 1995. **16**(2): p. 161-169.

63. Plueddeman, E. P., Journal of Paint Technology, 1968. **40**: p. 516.

64. Plueddeman, E. P., *Applied polymer symposium*. 1972, New York: Wiley.

65. Salon, M. C. B., Abdelmouleh, M., Boufi, S., Belgacem, M. N., and Gandini, A., *Silane adsorption onto cellulose fibers: Hydrolysis and condensation reactions.* Journal of Colloid and Interface Science, 2005. **289**(1): p. 249-261.

66. Vrancken, K. C., Coster, L. D., Voort, P. V. D., Grobet, P. J., and Vansant, E. F., *The role of silanols in the modification of silica gel with aminosilanes.* Journal of Colloid and Interface Science, 1995. **170**(1): p. 71-77.

67. Vrancken, K. C., Voort, P. V. D., Gillis-D'Hamers, I. , Etienne F. Vansant, E. F., and Grobet, P., *Influence of water in the reaction of γ-aminopropyltriethoxysilane with silica gel. A Fourier-transform infrared and cross-polarisation magic-angle-spinning nuclear magnetic resonance study.* Journal of the Chemical Society, Faraday Transactions, 1992. **88**: p. 3197-3200.

68. Osterholz, F. D. and Pohl, E. R., *Kinetics of the hydrolysis and condensation of organofunctional alkoxysilanes: a review.* Journal of Adhesion Science and Technology, 1992. **6**(1): p. 127.

69. Blum, F. D., Meesiri, W., Kang, H., and Gambogid, J. E., *Hydrolysis, adsorption, and dynamics of silane coupling agents on silica surfaces.* Journal of Adhesion Science and Technology, 1991. **5**(6): p. 479-496.

70. Nishiyama, N., Horie, K., and Asakura, T., *Adsorption behavior of a silane coupling agent onto a colloidal silica surface studied by ^{29}Si NMR spectroscopy* Journal of Colloid and Interface Science, 1989. **129**(1): p. 113-119.

71. Daniels, M. W., Sefcik, J., Francis, L. F., and McCormick, A. V., *Reactions of a trifunctional silane coupling agent in the presence of colloidal silica sols in polar media.* Journal of Colloid and Interface Science, 1998. **219**(2): p. 351-356.

72. González, D., Santos, V., and Parajó, J. C., *Silane-treated lignocellulosic fibers as reinforcement material in polylactic acid biocomposites.* Journal of Thermoplastic Composite Materials, 2012. **25**(8): p. 1005-1022.

73. Valadez-Gonzalez, A., Cervantes-Uc, J. M., Olayo, R., and Herrera-Franco, P. J., *Chemical modification of henequén fibers with an organosilane coupling agent.* Composites Part B: Engineering, 1999. **30**(3): p. 321–331.

74. Salon, M. C. B., Gerbaud, G., Abdelmouleh, M., Bruzzese, C., Boufi, S., and Belgacem, M. N., *Studies of interactions between silane coupling agents and cellulose fibers with liquid and solid-state NMR.* Magnetic Resonance in Chemistry, 2007. **45**(6): p. 473–483.

75. Abdelmouleh, M., Boufi, S., Belgacem, M. N., Duarte, A. P., Salah, A. B., and Gandini, A., *Modification of cellulosic fibres with functionalised silanes: development of surface properties.* International Journal of Adhesion and Adhesives, 2004. **24**(1): p. 43-54.

76. Lu, J., Askeland, P., and Drzal, L. T., *Surface modification of microfibrillated cellulose for epoxy composite applications.* Polymer, 2008. **49**(5): p. 1285-1296.

77. Monte, S. J., *Ken-React reference manual—titanate, zirconate and aluminate coupling agents*. 1995, Kenrich Petrochemicals, Inc.: Bayonne.

78. Lönnberg, H., Fogelström, L., Samir, M. A. S. A., Berglund, L., Malmström, E., and Hult, A, *Surface grafting of microfibrillated cellulose with poly(ε-caprolactone) – Synthesis and characterization.* European Polymer Journal, 2008. **44**(9): p. 2991-2997.

79. Kalia, S., Boufi, S., Celli, A., and Kango, S., *Nanofibrillated cellulose: surface modification and potential applications.* Colloid and Polymer Science, 2014. **292**(1): p. 5-31.

80. Syverud, K., Xhanari, K., Chinga-Carrasco, G., Yu, Y., and Stenius, P., *Films made of cellulose nanofibrils: surface modification by adsorption of a cationic surfactant and characterization by computer-assisted electron microscopy.* Journal of Nanoparticle Research, 2011. **13**(2): p. 773-782.

81. Nakagaito, A. N. and Yano, H., *Toughness enhancement of cellulose nanocomposites by alkali treatment of the reinforcing cellulose nanofibers.* Cellulose, 2008. **15**(2): p. 323-331.

82. Pahimanolis, N., Hippi, U., Johansson, L., Saarinen, T., Houbenov, N., Ruokolainen, J., and Seppälä, J., *Surface functionalization of nanofibrillated*

cellulose using click-chemistry approach in aqueous media. Cellulose, 2011. **18**: p. 1201-1212.

83. Lasseuguette, E., *Grafting onto microfibrils of native cellulose.* Cellulose, 2008. **15**(4): p. 571-580.
84. Maddah, H. A., *Polypropylene as a promising plastic: A review.* American Journal of Polymer Science, 2016. **6**(1): p. 1-11.
85. Anonymous. *Poly(propene) (Polypropylene)*. The Essential Chemical Industry - online 2014 January 2, 2014.
86. Shubhra, Q. T. H., Alam, A. K. M. M., and Quaiyyum, M. A., *Mechanical properties of polypropylene composites: A review.* Journal of Thermoplastic Composite Materials, 2011. **26**(3): p. 362-391.
87. Panaitescu, D. M., Donescu, D., Bercu, C., Vuluga, D. M., Iorga, M., and Ghiurea, M., *Polymer composites with cellulose microfibrils.* Polymer Engineering & Science, 2007. **47**(8): p. 1228-1234.
88. Ljungberg, N., Cavaillé, J.-Y., and Heux, L., *Nanocomposites of isotactic polypropylene reinforced with rod-like cellulose whiskers.* Polymer, 2006. **47**(18): p. 6285–6292.
89. Iwamoto, S., Yamamoto, S., Lee, S., and Endo, T., *Mechanical properties of polypropylene composites reinforced by surface-coated microfibrillated cellulose.* Composites Part A: Applied Science and Manufacturing, 2014. **59**: p. 26-29.
90. Nakatani, H., Hashimoto, K., Miyazaki, K., and Terano, M., *Cellulose/syndiotactic polypropylene composites: Effects of maleated polypropylene as a compatibilizer and silanized cellulose on the morphology and tensile properties.* Journal of Applied Polymer Science, 2009. **113**(3): p. 2022–2029.
91. Cheng, Q., Wang, S., Rials, T. G., and Lee, S., *Physical and mechanical properties of polyvinyl alcohol and polypropylene composite materials reinforced with fibril aggregates isolated from regenerated cellulose fibers.* Cellulose, 2007. **14**(6): p. 593-602.
92. Lim, L.-T., Auras, R., and Rubino, M., *Processing technologies for poly(lactic acid).* Progress in Polymer Science, 2008. **33**(8): p. 820–852.

93. Garlotta, D., *A literature review of poly(lactic acid).* Journal of Polymers and the Environment, 2001. **9**(2): p. 63-84.

94. Auras, R., Harte, B., and Selke, S., *An overview of polylactides as packaging materials.* Macromolecular Bioscience, 2004. **4**(9): p. 835-864.

95. Sinclair, R. G., *The case for polylactic acid as a commodity packaging plastic.* Journal of Macromolecular Science, Part A: Pure and Applied Chemistry, 1996. **A33**(5): p. 585–597.

96. Weber, C. J., Haugaard, V., Festersen, R., and Bertelsen, G., *Production and applications of biobased packaging materials for the food industry.* Food Additives & Contaminants, 2002. **19**(1): p. 172-177.

97. Gupta, B., Revagade, N., and Hilborn, J., *Poly(lactic acid) fiber: An overview.* Progress in Polymer Science, 2007. **32**(4): p. 455-482.

98. Griffith, L. G., *Polymeric biomaterials.* Acta Materialia, 2000. **48**(1): p. 263-277.

99. Nampoothiri, K. M., Nair, N. R., and John, R. P., *An overview of the recent developments in polylactide (PLA) research.* Bioresource Technology, 2010. **101**(22): p. 8493–8501.

100. Henton, D. E., Gruber, P., Lunt, J., and Randall, J., *Polylactic acid technology*, in *Natural Fibers, Biopolymers, and Biocomposites*. 2005, CRC Press. p. 528-569.

101. Lasprilla, A. Jr., Martinez, G. A. R., Lunelli, B. H., Jardini, A. L., and Filho, R. M., *Poly-lactic acid synthesis for application in biomedical devices — A review.* Biotechnology Advances, 2012. **30**(1): p. 321-328.

102. Auras, R. A., Harte, B., Selke, S., and Hernandez, R., *Mechanical, physical, and barrier properties of poly(lactide) films.* Journal of Plastic Film and Sheeting, 2003. **19**(2): p. 123-135.

103. Auras, R., Harte, B., and Selke, S., *Effect of water on the oxygen barrier properties of poly(ethylene terephthalate) and polylactide films.* Journal of Applied Polymer Science, 2004. **92**(3): p. 1790-1803.

104. Auras, R. A., Singh, S. P., and Singh, J. J., *Evaluation of oriented poly(lactide) polymers vs. existing PET and oriented PS for fresh food service containers.* Packaging Technology and Science, 2005. **18**(4): p. 207-216.

105. Lehermeier, H. J., Dorgan, J. R., and Way, D., *Gas permeation properties of poly(lactic acid).* Journal of Membrane Science, 2001. **190**(2): p. 243-251.

106. Auras, R., Harte, B., and Selke, S., *Sorption of ethyl acetate and d-limonene in poly(lactide) polymers.* Journal of the Science of Food and Agriculture, 2006. **86**(4): p. 648-656.

107. Dorgan, J. R., Lehermeier, H., and Mang, M., *Thermal and rheological properties of commercial-grade poly(lactic acid)s.* Journal of Polymers and the Environment, 2000. **8**(1): p. 1-9.

108. Siebott, V., *PLA—the future of rigid packaging?* , in *Bioplastics Mag* 2007. p. 28-29.

109. Anonymous, *Making preforms for PLA bottles*, in *Bioplastics Mag* 2006. p. 16-18.

110. Kimura, K. and Horikochi, Y., *Bio-based polymers.* Fujitsu Scientific & Technical Journal, 2005. **41**: p. 173-180.

111. Serizawa, S., Inoue, K., and Iji, M., *Kenaf-fiber-reinforced poly(lactic acid) used for electronic products.* Journal of Applied Polymer Science, 2006. **100**(1): p. 618-624.

112. Anonymous, *Complete mobile phone housing made of PLA reinforced with Kenaf fibres*, in *Bioplastics Mag*. 2006. p. 18-19.

113. Huda, M. S., Drzal, L. T., Mohanty, A. K., and Misra, M., *The effect of silane treated- and untreated-talc on the mechanical and physico-mechanical properties of poly(lactic acid)/newspaper fibers/talc hybrid composites.* Composites Part B: Engineering, 2007. **38**(3): p. 367–379.

114. Pluta, M., *Morphology and properties of polylactide modified by thermal treatment, filling with layered silicates and plasticization.* Polymer, 2004. **45**(24): p. 8239–8251.

115. Liu, X., Wang, T., Chow, L. C., Yang, M., and Mitchell, J. W., *Effects of inorganic fillers on the thermal and mechanical properties of poly(lactic acid).* International Journal of Polymer Science, 2014. **2014**: p. 1-8.

116. Suryanegara, L., Nakagaito, A. N., and Yano, H., *Thermo-mechanical properties of microfibrillated cellulose-reinforced partially crystallized PLA composites.* Cellulose, 2010. **17**(4): p. 771-778.

117. Lu, T., Jiang, M., Xu, X., Zhang, S., Hui, D., Gou, J., and Zhou, Z., *The effects on mechanical properties and crystallization of poly (l-lactic acid) reinforced by cellulosic fibers with different scales.* Journal of Applied Polymer Science, 2014. **131**(22).

118. Petersson, L., Kvien, I., and Oksman, K., *Structure and thermal properties of poly(lactic acid)/cellulose whiskers nanocomposite materials.* Composites Science and Technology, 2007. **67**(11-12): p. 2435-2544.

119. Jonoobi, M., Harun, J., Mathew, A. P., and Oksman, K., *Mechanical properties of cellulose nanofiber (CNF) reinforced polylactic acid (PLA) prepared by twin screw extrusion.* Composites Science and Technology, 2010. **70**(12): p. 1742–1747.

120. Jonoobi, M., Mathew, A. P., Abdi, M. M., Makinejad, M. D., and Oksman, K., *A comparison of modified and unmodified cellulose nanofiber reinforced polylactic acid (PLA) prepared by twin screw extrusion.* Journal of Polymers and the Environment, 2012. **20**(4): p. 991-997.

121. Pei, A., Zhou, Q., and Berglund, L. A., *Functionalized cellulose nanocrystals as biobased nucleation agents in poly(l-lactide) (PLLA)–Crystallization and mechanical property effects.* Composites Science and Technology, 2010. **70**(5): p. 815–821.

122. Raquez, J.-M., Murena, Y., Habibi, Y., Ruelle, B., DeBuyl, F., and P. Dubois, *Surface-modification of cellulose nanowhiskers and their use as nanoreinforcers into polylactide: A sustainably-integrated approach.* Composites Science and Technology, 2012. **72**(5): p. 544-549.

123. Frone, A. N., Berlioz, S., Chailan, J.-F., Panaitescu, D. M., and Donescu, D., *Cellulose fiber-reinforced polylactic acid.* Polymer Composites, 2011. **32**(6): p. 976-985.

124. Luo, X. and Zhang, L., *New solvents and functional materials prepared from cellulose solutions in alkali/urea aqueous system.* Food Research International, 2013. **52**(1): p. 387–400.

125. Zhang, S., Li, F., Yu, J., and Hsieh, Y., *Dissolution behaviour and solubility of cellulose in NaOH complex solution.* Carbohydrate Polymers, 2010. **81**(3): p. 668–674.

126. Ruan, D., Zhang, L., Mao, Y., Zeng, M., and Li, X., *Microporous membranes prepared from cellulose in NaOH/thiourea aqueous solution.* Journal of Membrane Science, 2004. **241**(2): p. 265–274.

127. Jin, H., Zha, C., and Gu, L., *Direct dissolution of cellulose in NaOH/thiourea/urea aqueous solution.* Carbohydrate Research, 2007. **342**(6): p. 851–858.

128. Qi, H., Liebert, T., Meister, F., and Heinze, T., *Homogenous carboxymethylation of cellulose in the NaOH/urea aqueous solution.* Reactive and Functional Polymers, 2009. **69**(10): p. 779–784.

129. Qi, H., Chang, C., and Zhang, L., *Effects of temperature and molecular weight on dissolution of cellulose in NaOH/urea aqueous solution.* Cellulose, 2008. **15**(6): p. 779-787.

130. Cai, J. and Zhang, L., *Rapid dissolution of cellulose in LiOH/urea and NaOH/urea aqueous solutions.* Macromolecular Bioscience, 2005. **5**(6): p. 539-548

131. Ratanakamnuan, U., Atong, D., and Aht-Ong, D., *Cellulose esters from waste cotton fabric via conventional and microwave heating.* Carbohydrate Polymers, 2012. **87**(1): p. 84-94.

132. Kiangkitiwan, N. and Srikulkit, K., *Poly(lactic acid) filled with cassava starch-g-soybean oil maleate.* The Scientific World Journal, 2013. **2013**: p. 1-7.

133. Thanomchat, S. and Srikulkit, K., *Effects of soybean oil modified cellulose fibril and organosilane modified cellulose fibril on crystallization of polypropylene.* Advances in Materials Science and Engineering, 2015. **2015**: p. 1-9.

134. Jacquet, N., Vanderghem, C., Danthine, S., Quiévy, N., Blecker, C., Devaux, J., and Paquot, M., *Influence of steam explosion on physicochemical properties*

and hydrolysis rate of pure cellulose fibers. Bioresource Technology, 2012. **121**: p. 221-227.

135. Olley, R. H. and Bassett, D. C., *An improved permanganic etchant for polyolefines.* Polymer, 1982. **23**(12): p. 1707-1710.

136. Garcia, M., Vliet, G. V., Jahin, S., Schrauwen, B. A. G., Sarkissov, A., Zyl, W. E. V., and Boukamp, B., *Polypropylene/SiO_2 nanocomposites with improved mechanical properties.* Reviews on Advanced Materials Science, 2004. **6**: p. 169-175.

137. Turner, J. F., Riga, A., O'Connor, A., Zhang, J., and Collis, J., *Characterization of drawn and undrawn poly-L-lactide films by differential scanning calorimetry.* Journal of Thermal Analysis and Calorimetry, 2004. **75**(1): p. 257-268.

138. Henrick, F. W., Casebier, R. L., Hamilton, J. K., and Sandberg, K. R., *Microfibrillated cellulose: morphology and accessibility.* Journal of Applied Polymer Science: Applied Polymer Symposium, 1983. **37**: p. 797-813.

139. Zhang, J., Song, H., Lin, L., Zhuang, J., Pang, C., and Liu, S., *Microfibrillated cellulose from bamboo pulp and its properties.* Biomass and Bioenergy, 2012. **39**: p. 78-83.

140. Thanomchat, S., Srikulkit, K., Suksut, B., and Schlarb, A. K., *Morphology and crystallization of polypropylene/microfibrillated cellulose composites.* KMUTNB : International Journal of Applied Science and Technology, 2014. **7**(4): p. 23-34.

141. Li, W. Y., Jin, A. X., Liu, C. F., Sun, R. C., Zhang, A. P., and Kenedy, J. F., *Homogeneous modification of cellulose with succinic anhydride in ionic liquid using 4-dimethylaminopyridine as a catalyst.* Carbohydrate Polymers, 2009. **78**(3): p. 389-395.

142. Dong, X., Dong, Y., Jiang, M., Wang, L., Tong, J., and Zhou, J., *Modification of microcrystalline cellulose by using soybean oil for surface hydrophobization.* Industrial Corps and Products, 2013. **46**: p. 301-303.

143. Sequeira, S., Evtuguin, D. V., Portugal, I., and Esculcas, A. P., *Synthesis and characterisation of cellulose/silica hybrids obtained by heteropoly acid*

catalysed sol–gel process. Materials Science and Engineering C, 2007. **27**(1): p. 172-179.

144. E. Fortunati, M. Peltzer, I. Armentano, L. Torre, A. Jimenez, and J. M. Kenny, *Effects of modified cellulose nanocrystals on the barrier and migration properties of PLA nano-biocomposites.* Carbohydrate Polymers, 2012. **90**(2): p. 948-956.

145. Ciolacu, D., Ciolacu, F., and Popa, V. I., *Amorphous cellulos–structure and characterization.* Cellulose Chemistry and Technology, 2011. **45**(1-2): p. 13-21.

146. Kadokawa, J., Murakami, M., Takegawa, A., and Kaneko, Y., *Preparation of cellulose-starch composite gel and fibrous material from a mixture of polysaccharides in ionic liquid.* Carbohydrate Polymers, 2009. **75**(1): p. 180-183.

147. Spoljaric, S., Genovese, A., and Shanks, R. A., *Polypropylene–microcrystalline cellulose composites with enhanced compatibility and properties.* Composites: Part A, 2009. **40**(6-7): p. 791-799.

148. Mamleev, V., Bourbigot, S., and Yvon, J., *Kinetic analysis of the thermal decomposition of cellulose: The main step of mass loss.* Journal of Analytical and Applied Pyrolysis, 2007. **80**(1): p. 151-165.

149. Mamleev, V., Bourbigot, S., Bras, M. L., Yvon, J., and Lefebvre, J., *Model-free method for evaluation of activation energies in modulated thermogravimetry and analysis of cellulose decomposition.* Chemical Engineering Science, 2006. **61**(4): p. 1276-1292.

150. Rachini, A., Troedec, M. L., Peyratout, C., and Smith, A., *Comparison of the thermal degradation of natural, alkali-treated and silane-treated hemp fibers under air and an inert atmosphere.* Journal of Applied Polymer Science, 2008. **112**(1): p. 226-234.

151. Shen, W., He, H., Zhu, J., Yuan, P., and Frost, R. L., *Grafting of montmorillonite with different functional silanes via two different reaction systems.* Journal of Colloid and Interface Science, 2007. **313**(1): p. 268-273.

152. Joseph, P. V., Joseph, K., Thomas, S., Pillai, C. K. S., Prasad, V. S., Groeninckx, G., and Sarkissova, M., *The thermal and crystallisation studies of short sisal fibre*

reinforced polypropylene composites. Composites Part A: applied science and manufacturing, 2003. **34**(3): p. 253-266.

153. Yang, H., Kiziltas, A., and Gardner, D. J., *Thermal analysis and crystallinity study of cellulose nanofibril-filled polypropylene composites.* Journal of Thermal Analysis and Calorimetry, 2013. **113**(2): p. 673-682.
154. Wang, M., Lin, L., Peng, Q., Ou, W., and Li, H., *Crystallization and mechanical properties of isotactic polypropylene/calcium carbonate nanocomposites with a stratified distribution of calcium carbonate.* Journal of Applied Polymer Science, 2013. **131**(10): p. 1-9.
155. Yang, K., Yang, Q., Li, G., Sun, Y., and Feng, D., *Morphology and mechanical properties of polypropylene/calcium carbonate nanocomposites.* Materials Letters, 2006. **60**(6): p. 805-809.
156. Wang, Y., Shen, H., Li, G., and Mai, K., *Crystallization and melting behavior of PP/nano-$CaCO_3$ composites with different interfacial interaction.* Journal of Thermal Analysis and Calorimetry, 2010. **99**(2): p. 399-407.
157. Ning, N., Yin, Q., Luo, F., Zhang, Q., Du, R., and Fu, Q., *Crystallization behavior and mechanical properties of polypropylene/halloysite composites.* Polymer, 2007. **48**(25): p. 7374-7384.
158. Ferrage, E., Martin, F., Boudet, A., Petit, S., Fourty, G., Jouffret, F., Micoud, P., De Parseval, P., Salvi, S., Bourgerette, C., Ferret, J., Saint-Gerard, Y., Buratto, S., and Fortune, J. P., *Talc as nucleating agent of polypropylene: morphology induced by lamellar particles addition and interface mineral-matrix modelization.* Journal of Materials Science, 2002. **37**(8): p. 1561-1573.
159. Zanetti, M., Camino, G., Reichert, P., and Mu¨lhaupt, R., *Thermal Behaviour of Poly(propylene) Layered Silicate Nanocomposites.* Macromolecular Rapid Communications, 2001. **22**(3): p. 176-180.
160. George, J., Bhagawan, S. S., and Thomas, S., *Thermogravimetric and dynamic mechanical thermal analysis of pineapple fibre reinforced polyethylene composites.* Journal of Thermal Analysis, 1996. **47**(4): p. 1121-1140.

161. Dai, J., Shen, Y., Yang, J., Huang, T., Zhang, N., and Wang, Y., *Crystallization and melting behaviors of polypropylene admixed by graphene and β-phase nucleating agent.* Colloid and Polymer Science, 2014. **292**(4): p. 923-933.

162. Duan, J. and Dou, Q., *Investigation on b-Polypropylene/PP-g-MAH/Surface Treated Talc Composites.* Journal of Applied Polymer Science, 2013. **130**(1): p. 206-221.

163. Huson, M. G. and McGill, W. J., *Transcrystallinity in polypropylene.* Journal of Polymer Science: Part A. **22**(11): p. 3571-3580.

164. Amash, A. and Zugenmaier, P., *Morphology and properties of isotropic and oriented samples of cellulose fibre–polypropylene composites.* Polymer, 2000. **41**(4): p. 1589-1596.

165. Qiu, W., Endo, T., and Hirotsu, T., *Structure and properties of composites of highly crystalline cellulose with polypropylene: Effects of polypropylene molecular weight.* European Polymer Journal, 2006. **42**(5): p. 1059–1068.

166. Qin, H. L., Zhang, S. M., Zhao, C. G., Feng, M., Yang, M. S., Shu, Z. J., and Yang, S. S., *Thermal stability and flammability of polypropylene/montmorillonite composites.* Polymer Degradation and Stability, 2004. **85**(2): p. 807-813.

167. Panaitescu, D. M., Donescu, D., Bercu, C., Vuluga, D. M., Iorga, M., and Ghiurea, M., *Polymer composites with cellulose microfibrils.* Polymer Engineering and Science, 2007. **47**(8): p. 1228-1234.

168. Wu, C. L., Zhang, M. Q., Rong, M. Z., and Friedrich, K., *Tensile performance improvement of low nanoparticles filled-polypropylene composites.* Composites Science and Technology, 2002. **62**(10-11): p. 1327-1340.

169. Kalaitzidou, K., Fukushima, H., and Drzal, L. T., *Mechanical properties and morphological characterization of exfoliated graphite–polypropylene nanocomposites.* Composites Part A: Applied Science and Manufacturing, 2007. **38**(7): p. 1675-1682.

170. Demir, H., Atikler, U., Balkose, D., and Tihminlioglu, F., *The effect of fiber surface treatments on the tensile and water sorption properties of polypropylene-luffa fiber composites.* Composites Part a-Applied Science and Manufacturing, 2006. **37**(3): p. 447-456.

171. Yang, H., Gardner, D. J., and Nader, J. W., *Morphological properties of impact fracture surfaces and essential work of fracture analysis of cellulose nanofibril-filled polypropylene composites.* Journal of Applied Polymer Science, 2013. **128**(5): p. 3064–3076.

172. Sui, G., Zhong, W. H., Fuqua, M. A., and Ulven, C. A., *Crystalline structure and properties of carbon nanofiber composites prepared by melt extrusion.* Macromolecular Chemistry and Physics, 2007. **208**(17): p. 1928-1936.

173. Bao, S. P. and Tjong, S. C., *Temperature and strain rate dependences of yield stress of polypropylene composites reinforced with carbon nanofibers.* Polymer Composites, 2009. **30**(12): p. 1749-1760.

174. Iwamoto, S., Yamamoto, S., Lee, S. H., and Endo, T., *Mechanical properties of polypropylene composites reinforced by surface-coated microfibrillated cellulose.* Composites Part a-Applied Science and Manufacturing, 2014. **59**: p. 26-29.

175. Nakatani, H., Iwakura, K., Hamadate, M., Okazaki, N., Aoyama, M., and Terano, M., *Interface adhesion properties of syndiotactic polypropylene/cellulose group composite: Relationship between chemical structure of coupling agent and reactivity for cellulose group.* Journal of Applied Polymer Science, 2011. **122**(4): p. 2798-2806.

176. Qiu, W. L., Zhang, F. R., Endo, T., and Hirotsu, T., *Milling-induced esterification between cellulose and maleated polypropylene.* Journal of Applied Polymer Science, 2004. **91**(3): p. 1703-1709.

177. Kokta, B. V., Chen, R., Daneault, C., and Valade, J. L., *Use of wood fibers in thermoplastic composites.* Polymer Composites, 2004. **4**(4): p. 229-232.

178. Van der Wal, A. and Gaymans, R. J., *Polypropylene–rubber blends: 3. The effect of the test speed on the fracture behaviour.* Polymer, 1999. **40**(22): p. 6045-6055.

179. Luiz de Paula, E., Mano, V., and Pereira, F. V., *Influence of cellulose nanowhiskers on the hydrolytic degradation behavior of poly(d,l-lactide).* Polymer Degradation and Stability, 2011. **96**(9): p. 1631-1638.

180. Lee, J. H., Park, S. H., and Kim, S. H., *Preparation of cellulose nanowhiskers and their reinforcing effect in polylactide.* Macromolecular Research, 2013. **21**(11): p. 1218-1225.

181. Suryanegara, L., Nakagaito, A. N., and Yano, H., *Thermo-mechanical properties of microfibrillated cellulose-reinforced partially crystallized PLA composites.* Cellulose, 2010. **17**(4): p. 771-778.

182. Krishnamachari, P., Zhang, J., Lou, J. Z., Yan, J. Z., and Uitenham, L., *Biodegradable poly(lactic acid)/clay nanocomposites by melt intercalation: A study of morphological, thermal, and mechanical properties.* International Journal of Polymer Analysis and Characterization, 2009. **14**(4): p. 336-350.

183. Lee, J. H., Park, T. G., Park, H. S., Lee, D. S., Lee, Y. K., Yoon, S. C., and Nam, J. D., *Thermal and mechanical characteristics of poly(L-lactic acid) nanocomposite scaffold.* Biomaterials, 2003. **24**(16): p. 2773-2778.

184. Kang, K. S., Lee, S. I., Lee, T. J., Narayan, R., and Shin, B. Y., *Effect of biobased and biodegradable nucleating agent on the isothermal crystallization of poly(lactic acid).* Korean Journal of Chemical Engineering, 2008. **25**(3): p. 599-608.

185. Lorenzo, M. L. D., *Calorimetric analysis of the multiple melting behavior of poly(L-lactic acid).* Journal of Applied Polymer Science, 2006. **100**(4): p. 3145-3151.

186. Frone, A. N., Berlioz, S., Chailan, J. F., and Panaitescu, D. M., *Morphology and thermal properties of PLA-cellulose nanofibers composites.* Carbohydrate Polymers, 2013. **91**(1): p. 377-384.

187. Lu, T. J., Jiang, M., Xu, X. L., Zhang, S. L., Hui, D., Gou, J. H., and Zhou, Z. W., *The effects on mechanical properties and crystallization of poly(L-lactic acid) reinforced by cellulosic fibers with different scales.* Journal of Applied Polymer Science, 2014. **131**(22): p. 1-8.

188. Mathew, A. P., Oksman, K., and Sain, M., *The effect of morphology and chemical characteristics of cellulose reinforcements on the crystallinity of polylactic acid.* Journal of Applied Polymer Science, 2006. **101**(1): p. 300-310.

189. Wang, T. and Drzal, L. T., *Cellulose-nanofiber-reinforced poly(lactic acid) composites prepared by a water-based approach.* Acs Applied Materials & Interfaces, 2012. **4**(10): p. 5079-5085.

190. Song, Y. N., Tashiro, K., Xu, D. G., Liu, J., and Bin, Y. Z., *Crystallization behavior of poly(lactic acid)/microfibrillated cellulose composite.* Polymer, 2013. **54**(13): p. 3417-3425.

191. Rhim, J., Mohanty, A. K., Singh, S. P., and Ng, P. K. W., *Effect of the processing methods on the performance of polylactide films: Thermocompression versus solvent casting.* Journal of Applied Polymer Science, 2006. **101**(6): p. 3736-3742.

192. Labrecque, L. V., Kumar, R. A., Dave, V., Gross, R. A., and McCarthy, S. P., *Citrate esters as plasticizers for poly(lactic acid).* Journal of Applied Polymer Science, 1997. **66**(8): p. 1507-1513.

193. Jacobsen, S. and Fritz, H. G., *Plasticizing polylactide-The effect of different plasticizers on the mechanical properties.* Polymer Engineering and Science, 1999. **39**(7): p. 1303-1310.

194. Jacobsen, S. and Fritz, H. G., *Filling of poly(lactic acid) with native starch.* Polymer Engineering and Science, 1996. **36**(22): p. 2799-2804.

195. Sarasua, J. R., Arraiza, A. L., Balerdi, P., and Maiza, I., *Crystallization and thermal behaviour of optically pure polylactides and their blends.* Journal of Materials Science, 2005. **40**(8): p. 1855-1862.

196. Li, Y. J. and Shimizu, H., *Improvement in toughness of poly(L-lactide) (PLLA) through reactive blending with acrylonitrile-butadiene-styrene copolymer (ABS): Morphology and properties.* European Polymer Journal, 2009. **45**(3): p. 738-746.

197. Thepthawat, A. and Srikulkit, K., *Improving the properties of polylactic acid by blending with low molecular weight polylactic acid-g-natural rubber.* Polymer Engineering & Science, 2014. **54**(12): p. 2770-2776.

APPENDIX

Elapsed Time	00:04:00
Median Diam.	567.2 nm
Mean Diam.	648.6 nm
Polydispersity	0.328
GSD	1.703

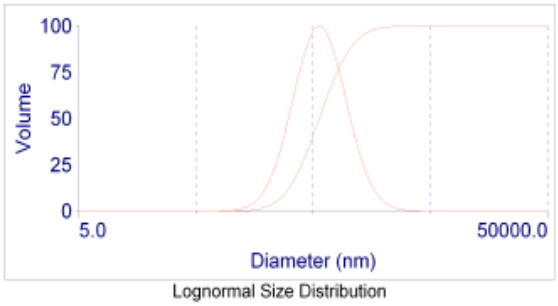

Lognormal Size Distribution

d(nm)	G(d)	C(d)	d(nm)	G(d)	C(d)	d(nm)	G(d)	C(d)
241.9	26	5	497.5	97	40	804.2	80	75
291.9	44	10	531.3	99	45	877.4	70	80
331.6	58	15	567.2	100	50	970.1	58	85
366.6	70	20	605.4	99	55	1102.0	44	90
400.0	80	25	646.6	97	60	1330.1	26	95
432.3	87	30	692.4	93	65			
464.6	93	35	744.1	87	70			

Figure A-1 Particle size distribution of cellulose fibril

Elapsed Time	00:03:00
Median Diam.	1687.9 nm
Mean Diam.	2069.0 nm
Polydispersity	0.523
GSD	1.912

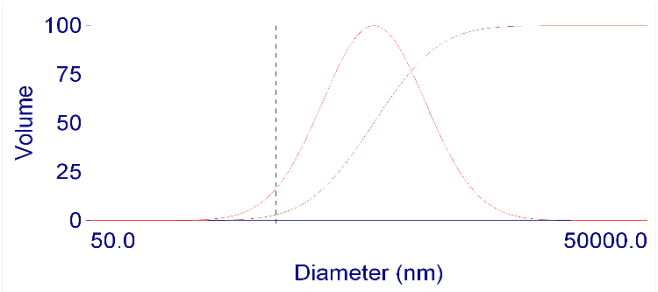

Lognormal Size Distribution

d(nm)	G(d)	C(d)	d(nm)	G(d)	C(d)	d(nm)	G(d)	C(d)
590.9	26	5	1436.3	97	40	2595.0	80	75
744.9	44	10	1557.5	99	45	2888.6	70	80
871.5	58	15	1687.9	100	50	3269.3	58	85
986.3	70	20	1829.2	99	55	3825.0	44	90
1097.9	80	25	1983.7	97	60	4821.9	26	95
1208.2	87	30	2158.0	93	65			
1320.3	93	35	2358.1	87	70			

Figure A-2 Particle size distribution of Oil-g-CF

Elapsed Time	00:05:00
Median Diam.	855.3 nm
Mean Diam.	978.2 nm
Polydispersity	0.328
GSD	1.703

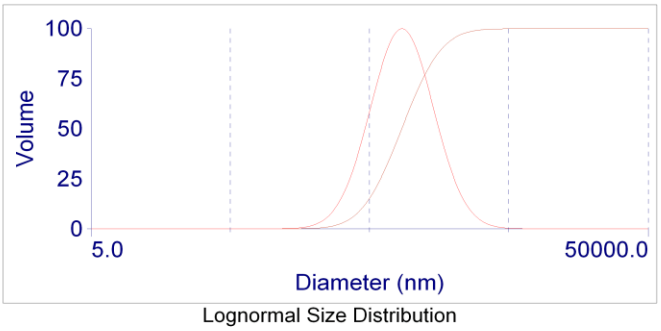

Lognormal Size Distribution

d(nm)	G(d)	C(d)	d(nm)	G(d)	C(d)	d(nm)	G(d)	C(d)
364.7	26	5	750.3	97	40	1212.8	80	75
440.2	44	10	801.3	99	45	1323.2	70	80
500.1	58	15	855.3	100	50	1463.1	58	85
552.9	70	20	913.1	99	55	1662.0	44	90
603.2	80	25	975.2	97	60	2005.9	26	95
652.0	87	30	1044.2	93	65			
700.7	93	35	1122.2	87	70			

Figure A-3 Particle size distribution of Silane-g-CF

Table A-1 Water retention value of CF, regenerated MCC and MCC

Sample	No.	Weight of wet sample (g.)				Weight of dried sample (g.)				WRV (%)	AV	SD
		1	2	3	Average	1	2	3	Average			
Cellulose	1	5.73	5.72	5.72	5.73	0.27	0.26	0.27	0.27	2054.48	2021.37	46.82
Fibril	2	5.61	5.61	5.60	5.61	0.27	0.27	0.27	0.27	1988.27		
Regenerated	1	8.36	8.35	8.35	8.35	0.45	0.46	0.45	0.45	1736.69	1739.58	4.09
MCC	2	8.26	8.26	8.25	8.26	0.45	0.45	0.45	0.45	1742.47		
	1	2.81	2.80	2.80	2.80	0.87	0.87	0.88	0.87	221.20	222.25	1.48
MCC	2	2.76	2.76	2.76	2.76	0.85	0.85	0.86	0.85	223.30		

Table A-2 Tensile strength (MPa) of neat PP, Silane-g-CF/PP composites and virgin CF/PP composite with various filler content

Sample	Neat PP	0.5 wt% Silane-g-CF	1.0 wt% Silane-g-CF	3.0 wt% Silane-g-CF	5.0 wt% Silane-g-CF	1.0 wt% virgin CF
1	38.16	39.77	38.68	36.10	34.52	38.41
2	37.83	38.44	36.63	36.85	33.79	38.99
3	37.38	39.93	35.98	36.34	34.05	37.87
4	37.37	38.35	37.11	34.00	35.58	38.13
5	37.15	38.45	38.10	35.49	33.19	38.07
Average	37.58	38.98	37.30	35.75	34.23	38.29
SD	0.410	0.790	1.092	1.097	0.897	0.433

Table A-3 Young's modulus (MPa) of neat PP, Silane-g-CF/PP composites and virgin CF/PP composite with various filler content

Sample	Neat PP	0.5 wt% Silane-g-CF	1.0 wt% Silane-g-CF	3.0 wt% Silane-g-CF	5.0 wt% Silane-g-CF	1.0 wt% virgin CF
1	1585.39	1684.24	1682.24	1782.69	1687.07	1730.33
2	1626.92	1773.52	1699.22	1708.77	1870.60	1683.26
3	1679.47	1649.13	1707.59	1782.03	1818.45	1798.29
4	1533.45	1738.16	1630.15	1779.24	1770.07	1753.56
5	1654.67	1675.53	1600.50	1818.48	1809.54	1734.13
Average	1615.98	1704.12	1663.94	1774.25	1791.15	1739.92
SD	57.870	50.530	46.505	40.001	68.327	41.619

Table A-4 Elongation at break (%) of neat PP, Silane-g-CF/PP composites and virgin CF/PP composite with various filler content

Sample	Neat PP	0.5 wt% Silane-g-CF	1.0 wt% Silane-g-CF	3.0 wt% Silane-g-CF	5.0 wt% Silane-g-CF	1.0 wt% virgin CF
1	451.94	382.22	175.07	13.95	9.93	97.28
2	445.52	320.40	135.04	13.91	9.79	97.10
3	459.90	314.03	126.39	13.46	9.67	89.71
4	467.75	245.12	81.14	13.06	9.57	78.98
5	439.22	238.90	75.37	13.00	9.43	75.00
Average	452.87	300.13	118.60	13.48	9.68	87.61
SD	11.315	59.408	41.209	0.450	0.191	10.263

Table A-5 Tensile strength (MPa) of neat PLA, Silane-g-CF/PLA composites and virgin CF/PLA composite with various filler content

Sample	Neat PLA	0.5 wt% Silane-g-CF	1.0 wt% Silane-g-CF	3.0 wt% Silane-g-CF	5.0 wt% Silane-g-CF	1.0 wt% virgin CF
1	69.06	63.76	57.40	54.89	49.21	65.82
2	65.15	63.87	60.37	53.71	49.71	67.67
3	68.10	61.54	56.66	54.84	45.38	65.63
4	68.06	59.98	58.18	52.28	45.39	64.99
5	69.81	63.12	57.46	55.76	48.98	65.31
Average	68.04	62.45	58.01	54.29	47.74	65.89
SD	1.772	1.666	1.426	1.342	2.160	1.049

Table A-6 Young's modulus (MPa) of neat PLA, Silane-g-CF/PLA composites and virgin CF/PLA composite with various filler content

Sample	Neat PLA	0.5 wt% Silane-g-CF	1.0 wt% Silane-g-CF	3.0 wt% Silane-g-CF	5.0 wt% Silane-g-CF	1.0 wt% virgin CF
1	3334.74	3349.33	2247.05	2696.81	2529.68	3337.61
2	3515.71	3305.63	3108.26	2474.61	2732.54	3462.04
3	3292.90	3517.87	3117.23	2894.56	2548.42	3247.42
4	3598.03	3328.97	2767.98	2616.68	2801.38	3429.72
5	3409.83	3042.34	2809.15	2861.68	2710.36	3251.04
Average	3430.24	3308.83	2809.94	2708.87	2664.47	3345.57
SD	126.350	170.857	354.270	174.180	119.499	99.094

Table A-7 Elongation at break (%) of neat PLA, Silane-g-CF/PLA composites and virgin CF/PLA composite with various filler content

Sample	Neat PLA	0.5 wt% Silane-g-CF	1.0 wt% Silane-g-CF	3.0 wt% Silane-g-CF	5.0 wt% Silane-g-CF	1.0 wt% virgin CF
1	5.50	7.43	7.68	3.94	3.46	4.90
2	5.49	7.30	6.88	3.80	3.39	4.88
3	4.31	7.27	6.50	3.79	3.34	4.87
4	4.29	6.69	5.55	3.78	3.12	4.86
5	4.08	6.41	5.50	3.67	3.11	4.51
Average	4.73	7.02	6.42	3.80	3.28	4.80
SD	0.698	0.442	0.921	0.098	0.160	0.163

Table A-8 Impact resistance (KJ/m^2) of neat PP, Silane-g-CF/PP composites and virgin CF/PP composite with various filler content

Sample	Neat PP	0.5 wt% Silane-g-CF	1.0 wt% Silane-g-CF	3.0 wt% Silane-g-CF	5.0 wt% Silane-g-CF	1.0 wt% virgin CF
1	2.21	2.23	2.23	2.28	2.21	1.90
2	2.08	2.23	2.24	2.34	2.33	1.81
3	2.05	2.21	2.22	2.28	2.22	1.72
4	1.83	2.19	2.21	2.17	2.17	1.61
5	1.83	2.16	2.24	2.31	2.27	1.45
6	1.75	2.11	2.10	2.30	2.21	1.43
7	1.73	2.11	2.26	2.23	2.24	1.42
8	1.73	2.11	2.10	2.17	2.24	1.40
9	1.85	1.84	2.14	2.24	2.20	1.11
10	1.70	1.81	2.12	2.26	2.15	1.02
Average	1.88	2.10	2.19	2.26	2.22	1.49
SD	0.18	0.15	0.06	0.06	0.05	0.28

Table A-9 Impact resistance (KJ/m^2) of neat PLA, Silane-g-CF/PLA composites and virgin CF/PLA composite with various filler content

Sample	Neat PLA	0.5 wt% Silane-g-CF	1.0 wt% Silane-g-CF	3.0 wt% Silane-g-CF	5.0 wt% Silane-g-CF	1.0 wt% virgin CF
1	2.04	2.06	2.34	2.63	2.25	1.39
2	2.10	2.11	2.43	2.63	2.27	1.42
3	1.96	2.12	2.11	2.47	2.13	1.40
4	1.96	1.98	2.23	2.58	1.98	1.39
5	1.75	1.95	2.07	2.13	1.67	1.37
6	1.61	2.03	1.96	2.10	1.76	1.09
7	1.59	1.65	1.97	2.09	1.74	1.07
8	1.55	1.73	2.03	2.05	1.86	1.12
9	1.40	1.65	1.83	2.03	1.78	1.08
10	1.22	1.72	1.82	1.89	1.73	1.02
Average	1.72	1.90	2.08	2.26	1.92	1.24
SD	0.29	0.19	0.20	0.28	0.22	0.17

VITA

Mr. Sarit Thanomchat was born on February 7, 1985, in Angthong, Thailand. In 2007, He graduated from the department of Materials Science and Engineering, Faculty of Engineering and Industrial Technology, Silpakorn University with a Bachelor's Degree in Engineering (Petrochemicals and Polymeric Materials). Afterwards, he continued to study in the department of Materials Science, Faculty of Science, Chulalongkorn University and received a Master of Science in Applied Polymer Science and Textile Technology in 2009. After working in an industrial company, he decided to study a Doctoral degree program in Materials Science, department of Materials Science, Faculty of Science, Chulalongkorn University in 2011 and graduated in 2016.

Publications:

1. Thanomchat, S. and Srikulkit, K., Thermal and mechanical properties of polylactic acid filled with organosilane modified cellulose fibril. Jurnal Teknologi, 2016. (In Press)

2. Thanomchat, S. and Srikulkit, K., Effects of soybean oil modified cellulose fibril and organosilane modified cellulose fibril on crystallization of polypropylene. Advances in Materials Science and Engineering, 2015. 2015: p. 1-9.

3. Thanomchat, S., Srikulkit, K., Suksut, B., and Schlarb, A. K., Morphology and crystallization of polypropylene/microfibrillated cellulose composites. KMUTNB : International Journal of Applied Science and Technology, 2014. 7(4): p. 23-34.

4. Thanomchat, S., Limpanart, S., and Srikulkit, K., Spinning and characterizations of polypropylene/alkylphosphonic acid treated montmorillonite nanocomposite fiber. Journal of Applied Polymer Science, 2010. 117(4): p. 1969-1977.

Patents

1. กาวี ศรีกูลกิจ และสาริศ ถนอมชาติ. 2558. มาสเตอร์แบทช์พอลิโอเลฟินส์ผสมเซลลูโลสไมโครไฟบริลดัดแปร และกรรมวิธีการเตรียมมาสเตอร์แบทช์ดังกล่าว. สิทธิบัตรไทย.

2. กาวี ศรีกูลกิจ และสาริศ ถนอมชาติ. 2556. กรรมวิธีการเตรียมเซลลูโลสไมโครไฟบริลด้วยวิธีละลายและตกตะกอน. สิทธิบัตรไทย.

Work Experience:

2009-2011: Chemist, Quality Control Department, Captain Coating Co., Ltd., Thailand.